Flexibility and Balancing in Active Distribution Networks

Kordheili, Reza Ahmadi

Publication date:
2015

Document Version
Publisher's PDF, also known as Version of record

FLEXIBILITY AND BALANCING IN ACTIVE DISTRIBUTION NETWORKS

by

Reza Ahmadi Kordkheili

AALBORG UNIVERSITY
DENMARK

A Dissertation Submitted to

The Faculty of Engineering and Science at Aalborg Universiy

In Partial Fulfillment for the Degree of

Doctor of Philosophy in Electrical Engineering

December 2015

.

Thesis Details

Title: Flexibility and Balancing in Active Distribution Networks

Thesis submitted:	December 20, 2015
PhD Student:	Reza Ahmadi Kordkheili,
PhD supervisors:	Prof. Josep M. Guerrero, Aalborg University Dr. Mehdi Savaghebi, Aalborg University
PhD committee:	Prof. Laszlo Mathe, Aalborg University Prof. Eleonora Riva Sanseverino, University of Palermo Prof. Moises Graells, University of Barcelona UPC
PhD Series:	Faculty of engineering, Aalborg University

Published by:
Aalborg University Press
Skjernvej 4A, 2nd floor
DK – 9220 Aalborg Ø
Phone: +45 99407140
aauf@forlag.aau.dk
forlag.aau.dk

Printed in Denmark by Rosendahls, 2015

ACKNOWLEDGEMENTS

It's been a great honor to have the chance of doing a PhD in Aalborg University. I'm very thankful to the Department of Energy Technology for their support and helps during my PhD period. I would also like to thank the *EDGE* project, which partly funded my PhD project.

I'm deeply grateful to my supervisor, Professor Josep M. Guerrero, and my co-supervisor, Mehdi Savaghebi, for their support during the final stage of my PhD. Their valuable support and understanding has been a great help for me. I would also like to thank Professor Birgitte bak-Jensen and Associate Professor Jayakrishnan R.Pillai for their feedbacks and helps during the PhD. Their comments have been a great help for improving the work and moving forward through the PhD.

I've had the honor and pleasure of collaborating with Professor Hashem Nehrir from Montana State University, USA, where I spent my study abroad. It's been a great experience to work with Professor Nehrir and his research group. I'm also very thankful to my very good friend, Seyyed Ali pourmousavi, to whom I had the pleasure of working and collaborating with.

My friends in the department of energy technology have been a great support through my PhD life. They have been a great support to me, regardless of the circumstances. Bishnu Prasad Bhattarai, Konstantinos Kouzelis, and Iker Diaz de Cerio Mendaza have been great friends and great roommates, and it's been a pleasure to work with and talk to them. I would like to express my gratitudes to my Iranian friends, especially Alireza Rezania, Hamid Soltani, Amir Sajjad Bahman, Qobad Shafiee, Mostafa Astaneh, Pooya Davari, Bakhtyar Hoseinzadeh, and Hamidreza Shaker for their friendship and their patience. I'm very thankful to all my Danish friends in the department who have been very kind to me during these years. It's been a great honor for me to find such good friends in Denmark, and they will always be in my memories.

My family have been a great support during my whole life, and supported me all the time, regardless of the circumstances. My deepest gratitudes to my parents, and to my brothers, for their support, understanding and patience during the whole PhD study.

ENGLISH SUMMARY

Environmental concerns, together with the fast-pacing changes in the renewable energy technologies, have led to significant growth of renewable energy sources (RESs) in energy systems. Among different sources of renewable energy, wind and solar energy are the most progressed sources so far. However, high penetration of RESs in the power network can cause serious problems in the power system, as these energy sources are hardly dispatchable. On the other hand, appearance of new electric loads in the power system, especially electric vehicles (EVs), increases the electric demand of the network, and causes higher fluctuations in the demand.

In countries such as Denmark, different incentives have been proposed and applied to encourage customers for investing on solar photovoltaic (PV) panels. These policies have increased the number of household PV panels. However, presence of such small energy sources in low voltage (LV) network affects the traditional behavior of these systems, as it leads to reverse power flow, from the customers to the upper network. Such reverse power flow brings new challenges to the system, while it also brings new potentials for transmission system operator (TSO) and distribution system operator (DSO) to use the reverse power flow for balancing purposes.

The first objective of this research is to quantify and analyze the impact of PV panels and EVs on LV network, and to determine the maximum capacity of LV network for hosting PV panels and EVs. Details of the studies are presented in chapter 2. In the first step, a proper modeling approach has been defined for loads, EVs, and PV panels. Details of the load modeling are presented in chapter 2. For EVs, the modeling is applied considering lithium-ion (Li-ion) batteries, considering the growing interest of industries in these batteries. A detailed modeling of Li-ion battery is presented in chapter 2 as well. PV panels are modelled as a function of solar irradiation and ambient temperature. In the next step, the impact of PV panels and electric vehicles on LV network was quantified separately. For PV panels, different placement of panels in the LV network has been analyzed and studied to find out the network operating limits in dealing with these small energy sources. Besides, an optimization study has been applied to the network to determine the maximum ancillary service which can be provided by PV panels for the power system, considering the operating limits of the power system and transformer capacity. On the other hand, different charging strategies have been proposed for EVs to determine maximum penetration of EVs in the LV network. These strategies are based on voltage measurement of LV grid nodes, and location and placement of EVs in the LV network. Different types of EVs, with different distance profiles (DP) have been considered in the studies. In the third step, the potential of PV panels and EVs for providing grid support and ancillary service for the power system has been analyzed. The main objective of this analysis was to quantify the capacity of LV

network for providing ancillary service for power system. To do so, an optimization problem has been proposed and applied to the network.

The second objective of this research is to evaluate the impact of active LV network on medium voltage (MV) network. To do so, an aggregated model of LV network in presence of PV panels and EVs has been proposed and simulated. The proposed aggregation technique is presented in chapter 3. Also, the impact of the LV network on the MV network has been quantified, considering residential, industrial, and commercial loads of the MV network. Chapter 4 presents the details of the analysis, as well as the details of the MV network. To generalize the analysis, a standard MV network has been used for the studies. The MV network is also an active network, i.e. it involves MV wind turbines and decentralized combined heat and power (DCHP). DCHP units play an important role in Danish power system, and they contribute to electricity production as well. Modeling of wind turbines is done considering real data of a Vestas wind turbine. For wind speed, a modified wind speed model has been used for wind turbines, considering the available wind measurement. Also, a detailed model of DCHP units has been used in this thesis. Details of wind turbine model, as well as details of DCHP are presented in the thesis.

The third objective of the research is to include the LV and MV networks in frequency response of the power system. Considering the increasing penetration of RESs in the power system, and the reducing role of traditional generation units, the power system frequency control needs to be modified as well. By other words, in the future grid scenario, active LV and MV networks are required to play a role in controlling the system frequency. Therefore, the traditional load frequency control (LFC) needs to be modified by including LV and MV networks. To do so, a modified LFC has been proposed in chapter 5 of this thesis. The main idea in this work was to use the fast response of DCHP units for frequency response of the system.

In conclusion, the main contribution of this thesis is to propose an intelligent strategy for managing high penetration of PV panels and EVs in the LV network, without reinforcing the network. Such solution helps DSOs to avoid or delay huge investments due to increase in demand, while it brings economic incentives for customers to consider RESs as a proper energy source. The other main contribution of this thesis is to propose a new aggregation technique for residential distribution networks, considering small energy sources and electric vehicles. Besides, this thesis proposes a modified LFC based on the DCHP units of MV network in order to improve system frequency response. The proposed modified LFC enables the LV and MV network to participate in system frequency response, and reduces the system dependency on central power plants for frequency regulation.

DANSK RESUME

Miljømæssige bekymringer sammen med hurtige ændringer i vedvarende energi teknologi har ført til betydelig vækst i vedvarende energikilder (RES) i energisystemer. Blandt forskellige vedvarende energikilder er vind- og solenergi de hidtil mest udviklede. Men en høj andel af RES i elnetværket kan medføre alvorlige problemer, da disse kilder ikke er særligt flexible. På den ande side giver de nye belastninger i elsystemet, specielt elbiler, et øget systemkrav og større variationer.

I lande som Danmark er der blevet foreslået og gennemført forskellige initiativer til at tilskynde kunder til at investere i solceller. Disse intitiativer har medført et øget antal solceller i husstandende. Men tilstedeværelsen af sådanne mindre energikilder i lav spænding (LV) netværket påvirker den traditionelle opførsel af disse, da det medfører tilbagestrøm fra kunderne til det øvre netværk. Sådanne tilbagestrømme giver nye udfordringer til systemet og samtidig nye potentialer transmissions system operatoren (TSO) og distributions system operatoren (DSO) til at anvende tilbagestrøm til stabiliserende formål.

Det første delmål for nærliggende forskning er at kvantificere og analysere virkningen af elbiler og solceller i LV netværk, samt at bestemme den maksimale kapacitet af LV netværk til solceller og elbiler. Detaljer er givet i kapitel 2. I første trin defineres en egentlig modeltilgang for belastning, elbiler og solceller. Detaljer for lastmodellen gives i kapitel 2. For elbiler er modellen anvendt med lithium-ion (Li-ion) batterier med henblik på den øgede industrielle interesse for disse. Detaljer gives ligeledes i kapitel 2. Solceller modelleres som funktion a solindstrålingen og den omgivende temperatur. I det andet trin kvantiseres effekten af solceller og elbiler på LV netværket separat. For solceller er forskellige placeringer blevet analyseret med det mål at bestemme begrænsningerne for disse mindre energikilder. Derudover et et optimeringstudie gennemført med henblik på at bestemme det maximale bidrag til elnetværket fra solceller ud fra betragninger om operative begrænsninger i elnetværket, såvel som transformerkapacitet. På den anden side er der blevet foreslået forskellige opladningstrategier til elbiler for at fastlægge den maximale inflydelse af elbiler på LV netværket. Disse strategier er baseret på spændingsmålinger samt placeringer af elbiler i LV netværket. Forskellige typer elbiler med forskellige rækkevidde (DP) er blevet betragtet. I det trejde trin analyseres potentialet for solceller og elbiler som bidragsydere til elnettet.Hovedformålet med denne analyse var at kvantisere kapaciteten af LV netværket som supplement til elnetværket.I den forbindelse opstilles og anvendes et optimeringsproblem.

Det andet delmål for nærliggende forskning er, at evaluere effekten af aktive LV netværk på (medium voltage) MV netværk. I den forbindelse opstilles og simuleres en akkumuleret model for LV netværket under tilstedeværelse af elbiler og solceller. Den foreslåede akkumuleringsteknik presenteres i kapitel 3. Derudover er effekten

af LV netværket på MV netværket kvantiseret under betragning af residual, industriel og kommerciel belastning af MV netværket. Kapitel 4 indeholder detaljerne af denne analyse samt detaljerne for MV netværket. For at bevare generallitet er et standard MV netværk anvendt i studiet. MV netværket er også et interaktivt netværk, dvs. Det inviolverer MV vindmøller samt de-centraliserede kombinerede kraftvarmeværker (DCHP). DCHP enheder spiller en vigtig rolle i det danske elnetværk, og de bidrager også til elproduktionen. Modellering af vindmøller er gennemført med ægte data fra en Vestas vindmølle. For vindhastighed er en modificeret model anvendt for vindmøller med de tilgænglige målinger. Endvidere er en detaljeret model for DCHP enheder blevet anvendt i denne afhandling.

Det tredje delmål for nærliggende forskning er at inkludere LV og MV netværk i vekselvirkingen med elnetværket. Under betragtning af den stigende inflydelse af RES's i elnetværket og den aftagende rolle fra traditionelle generatorer må vekselvirkning kontrollen ligelides modificeres. Med andre ord, i fremtidens elnetværk er det et krav, at aktive LV netværk og MV netværk kan spille en afgærende rolle. Derfor skal den ´traditionelle last frekvens kontrol (LFC) udviddes til at inkludere LV og MV netværk. I den forbindelse foreslåes en modificeret LFC i kapitel 5 i denne afhandling. Hovedideen i dette arbejde var at anvende det hurtige respons fra DCHP enheder til frekvens respons af systemet.

Som konklusion er hovedbidraget fra denne afhandling at foreslå en intelligent strategi til at kontrollere det store bidrag fra solceller og elbiler i LV netværket uden at forstærke det. Sådanne løsninger hjælper DSO'er med at undgå eller udsætte enorme inveteringer på grund af øget efterspørgsel, mens det fremkalder økonomiske motivationer hos kunder til at betragte vedvarende energikilder som egentlige energikilder. Det endet hovedbidrag fra denne afhandling er at foreslå en ny akkumuleringsteknik til residual fordelings netværk med henblik på mindre energikilder og elbiler. Derudover foreslås i denne afhandling et modificeret LFC baseret på DCHP enheder i MV netværk til forbedring af systemets frekvens respons. Den forslåede LFC model muliggør anveldese af LV og MV netværk i systemets frekvens respons og reducerer systemets afhængighed af centrale kraftværker for frekvens regulering.

TABLE OF CONTENTS

LIST OF FIGURES

LIST OF TABLES

COPYRIGHT STATEMENT

1. Thesis title: "Flexibility and Balancing in Active Distribuion Networks"

2. Name of PhD student. Reza Ahmadi Kordkheili

3. Name and title of supervisor and any other supervisors.

   Main supervisor: Prof. Josep M. Guerrero

   Co-supervisor: Dr. Mehdi Savaghebi

This present report combined with the above listed scientific papers has been submitted for assessment in partial fulfilment of the PhD degree. The scientific papers are not included in this version due to copyright issues. Detailed publication information is provided above and the interested reader is referred to the original published papers. As part of the assessment, co-author statements have been made available to the assessment committee and are also available at the Faculty of Engineering and Science, Aalborg University.

CHAPTER 1. INTRODUCTION

This chapter addresses a brief review of the project concepts, main objectives, and limitations of the project. The motivation behind this research is also highlighted.

1.1. CURRENT STATUS AND FUTURE TRENDS

Increasing interest in replacing fossil fuels with different renewable energy sources (RESs) is causing significant changes in the concepts and structure of energy systems. Different countries are defining new policies and long-term plans for minimizing the role of fossil fuels in the energy sectors by increasing the role of renewable energy sources. Accordingly, the European Union has also defined and identified certain targets and policies to depict a unified roadmap among European countries. The European Commission defined its new framework for 2030, considering the following pillars [1]:

- ✓ Increasing the renewable energy percentage to at least 27% of demand.
- ✓ Improving the energy efficiency by 30%.
- ✓ Reducing greenhouse gas (GHG) emissions to at least 40% below its level in 1990.
- ✓ Ensuring a new secure and competitive energy system by setting new indicators.

The EU has also defined a set of targets for the 2020 and 2050 horizons. Fig. 1.1 presents the RES indicators which are defined by EU Commission for different horizons. In Fig. 1.1, 'E' stands for electricity, 'T' represents transportation, and 'H&C' represents heating and cooling [1]-[3].

On the other hand, different countries in Europe have different policies and roadmaps toward the renewable energy integration. In Denmark, due to high potential for renewable energy sources, especially the wind power, the government policy is to achieve a 100% renewable energy penetration by 2050. Therefore, all the policies and roadmaps are with respect to the fact that by 2050, all the energy

consumption in Denmark will be provided by renewable energy sources (RESs). To achieve the 2050 milestone, different targets are defined for different years until 2050 as well. Fig. 1.2 presents the roadmap defined by Danish government toward the 100% RES-based energy system [2]. As can be seen in Fig. 1.2, there will be major changes in the energy sector in Denmark. The role of fossil fuel in the energy sector will decrease significantly, and it will be replaced by different renewable energy sources. Specifically, the share of coal in energy sector will be totally replaced by other energy sources, i.e. coal will phase out by 2030.

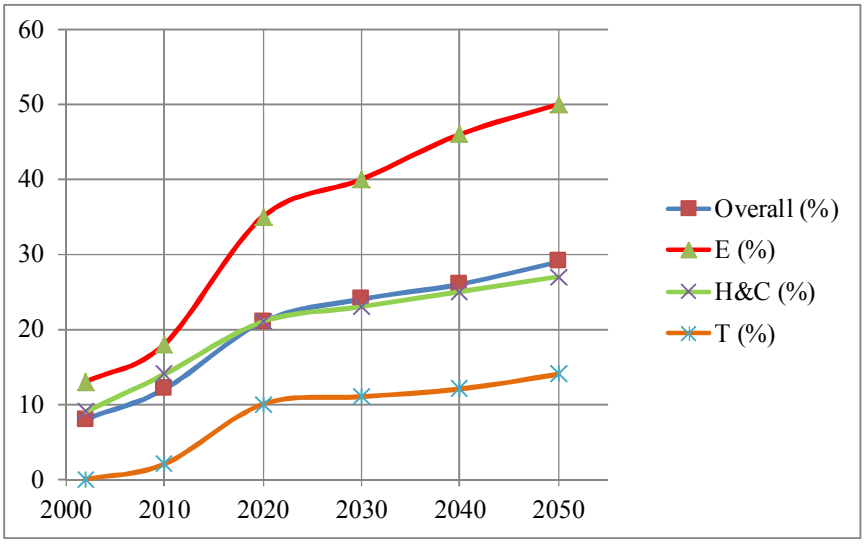

Fig. 1.1. EU Roadmap [1]

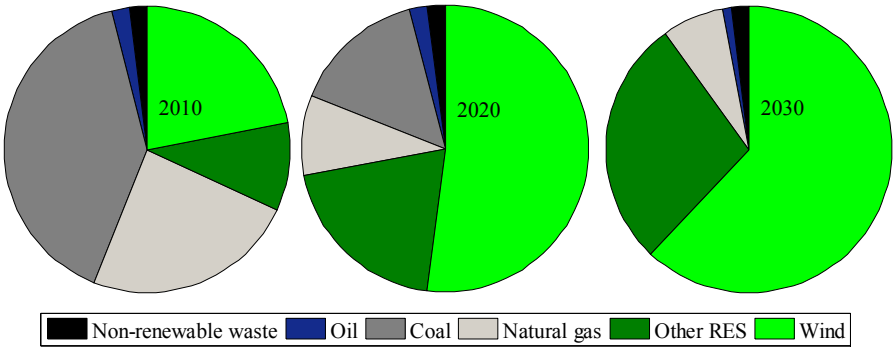

Fig. 1.2. Denmark roadmap toward 100% renewable energy [4]

However, moving toward high penetration of RES in the network has certain challenges which should be solved in advance. The uncertain nature of RESs, such as wind fluctuations and deviations in solar irradiation, brings a high level of

certainty to the system, as it will be more difficult to plan the required generation to match the demand. Such high level of uncertainty bolsters the role of power regulation services for stabilizing the power system frequency. On the other hand, phasing out the traditional power plants and replacing them with RESs in the network will decrease the overall inertia of the power system, which is an important factor in stabilizing the power system. Besides, replacing the fossil fuels with RESs means electrifying all the energy sectors, such as heating, gas, and transportation. Such renovation leads to new electric loads in the electric system, such as heat pumps (HPs) and electric vehicles (EVs), which in turn causes new challenges and new electric demand for the electric network. The motivation behind this project is to address the challenges caused by electric vehicles (EVs) in the network, and find out the potential of these new devices for supporting the network. The other objective of the project is to include new players in the system regulation and system frequency stabilization. Considering Danish scenario, decentralized combined head and power plants (DCHPs) play a major role in Danish energy sector. Therefore, the potential of these units in system frequency stabilization is also analyzed and quantified.

1.2. TRANSITION TOWARDS INTELLIGENT POWER GRIDS

In this section, the current status of RES in Denmark, as well as the role of electric vehicles (EVs) and DCHPs in Danish system are addressed. Also, different policies and incentives set by Danish authorities for encouraging customers and investigators are illustrated.

1.2.1. RES IN POWER SYSTEM

Danish power system has faced major changes during the last few decades, during which traditional central power plants have been replaced by new, decentralized small power plants. Considering Danish overall picture also clarifies tremendous changes in current Danish power system compared to the past. The trend is expected to continue, and more RESs, CHPs, and DCHPs are expected to contribute to Danish power system [5]. In particular, wind turbines have turned to a major player in Danish power system. Fig. 1.3 presents the share of wind power in total electric power consumption in Denmark. As demonstrated in Fig. 1.3, the wind turbine has provided 39.1% of total power consumption in Denmark [4]-[8].

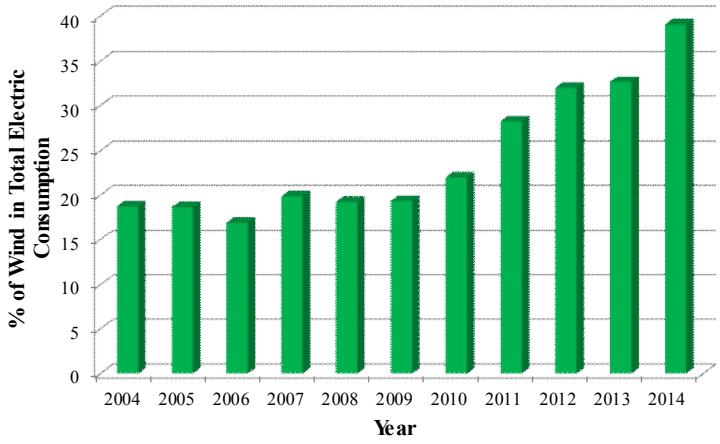

Fig. 1.3. Share of wind power in total electric consumption

Installing wind turbines, as an off-shore or on-shore wind turbines, or near-land wind turbines, has increased dramatically during the last couple of years. It is expected that the total installed capacity of wind turbines exceeds 8000 MW by 2035. The other source of renewable energy which got huge interest is solar photovoltaic (PV) panels. Although the total installed capacity of solar panels is not as significant as wind turbines, these panels are expected to have a steady increase during the next couple of years. Fig. 1.4 presents the forecast for installation of wind turbines and solar PV panels by Energinet [9]-[10].

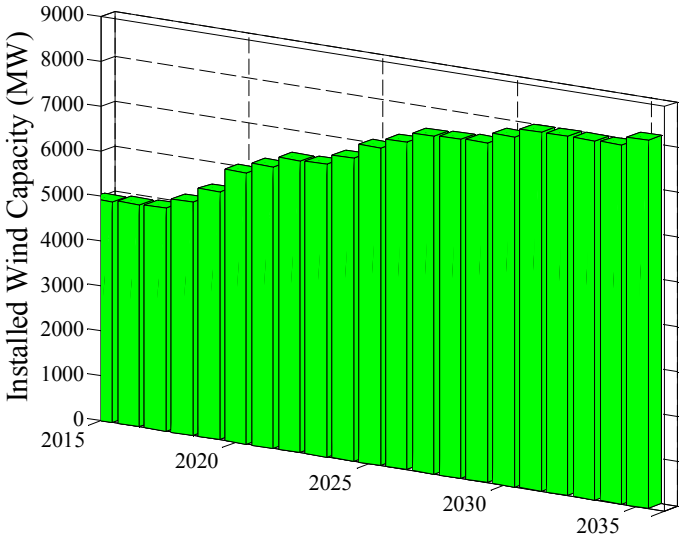

a)

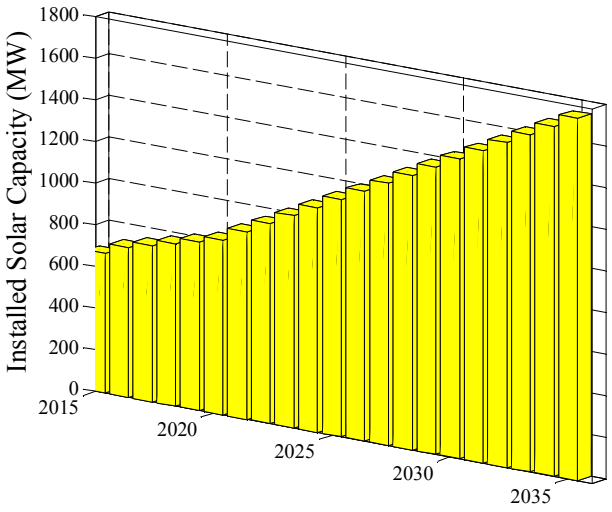

b)

Fig. 1.4. Forecast of total wind and solar installation [9]

Huge growth in penetration of RESs, particularly wind turbines in Denmark, and phasing out traditional central power plants leads to significant changes in power system characteristics. High penetration of wind and solar in power systems increases the system uncertainty significantly. Any loss of power production from wind turbines affects the system frequency and leads to system imbalance. Also, any extra power production raises the frequency above its nominal value. On the other hand, phase-out of the central power plants (CPPs) causes negative impact on system inertia, which in turn affects frequency. Therefore, it is necessary to provide necessary regulation power and ancillary services to bring the frequency back to its nominal value.

1.2.2. TRANSITION IN ENERGY AND TRANSPORTATION SECTORS

In general, electricity consumption is a fraction of energy demand in Denmark. The other main energy requirements are gas and heating, as well as transportation. Considering the Danish roadmap toward 100% fossil-free energy system, these areas of energy consumption should also be considered and be transformed toward 100% RES system [10].

1.2.2.1 Gas Sector

Gas system is a major sector of the Danish energy sector. However, serious concerns regarding the reduction in gas resources the North Sea as the main resource of the Danish gas system, has emphasized the need for finding proper replacements for these resources. Such issues bolster the necessity for the energy sector to move

toward the 100% renewable energy system. Some of the most promising alternatives are hydrogen and biogas. The other main solution is to electrify the customers' energy needs as much as possible. As a result, the electric load in the power system will increase significantly. Such loads have not been considered in the primary design of the network. Therefore, new solutions should be developed to enable the system to deal with its new loads and new demands [10].

1.2.2.2 Heating Sector

In Denmark, district heating (DH) plays a major role in providing heating for customers, especially big cities and population areas. Since the construction of the first combined heat and power plant in Denmark in 1903, there has been a continuous progress in the utilization of district heating for supplying the customers' heating requirements, such that in 1970's, around 30% of all Danish homes were heated using district heating systems. The energy crisis in the 1970s has accelerated the increasing penetration of district heating in Danish energy sector, especially the role of combined heat and power (CHP) and decentralized combined heat and power (DCHP), and these units appeared not only in big cities, but also in medium-size and small cities of Denmark [11]. Nowadays, district heating provides more than 60% of heat demand, as well as hot water demand, for private Danish houses. Apart from 6 large CHP plants, there are around 670 small-scale decentralized CHP (DCHP) units in Denmark. Fig. 1.5 presents the percentage of CHP and DCHP units in Danish district heating.

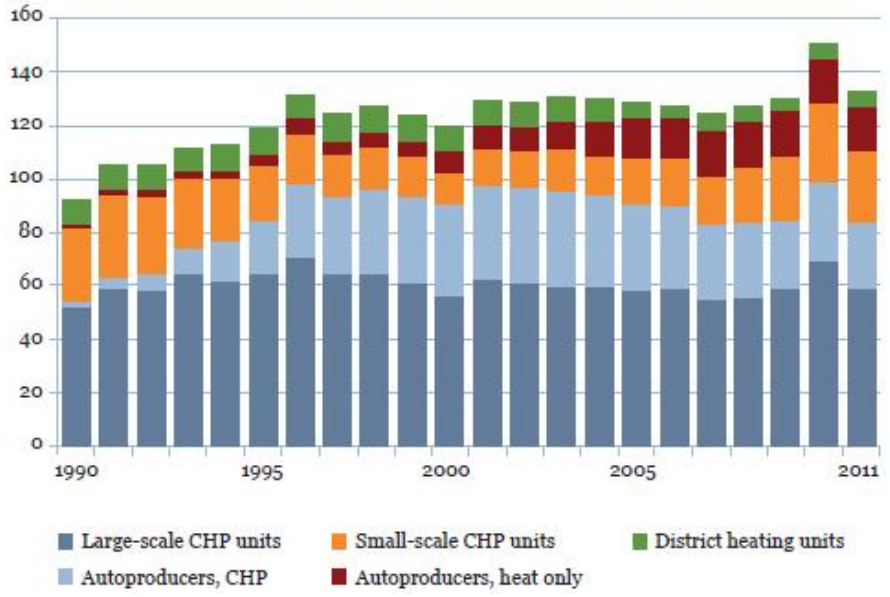

Fig. 1.5. The role of CHP and DCHP in Danish district heating sector [11]

The role of renewable energy, such as biomass and wind, in district heating has significantly increased in recent years. Considering the potential of DH, they're expected to be a major player in achieving two main targets:

- In 2020, wind turbines are expected to cover 50% of domestic electricity demand.
- By 2035, all the electricity and heating demand in Denmark have to be supplied by renewable energy sources.

The flexibility of DH in using different fuels gives a huge advantage to these units to play a major role toward a 100% renewable-energy-based energy network.

1.2.2.3 Transportation Sector

Transport sector consists of different equipment in Denmark, including private cars, motorcycles, buses, coaches, trains, ferries, and aircrafts. Cars and buses play a major role in transportation in Denmark. The share of different transportation equipment in transporting passengers in Denmark for 2013 is presented in Fig. 1.6 [12]. Considering the statistics provided by "Danish Ministry of Transport", the total number of private cars was around 2100000 cars in 2008, and it was around 2163000 cars in 2010. Table 1–1 presents the total number of cars, buses and motorcycles for 2014 and 2015 [13].

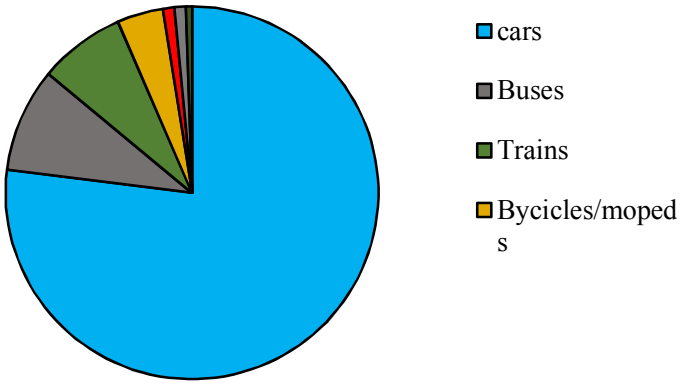

Fig. 1.6. Share of different equipment in passenger transportation (million passenger-km)

Table 1–1. Total number of vehicles in Denmark [13]

	2014	2015
Total passenger cars	2278121	2329578
Total number of buses	13270	13408
Total number of motorcycles	150360	151542

As can be seen in Table 1–1, the annual increase in total number of cars is not significant in Denmark. However, the number of electric vehicles (EVs) is predicted to grow significantly in Denmark. By 2020, 47000 EVs are expected to be utilized in Denmark, and the number is expected to reach 400000 EVs by 2035 in a "Moderate Scenario". Such number of EVs will represent 20% to 25% of total number of cars in Denmark, which brings certain challenges to the power system. In general, the charging power demand of EVs is much higher than a normal household. Therefore, appearance of EVs in the network brings a new significant power demand in the network which has to be handled by power system operators. Such high demand from EVs can also lead to congestions in power system, because the existing power system was not designed for dealing with such electric demands.

1.2.3. SMART GRID AND MICROGRID

As mentioned, the main policy in Denmark is toward a 100% renewable-energy system, in all the energy sectors. Obtaining such target requires certain transformations in different energy sectors, including transportation, heating, and gas. Such transformations bring new significant demand to power networks. The power networks were not designed to deal with such loads and demands. On the other hand, with respect to fluctuating inherent of RES, a 100% renewable energy network brings a huge uncertainty to the system. More precisely, it challenges the traditional consumption-production balance, since the production side will have higher fluctuations. Such situation demands certain changes and actions in the power system to deal with these problems. Considering the role of customers as major players in the system, having flexible customers, i.e. the ability to manage, control and interact with customers is considered as one of the key solutions. In this regard, the "Smart Grid" concept has been introduced and evolved in the last decade. Different definitions have been proposed for the term "Smart Grid" so far. In general, a smart grid is a platform for enabling the interaction between different stakeholders involved in the system, including customers and production units. The European Commission has proposed a definition for 'Smart Grid' in 2011, which is also utilized by Energniet.dk, the main Danish operator [14]:

"A Smart Grid is an electricity network than can cost-effectively integrate the behavior and actions of all users connected to it- generators, consumers, and those that do both- in order to ensure economically efficient, sustainable power system with low losses and high levels of quality and security of supply and safety."

However, to cover different aspects of the problem, a more comprehensive definition sounds necessary [14].

"Smart Energy Systems is defined as an approach in which Smart Electricity, Thermal and Gas Grids are combined and coordinated to identify synergies between

them in order to achieve an optimal solution for each individual sector as well as for the overall energy system." [14]

Microgrids are low-voltage distribution grids consisting of different distributed energy resources (DERs) and various kinds of loads, and have the ability to operate either interconnected to the main distribution grid or isolated from it. DERs may include both DGs and distributed storage units. Microgrids are considered as one of the main building blocks of the smart grids, as they are able to facilitate implementation of many smart grid functions. It is expected that in a near future, smart grid emerges as a well-planned plug-and-play integration of microgrids which interact through predefined highways for exchanging signals, data, and power.

A smart grid concept has been developed and defined jointly by Energinet.dk and Danish Energy Association. One of the main ideas in the proposed smart grid concept is the "flexibility" concept. The definition of flexibility in this framework is defined below.

1.2.3.1 Flexibility

In this context, flexibility means that a customer, or an appliance connected to the power system, changes its behavior to meet a need from the power system. For example, an electric vehicle that adapts its charging patterns to balance out fluctuating wind power or solar energy levels [15].

Different Roles and Responsibilities are defined for this concept. Fig. 1.7 presents different roles and responsibilities toward the flexibility concept in the smart grid framework. From Fig. 1.7, system operators, i.e. Energinet.dk and grid companies are the parties which are in need for flexibility. As the sole owner of transmission network in Denmark (> 100kV), Energinet.dk is responsible for running the network in a stable operating condition, either in normal operating condition or in the event of major outages. 'Grid Companies' own and operate Danish distribution grids (< 100kV). Their main task is to supply their customers with the least possible disruptions, while keeping the grid within standard operating limits [16]. On the other hand, private players, such as households and other grid consumers, as well as distributed energy resources (DERs) and small producers such as wind farms in the system, are capable of offering such flexibility.

Commercial players are responsible for the flexibility between the "Request" and the "Offer". Commercial players will compete freely and on equal terms in order to provide the most efficient and innovative solutions for the system. In today's market, Balance Responsible Parties (BRPs) play the major role between wholesale and retail markets, and they are responsible for submitting the plans of production and consumption. However, in the future power system, "Aggregator" is expected to be a major player.

Aggregators are expected to handle flexibility at the retail level by offering attractive solutions to customers for providing flexibility. On the other hand, they collect and aggregate individual flexibility in certain large volumes to be procured and activated through wholesale markets. Considering the definition of BRPs, the responsibilities of BRPs and Aggregators should be redefined in a proper way [17].

Fig. 1.7. Roles and responsibilities for flexibility in smart grid [15]

1.2.3.2 Flexibility based on market access

The central idea toward the concept of flexibility is that it should be market-based, i.e. private players must have the freedom to choose how much flexibility they want to offer, and through which commercial player they want to offer their flexibility. In general, two different mechanisms are defined in this regard: “Price-Based” method, and “Flexibility” method.

1.2.3.3 Advantages of flexibility concept

The main advantage of the flexibility for grid companies is that it enables collecting, organizing, and shifting flexible resources. Such potential can be realized as a real alternative to grid reinforcements without the need for the grid companies to be in direct commercial relations with customers. On the other hand, flexibility can be used by Energinet.dk for balancing purposes. Therefore, the concept guarantees optimum coordination and use of resources from a socio-economic point of view.

1.2.3.4 Converting power grid to a smart grid

The transition from traditional power grid to a smart grid can be seen as a two-step evolution. In the first step, the grid companies have to set up and organize required technological resolutions both for automating the grid and for monitoring the grid operating conditions and the grid utilization capacity. In the second step, the customer’s flexibility, either in consumption or in production, can be utilized to enable optimal utilization of grid capacity. It should be noticed that in practice, in order to reduce the cost of traditional grid expansion, the grid companies might initialize and implement both steps simultaneously.

1.3. POLICIES AND OBJECTIVES IN DENMARK

As the main Danish operator, Energinet.dk has defined certain set points and policies to deal with the changes and to develop Danish power system. These policies and objectives can be divided into some main categories, with different tools and methods to fulfill each objective [15].

1) Security of electricity supply:

Danish power system is connected with its neighboring countries, with both physical connections and market connections. In such case, it is necessary to ensure the security of the power system, especially on a regional level. An important tool for assuring the system security is ancillary service. In general, ancillary services ensure frequency and voltage stabilization, as well as short-circuit capacity in the power system. Considering the trend toward RES in Danish power system, conventional power plants are not expected to play the central role in providing ancillary services and guaranteeing the security of the power system in the future. Therefore, Energinet.dk is applying different studies in order to quantify the needs for ancillary service in the future, and different methods and solutions for providing the required ancillary service.

2) Means of Integrating wind power:

As explained in section 1.2.1 and presented in Fig. 1.2, wind power plays a major role in Danish future energy system. Therefore, numerous offshore, near-shore, and onshore wind turbines have been installed or will be installed in Denmark. As a result, different actions and solutions have to be considered by Energinet.dk in order to deal with such high penetration of wind turbines. The main solutions and approaches from Energinet.dk point of view are presented in Fig. 1.8, with short term, medium term, and long term objectives. It should be noted that some of these approaches can be considered for other objectives as well [15].

3) Expansion and reinforcement of the power system

Different projects are defined in Energinet.dk to reinforce Danish power system and make it more robust [18]. Due to different plans for connecting more large-scale offshore wind farms, and higher integration of different RESs in the network, reinforcing the network, either with new domestic connections or via external connections with neighboring countries is mandatory. Some of the ongoing and future projects are listed here as follows: 1) connection of the Anholt offshore wind farm; 2) Reinforcement of 400kV grid, including upgrade of the connection between Kassø (near Abenraa) and Tjele (near Viborg); 3- Undergrounding of the existing 132-150 kV overhead lines in a period of 20 years; 4) Visual enhancement projects;

5) reinforcement of interconnections: including “Skagerrak 4”, “COBRA Cable”, “Kriegers Flak” [18].

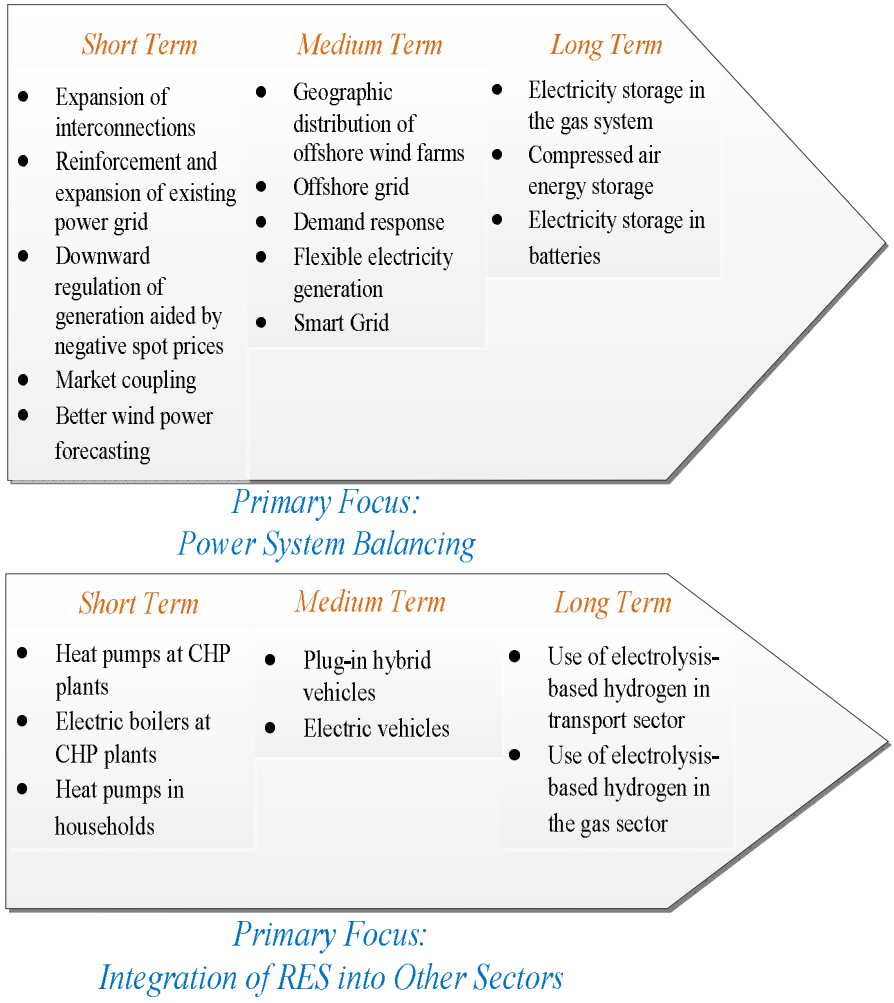

Fig. 1.8. Means of integrating wind power [15]

4) Offshore grid

Offshore wind farms play a major role, not only in Danish power system, but also in the other European countries, and it will be a major player in the future power system in Europe. One of the most promising locations for installing offshore wind turbines is the North Sea. All the ten countries around the North Sea are planning to install offshore wind farms in this area. Among different projects which are defined to determine the potential of the area, the “Kriegers Flak” project is considered as

one of the most important projects which can address some of the major issues of the offshore wind farms in this area, so that it can enable bilateral or trilateral connections between international wind farms. Besides, there is cooperation between ten countries to jointly investigate the possibilities of constructing an offshore grid in the North Sea.

5) Flexible electricity generation

Increasing penetration of wind power in Danish power system will lead to higher fluctuations in generation. In particular, the Danish power system will face more cases in which the wind generation exceeds the total demand and the capacity of the interconnections. Such situations are most likely to occur during the winter nights, with a windy weather. Therefore, proper frameworks and solutions are required to take care of such potential problems. Market-based incentives such as "Negative Price" are among the practices which can be applied for such conditions.

6) Demand response

Appearance of different types of new loads in system, such as heat pumps, electric vehicles, as well as small energy sources such as solar panels, has bolstered the need for contributing customers in the power system control and management. Demand Response has turned to one of the promising and attractive subjects during the last few years, and different types of demand response, such as incentive-based demand response and price-based demand response have been evolved in the last few years. Energinet.dk has also defined different projects to illustrate the potentials of demand response to boost the growth of RESs in Danish power system.

7) Electricity market

The electricity market has been an effective tool for keeping the balance between generation and consumption, by adapting the generation to the demand at the minimum cost. However, the increasing penetration of RESs in the power system and their inherent fluctuating nature will change the existing paradigm. Demand response is one of the promising tools to help ensuring continued balance between generation and consumption.

The increasing fluctuation in power generation, together with demand response of flexible loads such as electric vehicles (EVs) and heat pumps (HPs), will be a huge challenge to handle by the market, especially the 1-hour market. Therefore, Energniet.dk is looking for new solutions and market framework, especially considering the potential international market platforms, to deal with the future scenarios.

8) Smart Grid

As mentioned in Section 1.2.3, smart grid is considered as the future of the power system. Therefore, smart grid defines the main framework for different policies and solutions which are proposed to deal with the challenges toward the 100% RES energy network.

1.4. RESEARCH OBJECTIVES

Smart grid is considered as the future of the power systems. As explained, "Flexibility" concept is defined as a major player in the smart grid concept of Danish strategy plan [smart grid in Denmark 2], and the "Aggregator" is proposed as the new player in the system to handle flexibility. This project focuses on the effects of electric vehicles and renewable energy sources on the power system. It also investigates the potential of the LV and MV grid flexibility for power system balancing. The following bullet points mention the main objectives of the project:

- ✓ Analyzing the effect of solar panels and electric vehicles on the distribution grid;
- ✓ Developing a control strategy for handling electric vehicle charging in distribution grid without violating grid operating limits;
- ✓ Determining maximum potential of distribution grid for providing flexibility and ancillary service which can be offered to the upper network (power system);
- ✓ Proposing a new aggregation technique for aggregating distribution grid feeders, customers, and renewable energy sources from distribution system operator (DSO) point of view;
- ✓ Analyzing the effect of distribution grid loads, as well as the effects of wind turbines and DCHP units on the MV grid and on the upper network (power system);
- ✓ Enabling active participation of MV and LV grid in the power system balancing and regulation: The participation of the MV grid in the load frequency control (LFC) is investigated. A modified load frequency control (LFC) with the MV and LV grid is developed. Potential of DCHP units and electric vehicles (EVs) for regulating frequency has been realized through the modified LFC control.

1.5. THESIS OUTLINE

Written as a collection of papers, the thesis is organized in two parts. In the first part, the research contribution and the related results are briefly explained and addressed, whereas the second part consists of the scientific publications related to the research. The first part of the thesis is organized in the format of 7 chapters, as explained below:

- ***Chapter 1*** addresses the changes in traditional power system caused by high penetration of RESs, as well as changes in transportation, gas, and heating sectors. The transition of the traditional power system toward the Smart Grid (SG) and microgrid (MG) is also addressed in this chapter. Different policies and objectives which are set by Energinet.dk, the main operator of Danish power and energy system, are explained and addressed. Also, the scope, objectives, and the limitations of the current research are elaborated and discussed.

- ***Chapter 2*** analyzes the distribution grid in presence of solar photovoltaic (PV) panels and electric vehicles (EVs). The details of the load modeling, as well as the PV modeling are explained in detail in this chapter. Also, the modeling details of EVs are presented in this chapter. The effects of solar PV panels on residential distribution grid are investigated in this chapter. Also, the grid maximum hosting capability for solar panels is analyzed and addressed in this chapter. Besides, the effect of EVs on the distribution grid is discussed in details. Furthermore, the potential of EVs for providing and offering flexibility to the grid is analyzed and evaluated.

- ***Chapter 3*** proposes an aggregation technique for distribution networks. As mentioned in Chapter 1, flexibility is one of the main concepts toward the smart grid (SG). In the future power system scenarios, 'Aggregators' play an important role in handling flexibility, by connecting the private parties (customers) with the system operators (Energinet.dk and grid companies). Considering the significant number of distribution transformers in the system and the large number of customers connected to each transformer, having a proper aggregation model for distribution networks will be a great advantage for Aggregators. The proposed aggregation technique, together with its mathematical proof, is explained in this chapter. The results of applying the method on a part of the Danish distribution network is presented and discussed in this chapter. The method is also tested in presence of solar PV panels, as small energy resources, and electric vehicles (EVs).

- ***Chapter 4*** includes the analysis and studies of the medium voltage (MV) grid. The study considers different distributed energy resources (DER) in the medium voltage, including wind turbines and decentralized combined heat and power (DCHP) units, to match the Danish scenario. The modeling details of wind turbines and DCHP units are presented in this chapter. The study also includes the effect of distribution grid players on the medium voltage, i.e. customers, solar PV panels, and electric vehicles (EVs).

- ***Chapter 5*** introduces the concepts of load frequency control (LFC). The potential of MV and LV grids for participating in balancing services in the transmission level is analyzed. Then, a framework is presented for participating DCHP units and their capacity for participating in frequency stabilization issues.

Also, a control method is proposed for utilizing the EVs and DCHPs in the LFC control.

- ***Chapter 6*** provides a conclusion of the work and highlights the outcomes of the project. Also, some of the future works with respect to the outcomes of the project are highlighted in this chapter.

The second part of the thesis consists of the documentation of the research contributions in peer-reviewed journal and conference proceedings. The list of the publications is provided below. The relationship between the thesis chapters and the published papers is presented in Table1–2.

Table1–2. The relation between thesis chapters and published papers

Chapters	1	2	3	4	5	6
Related Publications	-	Conf1, Conf2, Conf3, J3	Conf4, J2	Conf3, Conf5, J1	Conf1, Conf3, J1	-

Peer-reviewed Conferences

- ***Conf 1:***

Kordkheili, R.A.; Bak-Jensen, B.; R-Pillai, J.; Mahat, P., "Determining Maximum Photovoltaic Penetration in a Distribution Grid Considering Grid Operation Limits", in Proc. IEEE PES General Meeting, pp.1-5, July 27-31, 2014

- ***Conf 2:***

Kordkheili, R.A.; Pourmousavi, S.A.; Pillai, J.R.; Hasanien, H.M.; Bak-Jensen, B.; Nehrir, M.H., "Optimal Sizing and Allocation of Residential Photovoltaic Panels in a Distribution Network for Ancillary Services Application", in Proc. IEEE OPTIM 2014, pp.681-687, 2014.

- ***Conf 3:***

Kordkheili, R.A.; Bak-Jensen, B.; R-Pillai, J.; Bhattarai, B. P., "Improving and Handling Electric Vehicle Penetration Level by Different Smart Charging Algorithms in Distribution Networks", in Proc. IEEE PES PowerTech, 29 June- 2 July, 2015.

- ***Conf 4:***

Kordkheili, R.A.; Bak-Jensen, B.; R-Pillai, J.; Bhattarai, B. P., "A Fast Approach for Calculating the Available Flexibility of a Residential Distribution Grid", in Proc. IEEE PowerEng, May 2015.

- ***Conf 5:***

Kordkheili, R.A.; Bak-Jensen, B.; R-Pillai, J., Savaghebi, M., and Guerrero, J. M., "Managing High Penetration of Renewable Energy in MV Grid by Grid Flexible Loads", in Proc. IEEE Cigre EDST, May 2015.

Peer-reviewed Journals

- ***J1:***

Kordkheili, R.A.; Pourmousavi, S.A., Savaghebi, M.; and Guerrero, Josep M., "DCHP-Based Secondary Control Scheme for High RES-Penetrated MV Microgrids," *IEEE Transactions on Smart Grid* (Revised)

- ***J2:***

Kordkheili, R.A., Savaghebi, M.; and Guerrero, Josep M., "Aggregated Modeling Approach for Electric-Vehicle-Supported Active Distribution Networks," *European Transactions on Electrical Power* (Under Review).

- ***J3:***

Kordkheili, R.A.; Pourmousavi, S.A.; Savaghebi, M.; Guerrero, Josep M.; and Nehrir, M.H., "Assessing the Potential of Plug-in Electric Vehicles in Active Distribution Networks," *Journal of Energies* (Revised. Under Final Review)

CHAPTER 2. MICROGRIDS IN INTERCONNECTED MODE: IMPACT OF PV PANELS AND ELECTRIC VEHICLES ON DISTRIBUTION NETWORKS

2.1. INTRODUCTION

In this chapter, the effect of solar panels as small energy resources, and electric vehicles (EVs) is investigated. Modeling details of solar PV panels and EVs are presented in the first step. The load modeling approach in this research, as well as the details of the distribution grid under study, is also presented in the first step. In the next step, the impacts of PV panels and EVs on distribution grid are analyzed. In the end, the maximum capability of the distribution grid for providing flexibility and ancillary service to the upper network is determined using an optimization technique. The optimization objectives, constraints, and the optimization technique, as well as the results are presented and discussed in this section.

2.2. MODELING APPROACH

In this section, the modeling details of PV panels, EVs, and load modeling approach are provided. The details of the distribution grid are also presented in this section, which is the case study in this research.

2.2.1. ELECTRIC VEHICLE MODELING

Electric vehicles have turned to a promising technology for the future of transport sector, and different manufacturers are trying to develop EVs and increase the share of EVs in the car market. Tesla, GM, and BMW are among the prominent companies in the EV category. The main part of an EV which defines the performance and efficiency of the car is the battery. Different battery technologies

have been used in cars so far. However, the most promising battery technology for EVs is the Lithium-ion (Li-ion) battery. The main focus of the research activities during the last couple of years, either in the industry or in the academia, has been on the Li-ion batteries. Therefore, this work also focuses on the Li-ion batteries to analyze the impact of EVs on the grid.

Fig. 2.1 presents the model of an EV battery. The parameters of the battery model are calculated using (2.1)-(2.5) [19].

$$R_{T,S}(DOD) = 0.04669 + 0.3208 * \exp\left[\left(-29.14 * (1 - DOD)\right)\right] \quad (2.1)$$

$$C_{T,S}(DOD) = 703.6 + 752.9 * \exp\left[\left(-13.51 * (1 - DOD)\right)\right] \quad (2.2)$$

$$R_{T,L}(DOD) = 0.04984 + 6.603 * \exp\left[\left(-155.2 * (1 - DOD)\right)\right] \quad (2.3)$$

$$C_{T,L}(DOD) = 4475 - 6056 * \exp\left[\left(-27.12 * (1 - DOD)\right)\right] \quad (2.4)$$

$$R_{series}(DOD) = 0.07446 + 0.1562 * \exp\left[\left(-24.37 * (1 - DOD)\right)\right] \quad (2.5)$$

In these equations, $R_{T,S}$ and $C_{T,S}$ represent the short transient response of the battery, while $R_{T,L}$ and $C_{T,L}$ represent the long transient response of the battery [19]. Also, 'DOD' stands for battery's 'depth of discharge'. This parameter is explained in the following. For simplicity, these parameters are replaced by an equivalent resistance (R_{eq}), as mentioned in (6) [19].

$$R_{eq}(DOD) = R_{T,S} * e^{\left[-1/\left(R_{T,S} * C_{T,S} * t_S\right)\right]} + R_{T,L} * \exp\left[-1/\left(R_{T,L} * C_{T,L} * t_L\right)\right] \quad (2.6)$$

The simplified equivalent circuit of the battery is presented in Fig. 2.2. In this model, V_{oc} is the internal voltage of the battery, which is a function of the battery state of charge (SoC) and type of the battery. For Li-ion batteries, the "V_{oc} -*DOD*" curve, shown in Fig. 2.3, can be used to obtain V_{oc} [19], [20]. 'DOD' represents the 'Depth of Discharge' of the battery, which is a function of battery's SoC.

Considering the charging power of the EV, the battery current can be calculated using (2.7). In (2.7), Pbat refers to charging power of the EV.

$$i_{bat} = \frac{V_{oc} - \sqrt{V_{oc} - 4 * (R_{series} + R_{transient}) * P_{bat}}}{2(R_{series} + R_{transient})} \quad (2.7)$$

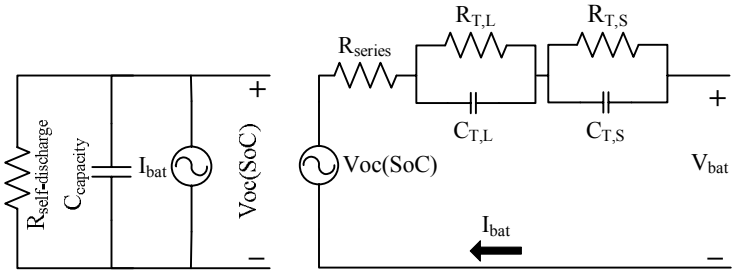

Fig. 2.1. Equivalent circuit for Li-ion EV [19], [20].

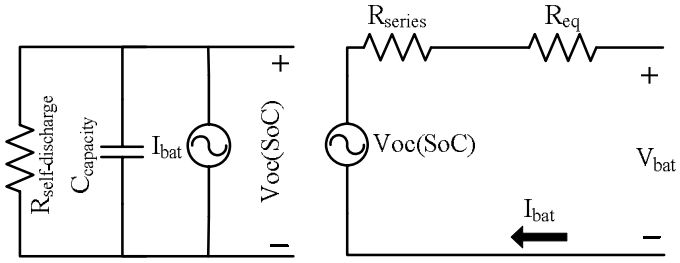

Fig. 2.2. Simplified equivalent circuit for Li-ion EV.

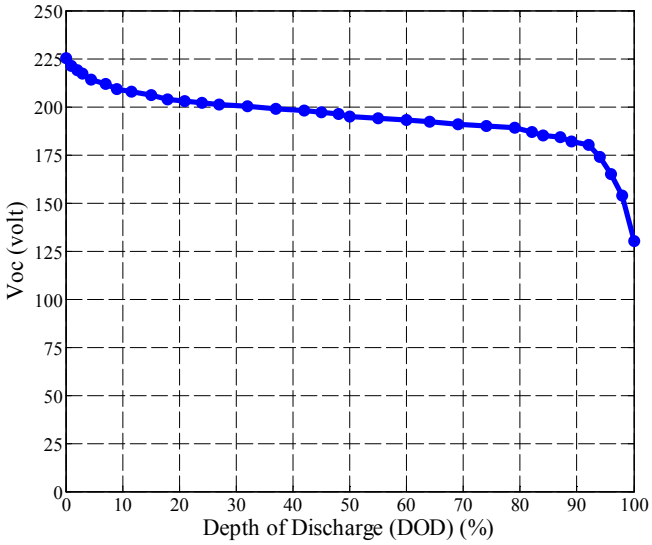

Fig. 2.3. Voltage curve for Li-ion battery [20].

Using the current and calculating the battery terminal voltage, the battery state of charge (SoC) in each time step can be obtained from (2.8).

$$SoC = \frac{CR(t_S) \pm \left(\frac{i_{bat}}{3600} \right)}{C_{bat}} \qquad (2.8)$$

In (2.8), Cbat represents the battery capacity, and CR(ts) is the previous state of charge of battery. The positive sign in (2.8) represents the charging state for the battery, while the negative sign stands for the discharging state. Also, the relation between the SoC and DOD of battery is simply calculated using (2.9).

$$DOD = 1 - SoC \qquad (2.9)$$

2.2.2. PV PANEL MODELING

Different models have been proposed so far for PV panels. Each of these models has different level of details and different parameters, depending on the scope of the work. In this research, the main focus is to determine the impact of solar panels on the steady state operating conditions of distribution grid, including voltage of grid buses, currents of the grid lines, and transformer power limits. Therefore, a simplified model of PV panels has been applied in this research [21], [22], which is based on the solar irradiation and the environment temperature.

The output power of a solar PV panel is presented in (2.10), in which G is solar irradiation, t is the ambient temperature, t0 is the standard temperature, $t_0 = 25℃$, and PSTC is the maximum power of the panel in standard test condition (*STC*).

$$P_{PV} = \frac{G}{1000} * P_{STC} \left[1 + \alpha \left(t - t_0 \right) \right] \qquad (2.10)$$

The distribution of solar PV panels in the grid is proportional to the number of customers on each bus of the system. It should be noted that in this study, the 3-kW solar panels are investigated.

2.2.3. LOAD MODELING AND GRID LAYOUT

The most common method for modeling the loads is to model the loads as constant power, constant current, or constant impedance loads [23]. However, considering the available data for the network under study, a different load modeling approach is applied in this study. The method is explained below, and its application on the grid under study is presented in the following.

2.2.3.1 Load modeling

An important part of the study is the loads in the system. Considering the main focus of the research, which is the impact of small energy resources and EVs on the operation of distribution grid, modeling the grid customers in a proper way is necessary. The case study in this research is a Danish residential distribution grid. However, there is no available measurement on the consumption of the customers. The only available data of the grid is the customers' annual energy demand, and the only available measurement was the transformer power profile. Therefore, modeling the loads has become tricky for the grid. Considering the available data of the grid, the "Velander method" has been selected in this work for modeling the grid customers [21], [24]. This method is a well-recognized method in Scandinavian countries, and different distribution system operators use this method for estimating the customer's demand. Using this method, the demand of different grid customers has been calculated. In the next step, the demand profile (load profile) of different customers has been created. To create the demand profile of different customers, it is assumed that all the grid customers have similar demand profile to transformer profile, and the only difference between different customers is the time delay between the peak consumption of different customers.

Velander Method:

As mentioned above, the "Velander method" is applied to cases where only the annual energy demand of customers is known [24]. The Velander formula is presented in (2.11):

$$P_{\max} = K_1 * E + K_2 * \sqrt{E} \qquad (2.11)$$

Here, K_1 and K_2 are empirical coefficients, E is the annual energy in kWh, and Pmax is the peak power demand (in kW). Some values of K_1 and K_2 are presented in Table 2–1 for different types of customers. Therefore, depending on the type of customers and their loading condition, proper coefficients should be selected.

Table 2–1. Velander coefficients for different types of loads [24]

Customer group (Domestic)	K_1	K_2
Customers without electric heating	0.00033	0.05
Cottage with electrical heating	0.00030	0.025
Large house with electrical heating	0.00028	0.025

2.2.3.2 Coincident load behavior

If the maximum power demand is known, it is still necessary to apply corrections to individual loads with similar behavior. The reason is that the sum of maximum

values of all the loads, if appearing at the same time, will lead to a very high current flow and therefore higher overall voltage drop [21]. Therefore, a correction is required to enable a reasonable load flow study in low voltage (LV) and medium voltage (MV) networks. Consider 'n' loads supplied through the same line. The instantaneous power can be written as (2.12).

$$instant\ \ power = \sum_{i=1}^{n} P_i \quad (2.12)$$

However, due to differences in load curves and peak demand time in different loads, peak power demand will be less than the sum of all load demands, i.e.:

$$P_{max} \leq \sum_{i=1}^{n} P_{max\,i} \quad (2.13)$$

Therefore, a 'coincidence factor' is used to determine the maximum demand of a group of loads, as mentioned in (2.14):

$$K = \frac{P_{\max}}{\sum_{i=1}^{n} P_{\max\,i}} \leq 1 \quad (2.14)$$

2.2.3.3 Demand in the grid

Part of a Danish distribution grid is selected as a case study in this work. The overall layout of the grid is presented in Fig. 2.4. The grid consists of 6 main feeders, and it has a radial layout. The number of customers on each feeder of the grid is presented in Table 2–2. From Table 2–2, feeder 2 and feeder 6 are the heavy-loaded feeders of the grid and the last bus of these feeders are far from transformer. The number of customers on each of grid buses is presented in Table 2–2, which clarifies that some feeders have higher number of customers and therefore, they have higher loading conditions. The data of the grid cables, i.e. the values of resistance of reactance of different cables in the grid, as well as cable length is presented in Appendix A. To obtain the (p.u.) value of the parameters, the voltage base is assumed to be 400V, and the base value of power is assumed to be 100MVA, i.e.:

$$Z_{base} = \frac{V_{base}^2}{S_{base}} = \frac{0.4^2}{100} = 0.0016\,\Omega \quad (2.15)$$

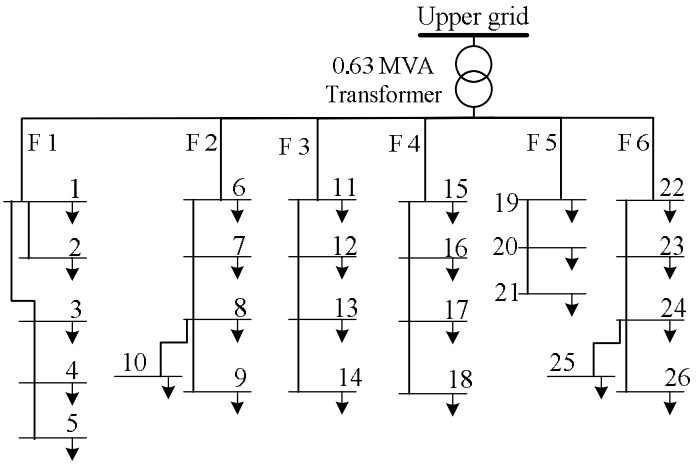

Fig. 2.4. Distribution grid layout.

Table 2–2. Number of households on each feeder [25]

Feeder	1	2	3	4	5	6
No. of house	20	33	27	28	17	42

2.3. IMPACT OF PV PANELS ON DISTRIBUTION GRID

To find out the impact of PV panels on the grid, different studies and analyses have been conducted and investigated. In this section, the studies regarding the impact of PV panels are discussed.

2.3.1. MAXIMUM ANCILLARY SERVICE VIA PV PANELS

It is well-known that ancillary service is a major concern in power system operation, where generation and demand should always remain balanced within power systems. Traditionally, spinning and non-spinning reserves were the only options to provide ancillary services. However, the large PV penetration level in the distribution systems provided a new opportunity for ancillary services which possibly can decrease operational cost and transmission congestion [22]. Because of the paradigm shift in ancillary services, maximum PV penetration in the distribution networks is desirable for the system operators, as long as it does not violate any technical limitations. To do so, a general approach is proposed to determine the maximum PV size and locations in a distribution network for maximum grid support without violating any technical constraint.

2.3.2. METHODOLOGY

In this study, three different objectives are considered which are structured as different single and multi-objective functions. The proposed objectives include: 1) maximizing power to the upper-hand grid (reserve), 2) minimizing voltage deviation, and 3) minimizing power loss. Because grid support is the primary goal of this study, the main objective is the first objective. Considering different grid requirements and their correlation, such as the correlation between power and voltage or power and losses, the optimization problem is complex. Due to the correlation between objectives, optimizing one function might lead to unwanted effects on other objectives, which might not be desirable. Therefore, simultaneous optimization of the objective functions can lead to better results, while grid constraints must also be met [26]-[44]. Therefore, two methods can be defined to deal with such problem: "single-objective method" and "multi-objective method". Single and multi-objective formulations are explained in the following sub-sections.

2.3.2.1 Single objective approach

In general, the single-objective method can be expressed as [26]-[28]:

$$\begin{aligned} & min \ \ f(x) \\ subject\ to: & \begin{cases} g_i(x) = 0 \ ; & i = 1,2,...,m \\ h_j(x) \le 0 \ ; & j = 1,2,...,n \end{cases} \end{aligned} \qquad (2.16)$$

Where '*m'* is the number of equality constraints and *'n'* is the number of inequality constraints. As mentioned before, different functions can be defined for this problem, with respect to what the user expects from the optimization. For our purpose, maximizing "power to the upper-hand network" (called $P_{upper}\ (x)$) is a priority. Therefore, the optimization problem with a single objective function is limited to maximize power to support the upper grid. Based on the convention used in this study, power flow to the upper grid is negative. As a result, the problem of maximizing power flow to the upper grid will alternatively be changed to minimizing power flow through transformer, as follows:

$$\max P_{upper}(x) = \min(\text{mean}(P_{trafo}(x))) \qquad (2.17)$$

In (2), the average power flowing through the transformer to the feeders during the day is obtained. Then, to maximize the power to the upper grid, this average value is minimized.

In this study, no equality constraint is involved in the optimization problem. Inequality constraints are similar to the alternative problem where transformer nominal capacity, standard voltage deviation for buses, and cable nominal currents

are considered, i.e.: 1) Voltage of all buses, $V_{b,s}$, must stay within a specific limit, i.e., $V_{min} \leq V_{b,s} \leq V_{max}$; $b= 1,2,...,l$. 2) Power flowing through transformer must be less than transformer nominal power. 3) Current limits of the cables. Here, V_{min} and V_{max} are the minimum and maximum voltage values of the grid buses, *'b'* is the number of the bus, and *'S'* is the time interval of the calculation. In this work, 15-minute time intervals are considered for calculations.

2.3.2.2 Multi-objective approach

Although the priority of the PV sizing and allocation optimization is given to the grid support objective, it is desired to consider other technical issues in the optimization simultaneously. Therefore, the multi-objective (MO) optimal structure is proposed as [27]:

$$\begin{aligned} &min\ F(x) \\ &F(x) = \left[f_1(x), f_2(x), ..., f_k(x) \right] \end{aligned} \tag{2.18}$$

From (2.18), k different functions (namely $f_k(x)$) might be considered in the MO problem. Similar constraints as in the single-objective function problem are utilized for the MO problem as well. Here, *'K'* is the number of objective functions. In our study, three objective functions are considered, as follows:

$$f_1(x) = \max P_{upper}(x) = \min(\text{mean}(P_{trafo}(x))) \tag{2.19}$$

$$f_2(x) = max(max(\left| V_{b,s} - 1 \right|)) \tag{2.20}$$

$$f_3(x) = P_{loss,total} \tag{2.21}$$

Where $V_{b,s}$ is the voltage at bus *'b'* at time interval *'S'*. As can be seen, the function defined in (2.19) is similar to that in (2.17). In (2.20), maximum voltage deviation at each grid bus is calculated during the day. Among all these voltage deviations, the maximum deviation is taken into account for optimization, where the optimization procedure according to (3) tries to minimize this maximum deviation. Also, the grid total loss during the day is calculated and taken as the third objective to be minimized, as mentioned in (2.21). Similar inequality constraints given for single-objective optimization problem in (2.16) are utilized for the MO problem as well.

As mentioned above, MO function can be obtained by combining different objectives. Different methods have been presented so far to deal with MO problems, among which Pareto optimality is a predominant method [27]. A comprehensive review of different Pareto optimality methods is presented in [27]. A common method for combining different objective functions is called "weighted-sum

approach". In this method, different objective functions are added together with a weighting factor to form a single objective function as given below:

$$min \sum_{i=1}^{k} w_i f_i(x) \qquad (2.22)$$

Objective functions are weighted, based on their significance in the optimization. In general, sum of all weighting factors are equal to one:

$$\sum_{i=1}^{k} w_i = 1 \qquad (2.23)$$

where $f_i(x)$ is 'i^{th}' objective function from *'K'* existing objectives. In this method, similar constraints can be employed for the optimization problem in hand. Typically, there are two methods to calculate weight factors: "rank order centroid" (ROC) method, and "rank sum" (RS) method [27]-[30].

ROC method:

In this method, a uniform distribution of the weights is assumed on the simplex of rank-order weights. Then, for $w_1 > w_2 > \ldots > w_m$, if 'i' is the rank position of 'w_i', and *'K'* is the number of objective functions:

$$w_i = \frac{1}{k} \sum_{l=i}^{k} \frac{1}{l} \qquad (2.24)$$

RS method:

This method is appropriate when there is a priority sequence among the objective functions. The weighting values can be calculated as follows:

$$w_i = \frac{2(k+1-i)}{k.(k+1)} \quad , \quad i = 1,2,\ldots,k \qquad (2.25)$$

As mentioned earlier, the highest priority is given to the first objective. Voltage deviation and power loss are second and third in the list, respectively. Minimizing voltage deviation has higher priority than power loss, since power loss does not change significantly with different PV sizes and allocation. This is due to the grid size under study and its low power loss.

2.3.3. OPTIMIZATION TECHNIQUE

With the objective functions and constraints in hand, it is required to utilize an appropriate optimization technique to solve the problem. The optimization problem in this study includes integer decision variables, namely the number of PV panels which can be installed on each bus. In addition, the objective functions (whether single objective or MO problems) are nonlinear functions, and might not converge. Therefore, heuristic optimization methods seem to be the best option for the problem in hand. There are several heuristic optimization techniques with their own weaknesses and strengths. However, only a few of them are capable of solving integer optimization problems. Amongst all, Genetic Algorithm (GA) is chosen in this study to solve the optimization problem. GA is a heuristic approach that imitates the process of natural selection by routinely providing solutions to optimization problems. Some main parameters of this method are: selection, crossover, mutation, and population. The principles of this technique, together with its different parameters are explained in [28], [30].

Details of GA parameters are presented in Table 2–3. For the MO problem, different weighting factors are calculated based on (2.24) and(2.25), and is reported in Table 2–4. As an example, to calculate the weight factor for the first objective function, $f_1(x)$, in ROC method, we would have:

$$i=1 \Rightarrow \quad w_1 = \frac{1}{3}\sum_{l=1}^{3}\frac{1}{l} = \frac{1}{3}\left(1+\frac{1}{2}+\frac{1}{3}\right) = \frac{11}{18}$$

Table 2–3. GA optimization parameters.

Parameter	Population	Number of generation	Stall generation	Tolerance function
Value	40	200	100	1e-8

Table 2–4. Weighting factors for different objectives in the MO problem.

Method	Objective Function		
	$f_1(x)$	$f_2(x)$	$f_3(x)$
ROC	11/18	5/18	2/18
RS	1/2	1/3	1/6

2.3.4. OPTIMIZATION RESULTS

Different simulation studies are carried out on the distribution system, shown in Fig. 2.4, to optimally size and locate the PV panels. In the first sub-section, simulation results for normal operation are presented and explained. In the second sub-section, a simulation study is performed to show that power loss minimization is not an effective objective function for a system of this size.

2.3.4.1 Single objective and multiobjective optimization

Table 2–5 presents the optimization results of each optimization method. With respect to optimization output, the grid parameters were measured. The transformer power profile from different optimization methods, together with normal transformer profile, is presented in Fig. 2.5 to ease the comparison. It should be mentioned that, while running optimization in single objective method, the results had a significant tolerance. The optimization was repeated several times. Despite a slight difference, the number of PV panels was similar in different tries. However, their arrangement would change significantly. Such problem didn't appear in multi-objective approaches. Running each multi-objective optimization several times, both the number and the arrangement of panels in the grid were almost the same. This is a much more promising result, as it can assure the accuracy of the results.

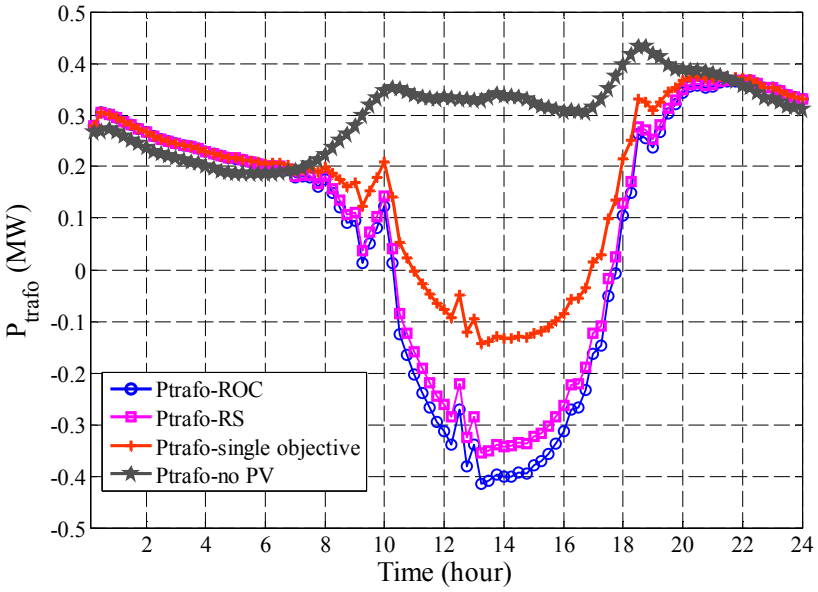

Fig. 2.5. Power profile at transformer level.

Table 2–5. Number of pv panels: single-objective vs. multi-objective approach.

Feeder	Bus	Single-objective	ROC approach	RS approach
1	1	2	4	4
	2	5	10	10
	3	4	8	4
	4	6	6	9
	5	3	0	0
2	1	5	10	10
	2	6	12	12
	3	9	10	13
	4	5	3	6
	5	6	6	1
3	1	5	14	14
	2	6	14	14
	3	0	10	9
	4	4	12	4
4	1	4	6	6
	2	2	16	15
	3	4	11	6
	4	4	5	3
5	1	5	10	10
	2	6	8	8
	3	6	5	5
6	1	6	12	12
	2	7	12	12
	3	10	18	15
	4	7	6	5

2.3.4.2 Power loss as single objective function

As mentioned in section II, for multi-objective optimization, the least weight is dedicated to “total power loss”, denoted as $f_3(x)$. The reason is that the total power loss value of the grid is small, as the grid is a small distribution network. To verify that assigning a higher priority to voltage rather than to total loss is reasonable, a separate single objective optimization is done. In this case, “total power loss”, $f_3(x)$, is the objective function. Optimization results are presented in Table 2–6. From the table, it can be realized that the network total power loss has not changed in different

optimization repeats, although the arrangement of the panels has changed. Also, to have a more accurate comparison, the total power loss of the network in different optimizations of Table 2–5 is presented inTable 2–7. From the results, one can realize the insignificant effect of optimization on grid total loss, comparing to grid normal power loss. The "total power loss" presented in Table 2–6 is almost the same as the "total power loss" of other methods in Table 2–7. Therefore, $f_3(x)$ doesn't have a significant effect on the optimization results. However, this might not be the case for a large-scale network with significant power loss. So, for different networks with different scales, this fact needs to be addressed.

Table 2–6. Number of pv panels: power loss as the objective function.

Feeder	Bus	1st optimization attempt	2nd optimization attempt	3rd optimization attempt
1	1	3	1	2
	2	4	6	5
	3	4	3	4
	4	5	6	6
	5	3	3	2
2	1	1	2	2
	2	8	5	7
	3	9	10	9
	4	5	4	5
	5	5	6	5
3	1	7	5	6
	2	2	8	3
	3	7	3	7
	4	4	5	4
4	1	5	4	4
	2	5	8	9
	3	5	1	4
	4	3	5	1
5	1	7	6	6
	2	7	8	8
	3	5	5	5
6	1	8	5	6
	2	5	8	7
	3	13	12	13
	4	7	8	7
	5	6	6	6
power loss (kW)		2.4084	2.4082	2.4081

Table 2–7. Total power loss of different optimization methods.

Method	Single objective	ROC	RS
Total power loss	2.508	2.571	2.493

2.4. EV IN PERSPECTIVE: CHALLENGES AND OPPORTUNITIES

New technologies and significant investments on electric vehicles (EVs) have led to increasing interest for these vehicles in recent years. Low-maintenance and consistent decrease in the price of EVs are of the main reasons which make EVs attractive choices for customers [33]. Considering the charging requirements of EVs and their potential challenges for the electric network, this study focuses on EVs' impact on distribution grid. The design and calculations of traditional distribution power systems are based on handling the customer peak demand. In these calculations, no EVs are included [34]. Considering the battery size of EVs, the demand of an EV would easily exceed the nominal demand of a typical household. As the number of EVs increase in the grid, their total demand can challenge the grid operation limits, among which voltage constraints, current limitations, and transformer capacity are the most important constraints [35].

Increase in the penetration of EVs in the grid, without having any charging strategy for them, forces the grid operators to reinforce the grid, which requires a significant investment and increases the costs [35]. On the other hand, applying smart charging algorithms in order to manage the charging time or charging level of EVs can defer the investment requirement to a huge extent [35]. Different charging strategies have been proposed for EVs so far. In [36], a decentralized charging method is proposed for EV charging. The main objective of this method is to increase the customer convenience. Doing so, grid constraints are not a concern. In [37], an optimum EV charging is proposed to minimize charging cost of EVs. The proposed algorithm mainly focuses on minimizing the customer cost. Also, a charging algorithm is proposed in [38], which is based on sensitivity of grid voltages and currents. On the other hand, the main part of the EV which affects the grid and EV performance is EV's battery type and its charging behavior [39]. As one of the most promising technologies, Lithium Ion (Li-ion) batteries have raised a huge interest among industries and research groups. High energy density, as well as their capability to provide perfect performance characteristics is among the main reasons for such interest [40]. 2 types of EVs are considered in this study: a) commuters; b) family cars [41]. Both types of EVs have a 30-kWh battery pack [25]. Commuters and family cars are assumed to have an average driving distance of 40km and 25km during the day, respectively. The required data for EVs are reported in Table 2–8 [41]. EVs are randomly distributed among the buses based on the number of households on each bus. Fig. 2.6 presents the distance profile (DP) of the commuters and family cars in the grid. From Fig. 2.6, commuters mainly drive during the morning and evening hours, from 7:00 A.M. until 9:00 A.M. in the morning, and from 17:00 to 19:00 in the evening. Family cars have more diverse profiles during the day, while their average driving distance is less than commuters.

2.4.1. PROPOSED CHARGING ALGORITHMS

High EV penetration can lead to challenges for the grid operation limit. Particularly, as a main operation index, voltage would be seriously affected by the new load. In the following, dumb charging is introduced as a base case. In the next subsections, two smart charging algorithms are proposed to deal with potential issues of the grid due to EVs. The results of the smart charging methods are compared with the dumb charging scenario to evaluate the effectiveness of the proposed algorithms.

Table 2–8. Details of EVs in the grid [11]

	% of EVs	Battery (kWh)	Average consumption (Wh/km)	Charger power (kW) (3-φ)	Average daily distance (km)
Commuter	80	30	150	7.2	40
Family car	20	30	150	7.2	25

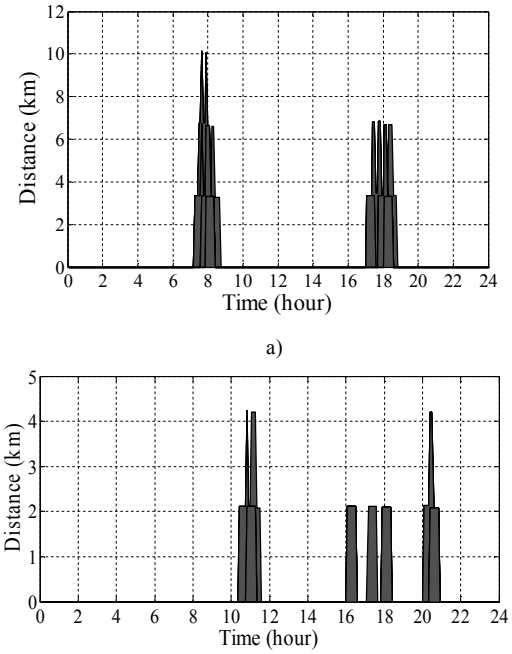

Fig. 2.6. Distance profile (DP) of some EVs in the grid: a) commuter; b) family car.

2.4.1.1 Simple (dumb) charging

In this case, EV owners connect their EVs to the grid while they're at home, i.e. there's no control on charging of EVs. Since the maximum battery charging is limited to 90%, if the EV's state of charge (SoC) decreases below this value, it starts consuming power. Such case might not be challenging at the moment, since the EV penetration is low. However, high penetration of EVs can lead to undesirable issues

in the grid, as the grid voltages or transformer nominal power might be violated. Fig. 2.7 presents the flowchart of the dumb charging case in this study, which is considered as a base case. In this figure, the algorithm takes the data of EVs as an input. 'EV data' includes type of EVs (commuter/family car), EVs' distance profile (DP), EVs' location in the grid (the bus that each EV is connected to), and the SOC of each EV from previous time interval. In the first step, the moving EVs will be separated from the idle EVs. If the EV is on the road, then it loses part of its battery charge. Therefore, for the moving EVs, the algorithm should calculate the EV's new SOC based on the distance that the EV moves in that time interval (obtained from DP data) and its battery size. On the other hand, if the EV is idle, the algorithm checks the SOC of EVs. If the EV's SOC is below its upper limit, it starts charging. Otherwise, the EV's SOC does not change. If the EV starts charging, the EV's bus data should be updated with respect to the EV's charging power. In this study, it is assumed that the EV only consumes active power, and it has no reactive power consumption [41]. The algorithm checks the status of all EVs, and modifies the bus data of all the EVs. The modified bus data of the grid (bus data including the effect of EVs) together with the 'input data' act as inputs for the 'Grid Power Flow (GPF)' block. 'Input data' includes the grid line data, and the grid load data (demand profile of grid buses of Fig. 2.4). Using these data, 'GPF' block performs a steady state analysis and obtains the voltages of different grid buses for each time interval.

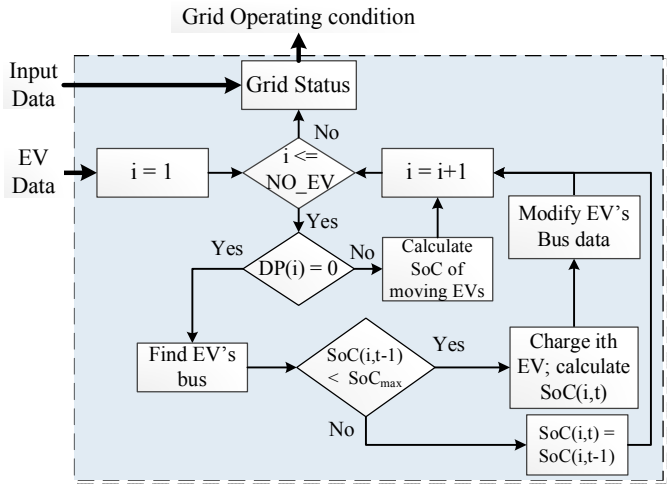

Fig. 2.7. Dumb charging of EVs.

2.4.1.2 Smart charging: plan A

In this scenario, a smart method of charging EVs is proposed. It is assumed that EVs are getting charged during the night time. Therefore, the algorithm manages EV charging from 22:00, where EV owners are most likely to be at home, until 7 A.M., where the EV owners start driving. In this plan, the charging power of EVs for simultaneous charging is similar, i.e. the EVs use their charger nominal power, as

mentioned in Table 2–8. The main idea in this algorithm is to use the EV's bus voltage measurement to decide whether to charge EV or not. The proposed algorithm for 'plan A' of EV charging is presented in Fig. 2.8. The "GPF 1" (Grid Power Flow) block in Fig. 2.8 takes the input data and analyses the grid initial operating condition. The 'input data' includes load data of the grid buses (demand profile of different grid buses of Fig. 2.4), grid line data, and grid bus data. Having these data as inputs, the 'GPF 1' block obtains the voltages of different grid buses for each time interval. The time intervals are assumed to be 15-minute intervals in this study. In the next step, the 'EV data' are added to the algorithm as the input data of the EVs in the grid. 'EV data' includes the DP of EVs, type of EVs, the location of each EV in the grid, and each EV's SoC from previous time interval. Having the data of the grid voltage values and the data of the EVs, the algorithm determines the charging status for each EV. The moving EVs and the idle EVs are separated by algorithm first. As mentioned earlier, it is assumed that if the EV is idle, then it is connected to the grid.

For idle EVs, the algorithm sorts EVs based on their SoC in ascending order, i.e. the EVs with lower SoC will have higher priority. In the next step, the EV location in the grid (EV's bus) is identified. Using the grid initial operating conditions, which are obtained from 'GPF 1' block, the voltage of the EV's bus will be obtained. If the bus voltage is within standard operating condition [16], the EV starts charging. Otherwise, the EV's SoC does not change. The charging state for the EV represents the presence of a new load for the grid bus. Therefore, the algorithm needs to modify the EV's bus data. After checking the status of all the EVs in the grid, the grid bus data will be modified. The modified bus data will be sent to 'GPF 2' (Grid Power Flow) block. The 'GPF 2' block analyses the grid operating conditions in presence of EVs. The process repeats for each time interval.

Apart from night-time charging, the main feature of this method is that it only considers the EV bus voltage to decide whether to charge EV or not. This could be an advantage for the algorithm, as the algorithm only needs voltage measurement of the EV bus which makes the algorithm simple. However, this could be a disadvantage for the algorithm as well, especially for high number (penetration) of EVs. The reason is that for the EVs which are located on the buses near transformer or in the middle of the feeder, the algorithm only checks the voltage of the EV bus for decision. In such cases, EV charging could lead to voltage issues for the buses which are at the far end of the feeders.

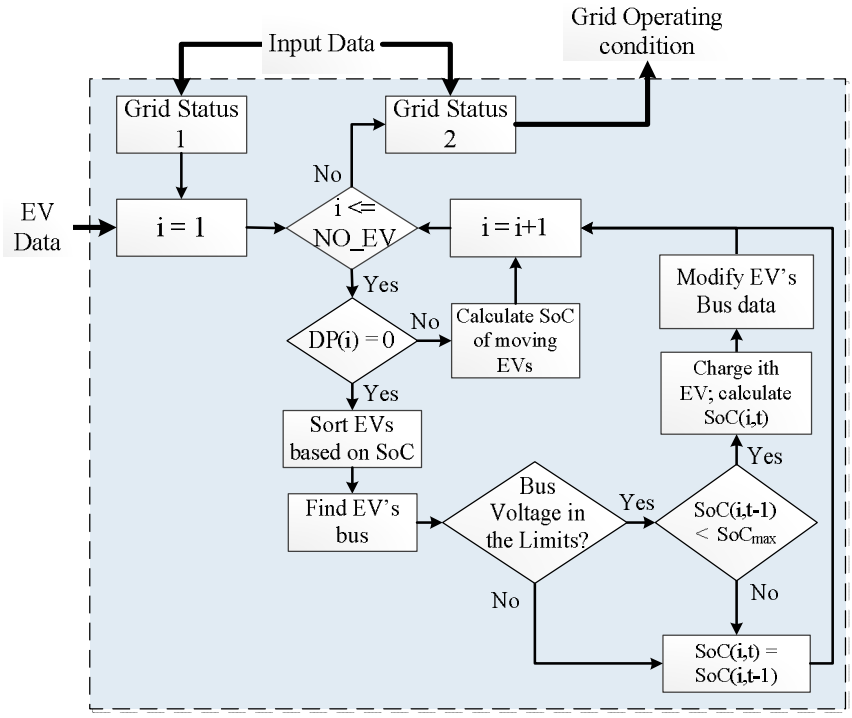

Fig. 2.8. Smart charging: plan A.

2.4.1.3 Smart charging: plan B

The proposed algorithm of 'plan B' is presented in Fig. 2.9. Similar to 'plan A' in Fig. 2.8, the 'GPF 1' block analyses the grid operating conditions without the EVs in the grid. Then, the algorithm separates the moving EVs from the idle EVs, and sorts the idle EVs based on their SOC. The first difference between 'plan B' and 'plan A' is that in 'plan B', in addition to recognizing EV's bus, the algorithm identifies EV's feeder as well. When the EV's bus and feeder is identified, the maximum voltage among all the feeder buses, V_{max}, as well as the minimum voltage in the feeder, 'Vmin', will be determined, using the results of the 'GPF 1' block. Having these values enables the algorithm to decide whether to charge the EV or not. If the voltages are not within the standard limits [16], the EVs will not be charged and their SoC remains unchanged. If the voltages allow, the algorithm determines the charging rate of EVs. Considering the charging rate of each EV, the new SoC of EVs will be calculated. The next step in the algorithm is to modify the grid 'bus data'. The bus data of the EV buses will be modified, if the EV in that bus is in the charging state. After checking all the EVs, the modified bus data will be sent to 'GPF 2' (Grid Power Flow) block for analyzing grid operating conditions in presence of EVs.

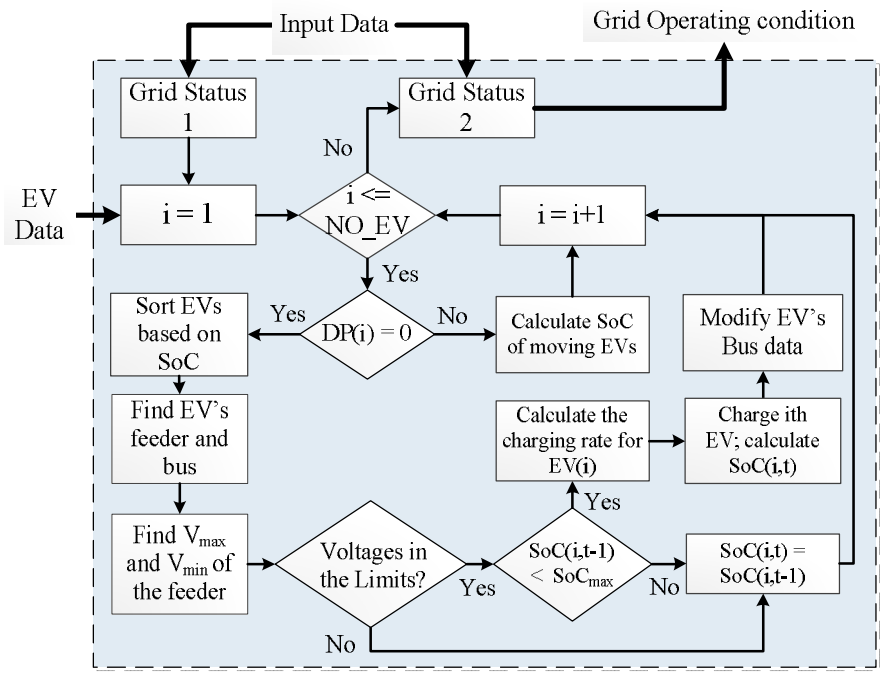

Fig. 2.9. Smart charging: plan B.

As mentioned, the charging rates of EVs are variable in this algorithm. The idle EVs will be sorted based on their SOC. For the EVs with lower SOC values, the charging power of the EVs will be equal to the nominal charging value, i.e. 7.2 kW. For the next EVs, the charging power will decrease linearly. The lowest charging rate is set to 25% of the nominal charging power. The other difference between 'plan A' and 'plan B' is that in 'Plan B', the charging time is not limited, and the algorithm charges the EVs for the 24-hour period. Compared to 'plan A', this plan might be more complex, as it uses all the voltages of each feeder to determine whether to charge EV or not. It also changes the charging rate of different EVs. However, these features will be an advantage for the algorithm under high penetration of EVs in the grid, since it can handle the grid voltages for high number of EVs. The algorithm also increases the grid potential for handling higher EV penetration in the grid, without reinforcing the grid.

2.4.2. SIMULATION STUDIES AND RESULTS

To figure out the grid operating conditions and to evaluate each of the charging methods, different scenarios with different EV penetration are simulated and analyzed. Considering the loading condition of different feeders in the grid, two of the buses in Fig. 2.4, bus10 and bus26, are considered as weak buses of the grid, i.e. their voltage profiles are more prone to violate the standard voltage [16]. Going

through simulation results, bus10 has shown worst voltage behavior in different scenarios and under different EV penetration levels. Therefore, the voltage profile of this bus is presented for comparing different scenarios.

Considering the number of households in the grid, presented in Table 2–2, it is assumed that 10% EV penetration in this study means that 16 EVs are in the grid, and 20% EV penetration represents 32 EVs in the grid. The distribution of EVs in the grid is proportional to the number of households on each feeder, i.e. the feeders with higher number of households are more likely to have higher number of EVs.

2.4.2.1 Dumb charging

As a base case, EV charging is done using dumb charging. From the results, if there is no smart charging plan in the grid, the EV penetration cannot exceed 20%. As the penetration level reaches 25%, the voltage violates its lower limit. From Fig. 2.10, the voltage of bus10 decreases below 0.9 (p.u.), as the penetration level reaches 25%. The morning spike in the voltage curve is due to the fact that all the commuters become idle after 9 A.M. and are connected to the grid. Also, in the evening time, most EVs become idle after 20:00, and therefore, they start charging.

2.4.2.2 Smart charging: plan A

In this case, the first smart charging algorithm, i.e. 'plan A', is applied in the grid. Using 'plan A', the EV penetration can increase to 50% (80 EVs), without violating grid operating limits. If the number of EVs goes beyond this number, then full charging of EVs violates voltage limits. Fig. 2.11 plots the voltage profile of bus10 for two cases in this plan: 50% EV penetration, and 75% EV penetration. The spikes in the voltage profile in Fig. 2.11 are due to the charging power of the EVs. As mentioned, the algorithm sorts EVs based on their SoC, and decides whether to charge EV or not based on the EV's bus voltage. However, the charging power of EVs is not controlled. Therefore, the EVs which are selected by algorithm will use the charger nominal power.

2.4.2.3 Smart charging: plan B

In the third simulation case, the grid is simulated using 'plan B' for EV charging. Results clarify that, although this algorithm is more complex compared to 'plan A', it increases the EV penetration level up to 75%. The reason is that since the charging power of different EVs are controlled by the algorithm, the voltage profiles of the grid are more smooth, compared to plan 'A'. Also, the algorithm checks the voltage of all the buses among the EV feeder to decide whether to charge the EV or not. The other point which affects the grid operating condition in this algorithm is that some EVs get charged during the daytime. Therefore, the EV loading for the night time decreases. Besides, since some of the EVs are partially charged during the day, they

can be charged by a lower charging rate. As a result, higher number of EVs can be charged by the grid. Fig. 2.12 presents the voltage profile of bus10, using plan 'B' for smart charging of EVs in the grid. Fig. 2.13 presents maximum EV penetration under each charging scenario.

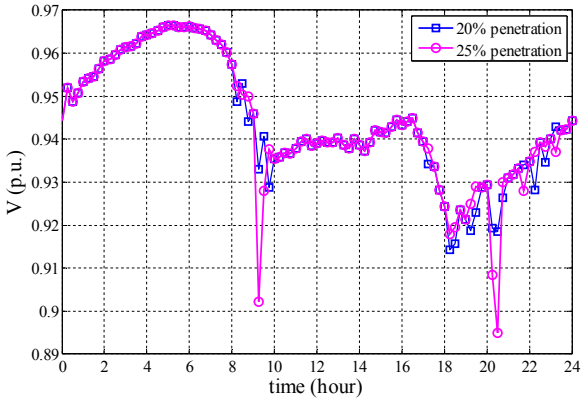

Fig. 2.10. Voltage profile of bus10: dumb charging.

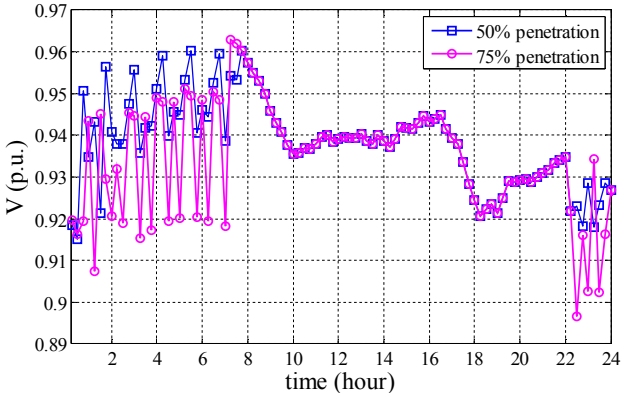

Fig. 2.11. Voltage profile of bus10: plan A.

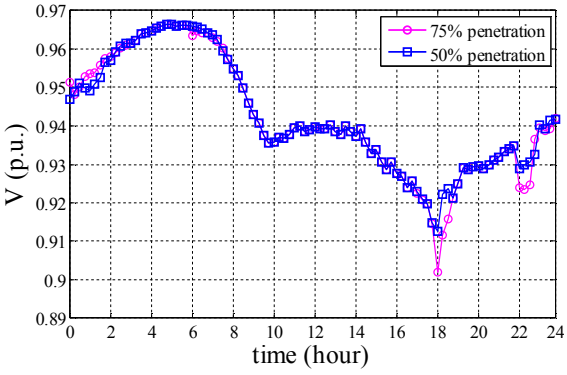

Fig. 2.12. Voltage profile of bus10: plan B.

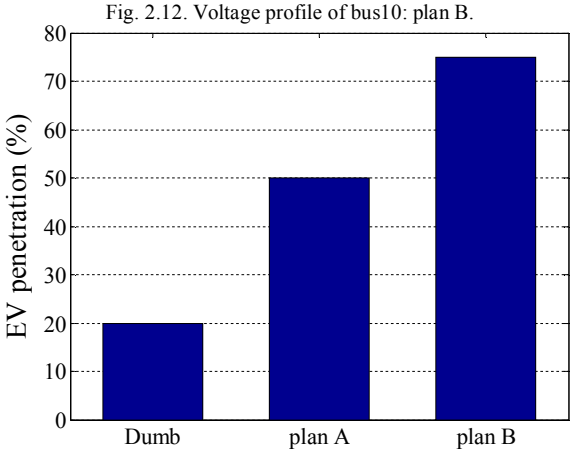

Fig. 2.13. Proposed optimization method.

Table 2–9. Minimum voltage of bus10 for different scenarios

EV penetration	Dumb Charging	Smart charging: plan A	Smart charging: plan B
10%	0.9139	0.9207	0.9176
20%	0.9017	0.9207	0.9175
25%	0.8984	0.9205	0.9165
50%		0.9126	0.9132
75%		0.8942	0.9018

2.5. GRID CAPABILITY FOR PROVIDING ANCILLARY SERVICE FOR UPPER NETWORK

In this section, an algorithm is proposed based on optimal management of PEV storage, in order to maximize LV participation in ancillary services. This way, part of the required ancillary services will be provided by the PV panels installed in distribution networks to alleviate the system operational costs [41]-[52]. Also, the total power loss of the system is included in the optimization procedure, so that the system losses will also be minimized. A multi-objective optimization procedure is proposed to obtain the best viable solution for this purpose [26], [27]. Appropriate voltage profile at different buses and the quality of service (QoS) for the PEV owners are among the major constraints in the proposed algorithm. Considering the physical constraints of electric equipment in the system, i.e. transformer nominal power and nominal currents of the cables, the problem formulation should take these limits into account as well. On the other hand, since PEVs are utilized by the algorithm for grid support, the proposed algorithm should include a proper charging algorithm for PEVs to avoid any inconvenience for PEV owners.

2.5.1. APPLIED INTELLIGENT ALGORITHM

An overview of the proposed algorithm is shown in Fig. 2.14. At the beginning, the optimization block generates appropriate PV sizes and locations based on the optimization data. The generated PV sizes and locations along with solar irradiation and ambient temperature data will be utilized to prepare the power flow matrices. Then, the first power flow study (PF-1 Block) will be carried out to calculate the voltage magnitudes of different buses. The calculated voltages will be used in the PEV Block to compute PEV charging pattern, and PEV for grid support. Then, the load flow matrices will be modified based on the impact of the PEVs, and the load flow runs again (PF-3 Block). Finally, the required data for the Optimization Block will be calculated based on the recent load flow. In the following sub-sections, each block will be discussed in details.

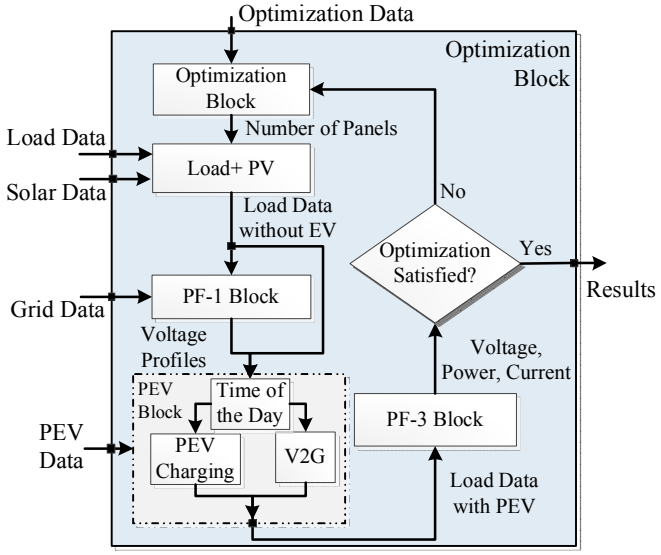

Fig. 2.14. Proposed optimization method.

2.5.1.1 Optimization Block

This block is responsible for finding the optimal size and location of the PV panels. Optimization data includes the maximum and minimum number of panels which can be installed at each bus, and optimization technique parameters. The maximum number of panels is obtained by assuming that each household cannot install more than 2 '3-kW' PV panel units. This is a fair assumption, considering the available roof area of a house. As a standard procedure for optimization problems, the first step is to define an appropriate objective function. As mentioned earlier, the main objective is to maximize the power flow to the upper-hand network. Two other objectives are defined as minimizing the voltage deviation, and minimizing power losses. The voltage profile is known as an important operational index in the

distribution networks. A multi-objective problem can be expressed similar to section 2.3.2:

$$Optimize\ F(x):\ F(x)=\left[f_1(x), f_2(x), ..., f_k(x)\right] \tag{2.26}$$

$$subject\ to: \begin{cases} g_i(x)=0\ ; & i=1,2,...,m \\ h_j(x)\le 0\ ; & j=1,2,...,n \end{cases}$$

The first objective can be equivalently replaced by minimizing the power from the upper grid to the distribution network, as follows:

$$f_1(x)=\min\left(\text{mean}(P_{trafo}(x))\right) \tag{2.27}$$

P_{trafo} is the power through the transformer from the upper network to the distribution grid. The second objective is the voltage deviation among the grid buses, which can be obtained as follows:

$$f_2(x)=\min\ \ max(max(\left|V_{b,t}-1\right|)) \tag{2.28}$$

where $V_{b,t}$ is the voltage at bus b at time interval t. Here, first the maximum voltage among all grid buses for different time intervals is selected. Then, the maximum voltage amongst all time intervals is chosen to be minimized. This approach is selected to simplify the second objective function without jeopardizing the overall performance and accuracy. Minimizing the maximum voltage deviation amongst all buses guarantees that every bus voltage deviation will also be minimized. The last objective function is expressed as:

$$f_3(x)=\min\ \ P_{loss,total} \tag{2.29}$$

At the end of each interval, total power loss of the network is calculated. Then, total power losses for a day of simulation (i.e., $P_{loss,total}$) is computed by adding values of all intervals together. Three inequality constraints in this study are: 1) voltage of all buses must stay within a specific limit; 2) power flow through the transformer must be less than transformer nominal power; 3) line currents should never exceed the cables' nominal current. Also, the equality constraints, regarding the generation-consumption balance are considered.

2.5.1.2 "Load +PV" block

This block prepares bus and line data matrices based on grid topology and grid demand data. Bus data, which contains generation and load data at each bus, will be

modified based on the generated PV sizes and locations by the Optimization Block. Therefore, it is primarily required to calculate PV generation based on irradiation and ambient temperature.

2.5.1.3 PF-1 Block

In this study, the voltage level at different buses in presence of PV is used to design a charging/discharging algorithm for the PEVs in order to increase PV penetration and support the upper grid. Once the PV generation is too much, voltage at the bus of connection (and probably at the neighbor buses) shows undesired increase. On the other hand, low voltage at different buses shows deficiency of power, which can be compensated by PEV discharging, if available. So, the voltage magnitudes at different buses should be computed before the utilization of PEVs. The PF-1 Block takes the data and calculates voltage magnitudes for the next time slot.

2.5.1.4 PEV Block

The PEV Block is responsible for computing the charging/discharging pattern for the PEVs based on their DP and the grid condition at each interval. The Block receives PEV data and voltage magnitudes at different buses as the input. The PEV data includes: 1) the number and type of PEVs, 2) PEVs' battery size, 3) initial SoC of PEVs at the beginning of simulation, 4) average consumption of different PEVs (Wh/km), 5) DP of PEVs, 6) nominal power of PEV charger, 7) PEV buses with the number and types of PEVs on each bus. The SoC of PEVs changes during the day with respect to their DP and their average energy consumption. Therefore, in order to define a proper algorithm for PEVs, it is necessary to calculate the SoC of each PEV at the end of each interval. If the PEV is moving, the new SoC at the end of the interval will be calculated based on the PEV's DP for that interval, type of PEV, its previous SoC, and its battery capacity. Otherwise, when the PEV is idle, its SoC does not change. The SoC will be calculated within "PEV Block" in Fig. 2.14. From Fig. 2.14, the "PEV Block" includes two individual blocks, "PEV Charging" and "V2G". The reason is that a day of simulation is divided into two different blocks: 1) high irradiation; 2) low irradiation. The reason for the division is to find appropriate set points for the algorithm. The high solar irradiation and solar production during the daytime increases grid voltage levels especially during the daytime. However, the solar production reaches zero during the evening and night hours. Therefore, different set points are defined for the algorithm to efficiently charge the PEV battery for customer requirements in the morning, while enabling the grid to utilize PEV storage for grid support.

1) PEV Charging:

Considering the number of PEVs in the grid and their significant power demand, especially at night when most PEV owners plug their car for charging, a huge amount of load will be imposed on the grid which can result in voltage issues, as

well as overcurrent in the lines and transformer. Therefore, a proper algorithm is required to handle PEV charging appropriately. Fig. 2.15 presents the flowchart of the proposed algorithm for PEV charging. From Fig. 2.15, all the PEVs connected to the grid will be sorted in ascending order based on their available SoC from the last interval. Sorting PEVs will enable the algorithm to only charge certain PEVs least SoC for simultaneous charging. Furthermore, the random displacement of different PEV types in different feeders and different buses, performed only once at the initialization of the whole optimization program, enhance the algorithm performance and voltage profile at different buses, as it minimizes the probability of simultaneous charging of too many PEVs at the same feeder. Additionally, when the number of PEVs increases, the random selection nature of the proposed algorithm helps to keep the diversity for PEV selection which results in higher probability of available PEV for charging at different buses at any time. After selecting the PEVs, each selected PEV will be examined for charging. If the i^{th} PEV is moving (i.e., $DP(i,t)\neq 0$), it cannot be charged and the algorithm only calculates its SoC at the end of the current interval. Otherwise, the PEV's SoC at the end of the last interval will be evaluated, i.e., $SoC(i,t-1)$. If the PEV's SoC is above SoC_{min}, the algorithm does not charge the PEV. This way, the SoC at the end of the current interval will be equal to its SoC from the last interval, i.e., $SoC(i,t)=SoC(i,t-1)$, since internal battery discharging is neglected in this study. Once the SoC of the i^{th} PEV is less than SoC_{min}, the PEV will be charged. Here, the PEV's SoC at the end of the charging period will be calculated and the "load data" matrix will be modified, due to PEV charging impact.

2) V2G:

PEVs utilization is a random behavior because of human interaction as the driver. This way, a PEV's SoC at the end of each trip, charging and discharging preferences of the owner, and connectivity to the grid at the time of idling brings a new level of uncertainty in the power system. This results in higher operational cost due to the required ancillary services. In this study, the PEV behavior is represented by generating random driving patterns, selecting the type and their random displacement in the grid. This way, when an PEV is idle and connected to the grid, the grid can benefit in two ways: 1) Positive balance, where the storage capacity of PEV can be used to store extra energy [43], and 2) Negative balance, where the PEV can support upper grid [43]. It should be noted that a PEV can be used for grid support only when: 1) the PEV is idle; 2) the PEV is connected to the grid; 3) the PEV battery is available for such function. Due to the battery lifetime issues, batteries should not be charged more than a certain level (90%) [20]. On the other hand, batteries should always have a minimum level of charge to respond to the owners' requirements. So, battery availability is limited to certain "minimum" and "maximum" values. Determining "minimum" value can be done considering PEVs' DP and their daily distance. Fig. 2.16 presents the proposed algorithm for such functions. For each interval, PEVs' data (including locations, DP, and initial SoC) are given to PEV Block (Fig. 2.14 and Fig. 2.16). Then, each PEV will be examined for its potential for grid support based on different rules and constraints. Since

charging and discharging of PEV could affect the voltage of the whole feeder, the algorithm is designed to consider voltage of the feeder to which PEV is connected. Then, in the first iteration, the maximum and minimum voltage of the feeder (V_{max} and V_{min}, respectively) will be determined based on the data from PF-1 Block. However, for the next iterations these values will be determined by 'PF-2 Block', shown in Fig. 2.16. These values will be compared with predefined set points, V_{max} (upper) and V_{min}(lower), also mentioned in Fig. 2.16 by 'Cond1' and 'Cond2'.

Scenario 1 (charging and discharging): If both maximum and minimum voltages of the feeder at hand are beyond the thresholds, which might happen if the feeder is too long and there are many PV panels installed at certain buses, priority between discharging and charging is given to the one that the PEV bus is closer to. As a result, discharging is preferred if the bus with minimum voltage is closer to the current PEV ($D\_V_{min}<D\_V_{max}$). Conversely, if the bus with maximum voltage is closer to the PEV bus, then charging will happen ($D\_V_{max}<D\_V_{min}$). The desired operation on the PEV, however, depends on its availability and the SoC level.

Scenario 2 (only charging): If the maximum voltage is higher than a threshold (V_{max}) in the whole feeder, there is an excess power generated by the PVs in that feeder which can be possibly stored in PEVs. So, the current PEV will be examined to store the excess power. However, charging happens only if the PEV is idle and its battery SoC is less than the technical upper limit, i.e., 90% of its nominal capacity.

Scenario 3 (discharging): If the minimum voltage of the feeder is below V_{min}, a shortage in the generation will be recognized. In this condition, the PEV will be examined for discharging based on its availability and SoC level.

Scenario 4: If the maximum and minimum voltages are within the pre-defined values, and the PEV is idle, the SoC of the PEV does not change.).

In all the scenarios (except for Scenario 4), the bus matrix should be modified for the new power flow in the PF-3 Block.

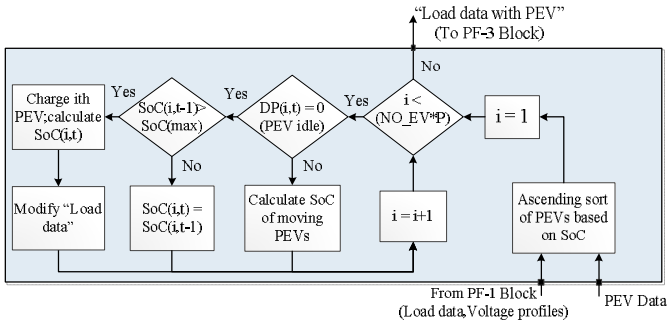

Fig. 2.15. Charging pattern for PEVs for each interval of simulation.

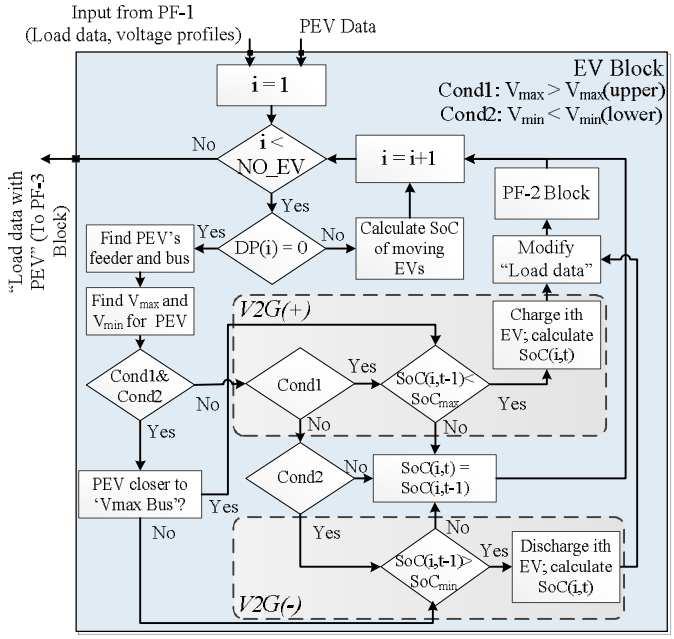

Fig. 2.16. Charging pattern for PEVs for each interval of simulation.

2.5.1.5 PF-3 Block

In this block, the modified "load data" matrix, considering charging and discharging operation of PEVs for the length of simulation, along with line matrix will be utilized to calculate new steady-state operating points. A similar power flow structure, similar to PF-1 Block, is used in this block; only the loads have changed. Final load flow results will be utilized to calculate the required data for the Optimization in order to generate new solutions for the PV sizes and locations.

2.5.2. SIMULATION RESULTS

Due to the nature of the optimization problem and variables (i.e., number of PVs), GA method is chosen for this study, as heuristic approaches are more effective than gradient-based techniques when it comes to nonlinear integer optimization. Different case studies, together with the optimization results, are presented in the following subsections.

2.5.2.1 Case Studies

1) CASE I: Original grid without PV and PEV

First, the original grid is simulated with actual load demand without PV panels and PEVs. The data used in this simulation belongs to the first day of July 2010. The

reason to pick a summer day is the fact that solar irradiation becomes maximum in the summer. Therefore, it's better to determine the penetration level of solar panels in the summer. This way, it will be guaranteed that the solar power production never exceeds the grid limits. The simulation reveals the possible issues with the grid which further can be utilized for comparison purposes. Voltages at some critical buses (i.e., at the end of the feeders) are shown in Fig. 2.17. Considering the standard voltage deviation limit [16], voltage violations at some buses can be recognized. Voltage violation is more severe for the end buses of feeders 2 and 6. The reason is the number of household on these feeders. It should be mentioned that, despite such voltage drop, such voltage profile is acceptable for Danish network. Since the "Velander" method is used for load modeling in this study, the voltage profiles obtained from simulations include more extremes comparing to the real situation. In reality, the voltage profiles in the grid have lower deviation and the voltage drop is also less than what is shown here.

2) CASE II: Optimization without grid support

In this case, it is assumed that the PEVs are considered as loads. PEVs are charged during the night time, using the smart charging algorithm, as presented in Fig. 2.15. During the daytime, PEVs can only be used for positive balancing (from grid to vehicle). The goal of the optimization-based simulation is to find the optimal number and location of PV panels considering the new PEV loads. Typically, PEVs are under charge during the night hours, where the household demand is normally minimal. However, connection of a large number of PEVs to the feeder imposes a significant amount of load and leads to a significant voltage drop. To overcome this issue, the charging algorithm presented in Fig. 2.15 is utilized. The lower and upper SoC of PEVs' batteries are 20% and 90%.

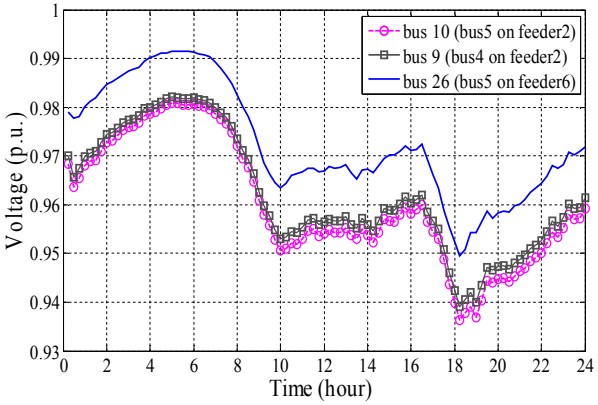

Fig. 2.17. Voltage profile of grid critical buses (no PV panels and no PEV).

3) CASE III: Optimization considering grid support

CASE III is similar to CASE II, except that the PEVs are utilized for V2G purposes (both positive and negative balance). So, CASE III contains the features of the

proposed method in section II. Considering customer's driving requirements, the lower limit of SoC is set to 35%, while the upper limit is 90% for night time charging, similar to CASE II.

4) CASE IV: Optimization considering grid support

Case IV is similar to case III. However, in order to increase the available PEV capacity, it is assumed that the grid operator is allowed to limit the upper limit of SoC for night-time charging to 50%. In such case, the available PEV storage for the daytime is higher.

2.5.2.2 Optimization Results

In this section, simulation results of CASE II, CASE III, and CASE IV are presented. The number of PEVs in the grid was increased gradually to have the maximum PEV penetration. Here, the results with 16 PEVs (10% PEV penetration) and 40 PEVs (25% penetration) in the grid are presented. The optimization results are shown in Table 2–10. To ease the comparison, the total number of PV panels for each case study is presented in Fig. 2.18 as well. Considering the total number of panels for each case, the effectiveness of the proposed algorithm can be realized. Activating the negative balance option (i.e. discharging PEVs for grid support), for both CASE III and CASE IV, has led to a higher number of panels in the grid. Besides, in CASE IV where the grid operator is allowed to limit the maximum charge of batteries (maximum 50% charging for the night time in this study), the number of panels has increased compared to CASE III. Such increase can be realized both with 10% PEV penetration, and with 25% PEV penetration, although the rate of increase is not the same. The reason for different rates is the fact that the placement of PEVs on different buses and the number of PEVs on different buses are not similar for the two cases. The maximum increase in the number of panels is in CASE IV with 40 PEVs in the grid (205 panels), which shows more than 32.7% increase compared to CASE II (138 panels). Since each panel's nominal capacity is 3 kW, such increase is equal to 201 kW more PV panels.

2.5.2.3 Analysis of PEV Impact

To show the impact of PEVs on the voltage profile at different buses, voltage profile of bus10 in Fig. 2.4 (bus5 on feeder2), is depicted in Fig. 2.19 for CASE II and CASE IV. As mentioned earlier, bus10 is the worst bus of the system. The role of PEVs for both negative and positive balance is also demonstrated in Fig. 2.19. In CASE II, the PEV is fully charged during the night, whereas in CASE IV the PEV charging is limited to 50%. The difference in settings causes the voltage difference between the two cases as well. PEV is on the road around 7:30 until 8:00, and it loses part of its charge. During the day time, as the solar irradiation increases, the PEV battery starts charging until around 14:00. However, after this time, although the solar power is still high, the battery reaches its maximum capacity (90 %) and

cannot participate in positive balance. This causes an increase in voltage. The PEV is on the road around 17:30 until 18:00 as well. As PEV becomes idle in the evening, it starts supporting the grid in CASE IV. The provided support by PEVs in this scenario is quite significant, and it clearly elevates the voltage profile of the bus. Besides, despite the higher PV penetration in CASE IV compared to CASE II (32.7% higher as mentioned above), the algorithm keeps voltage deviation in the grid less than 10%.

Table 2–10. Number of PV panels on grid buses of Fig. 2.4.

	case II		**case III**		**case IV**	
Bus	***10% (16PEV)***	***25% (40PEV)***	***10% (16PEV)***	***25% (40PEV)***	***10% (16PEV)***	***25% (40PEV)***
1	2	2	2	3	2	3
2	6	6	6	7	8	9
3	1	1	3	4	3	6
4	4	4	4	5	4	7
5	3	3	4	4	4	4
6	6	6	6	6	6	7
7	9	9	10	12	11	12
8	2	2	3	5	6	10
9	4	4	4	6	6	7
10	1	1	2	4	4	6
11	3	3	5	8	6	8
12	10	10	10	10	10	10
13	4	4	5	6	5	8
14	2	2	3	5	4	6
15	6	6	6	6	6	6
16	8	8	9	10	10	10
17	8	8	9	9	9	10
18	8	8	8	8	8	8
19	10	10	10	10	10	10
20	8	8	8	8	8	8
21	8	8	8	8	8	8
22	5	5	6	8	7	11
23	6	6	7	8	8	9
24	8	8	8	8	8	10
25	5	5	5	6	6	8
26	1	1	1	3	2	4
Total	138	138	152	177	169	205

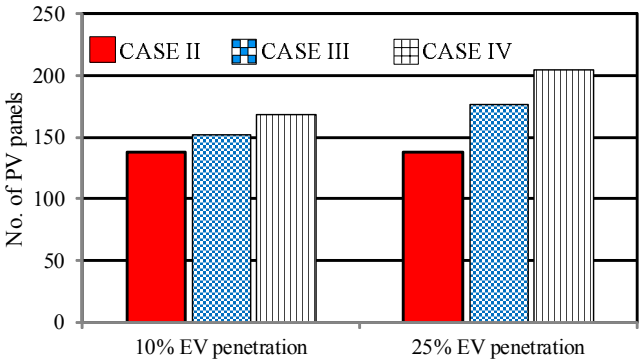

Fig. 2.18. Number of PV panels in different cases.

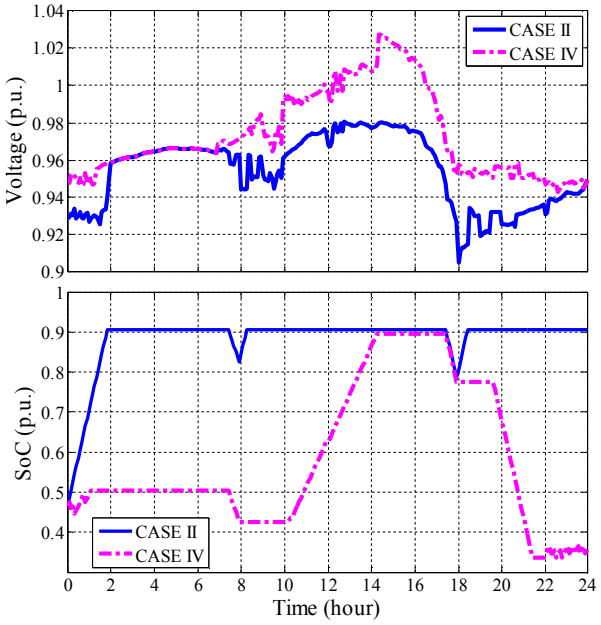

Fig. 2.19. Voltage profile and SoC for bus 10: CASE II and CASE IV.

Fig. 2.20 compares the voltage profile of bus 10, and the SoC of PEV for this bus, for CASE III and CASE IV. For CASE III the night charging is not limited, while it is limited to 50% for CASE IV. Therefore, voltage profile of bus 10 has lower values for night hours. On the other hand, when the PEV is idle during the day, the grid uses PEV storage for storing the solar production. However, since the available PEV storage is limited in CASE III compared to CASE IV, the PEV provides less grid support (positive balance) for the grid. Such scenario results in lower solar penetration, as presented in Table 2–10. Therefore, solar penetration is higher in CASE IV (205 panels) compared to CASE III (177 panels). Transformer power profile is presented in Fig. 2.21 for 40 PEVs (25% penetration) in the grid. Considering the results of CASE II as the base case, it can be seen that PEV

charging during the night time for CASE II occupies almost all the transformer capacity.

PV penetration provides extra power which can support the upper grid during the day. However, PV production doesn't exist during evening time, which the grid has a significant peak in demand. Therefore, the grid is forced to absorb power from the upper grid to support its consumption. Using PEVs for grid support, the excess available energy can be stored in PEV batteries during the daytime. The stored energy can then be used during the evening to respond to the peak demand of the grid. Such opportunity provides a great flexibility for the grid to provide some extra power to the upper grid, as well as dealing with its peak demand problem.

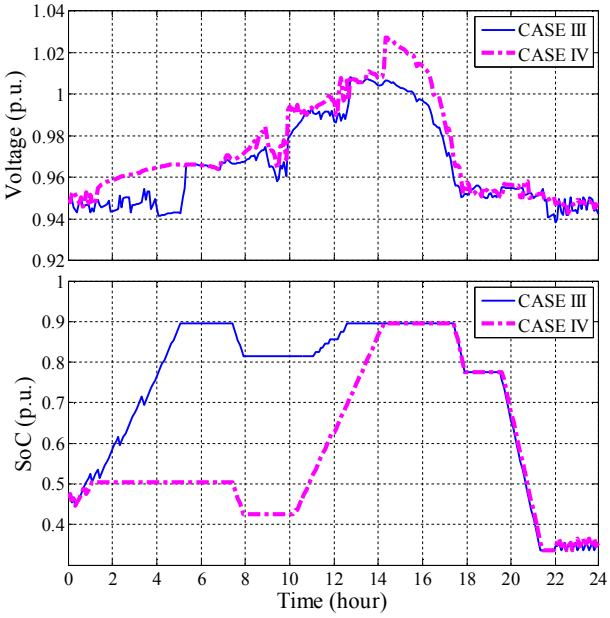

Fig. 2.20. Voltage profile and SoC for bus 10: CASE III and CASE IV.

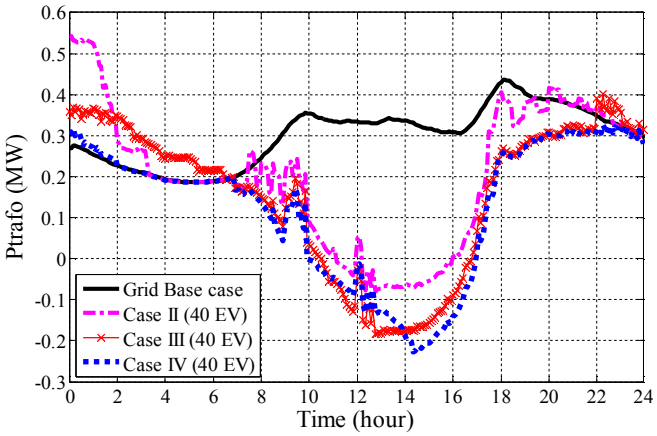

Fig. 2.21. Transformer power profile for different cases.

2.6. SUMMARY

The modeling details of PV panels and electric vehicles (EVs) are discussed in this chapter. Different studies have been applied to demonstrate the impact of PV panels and EVs on distribution networks. Besides, different charging algorithms are proposed in order to effectively deal with the impact of EVs on distribution neworks. On the other hand, different optimization methods are proposed and demonstrated to quantify the impact of distribution networks for providing ancillary service for the upper networks. Studies clarify the potential of low voltage (LV) distribution netwroks im providing support for the upper network (medium voltage and high voltage network).

CHAPTER 3. A NEW AGGREGATION METHOD FOR DISTRIBUTION NETWORKS

In this chapter, an aggregation method is proposed for distribution netwroks. The general concept of the method is based on the concepts of electric circuits. Applying the method requires certain assumptions, which are valid assumptions for distribution networks. Besides, a new solution is proposed for simplifying the calculations of parallel impedances. The proposed method simplifies the circuit and reduces the calculation time, while the error of the method is ignorable.

As a case study, the proposed aggregation method is applied to a Danish residential distribution network. Different scenarios have been defined and simulated to demonstrate the validity of the proposed method. The role of PV panels and electric vehicles (EVs) is also evaluated.

3.1. INTRODUCTION

Customers are getting more interested in installing PV panels, due to constant reduction in the price of PV panels, as well as interesting incentive policies by governments [31]. Furthermore, the increasing interest in the electric vehicles (EVs) and other new electric loads will change the customer characteristics and their power profile. These new changes in customer characteristics might lead to operating issues for the grid, such as voltage deviations and capacity issues [50],[62]. However, having such customers with the capability of providing power and energy for the electrical grid leads to new opportunities for the system operators, since the available power production of customers can be used for grid support [69]- [79]. On the other hand, utilizing the customers' potential in the grid requires an accurate measurement of the grid operating conditions. This would be a challenging and time-consuming task for the grid operators, considering the significant number of customers and feeders in the grid, especially in the low voltage (LV) grid. A typical medium voltage (MV) transformer supplies a certain number of distribution transformers through the MV bus-bar and medium voltage feeders. Each distribution transformer is connected to a significant number of customers through distribution

lines. In Danish distribution systems, each transformer has normally 4 to 7 feeders to feed its customers. The number of customers on each feeder varies, depending on the distance of the customers from the transformer, the type of the area (residential, commercial, etc.), and the demand of customers [21], [25]. Analyzing and controlling such complicated network in real time is highly challenging for system operators. Therefore, aggregation methods help distribution system operators (DSOs) to quickly realize the grid extra capacity under different operating conditions, as well as grid bottlenecks, and hence avoiding the requirement for continuously checking every customer of the grid. Most of the proposed aggregation methods so far deal with medium voltage and high voltage power system, and their main focus is on planning stage of the system. A common aggregation method, proposed in [80]- [83], is known as the Ward-type method. This method ignores unnecessary elements in power system, and also assumes that the system has no nonlinearity. Based on this method, some of the lines could be ignored in the equivalent model of these approaches [86]. The main drawback of this approach is that it is hard to aggregate the external generators [86]. In recent works, bus aggregation techniques have been the main focus for simplification of the power system [85], [86]. These methods use an equivalent Power Transfer Distribution Factor (PTDF) matrix, based on the dc-network equivalent of the system. However, the error of these aggregated models is considerable compared to the original network, even for the base case scenario [86]. Also, these methods are computationally complex. In [86], the network simplification problem is defined as a quadratic optimization problem. However, this method requires the definition of a proper objective function, as well as different constraints, which is complicated and computationally troublesome.

All the methods mentioned above are defined and applied for planning stage of large scale high voltage power systems. There is not much work on simplification and aggregation methods for LV systems. As one of the few works in this regard, an equivalent model of the low voltage grid is presented in [89]. This model, which is based on the impedance matrix of the system, is used for voltage control purposes. A Thevenin equivalent of the grid from the PV point of connection is proposed in the model [87]. However, the Thevenin model of the grid is different for every single PV in the grid. Also, the equivalent model changes for each PV from time to time. Ref [88] proposes a voltage control method based on X/R estimation of the network. The method uses Recursive Least Square (RLS) method for determining and identifying the equivalent circuit parameters. It requires online identification of the X/R ratio of the system, and uses Kalman filter for the estimation. Also, a ‘dynamic boundary technique’ is proposed in [89] for obtaining the equivalent of distribution systems, which is based on ‘Extended Ward method’ [90].

3.2. PROPOSED AGGREGATION METHOD

The main idea behind the proposed method is based on the fundamental concepts of the electric circuits, and operating conditions of distribution systems. The proposed method consists of two steps: a feeder-level aggregation, and a transformer-level aggregation. Such model would be very convenient, especially for controlling the extra capacity of distribution grid under different operating conditions, and for providing regulation power for the upper network.

3.2.1. FEEDER-LEVEL AGGREGATION

In this step, all the loads of each feeder are moved to the ending bus of the feeder. In general, such change would create a worst case scenario of each feeder.

For a feeder with 'k' buses, the voltage drop across the ending bus of each feeder in the original grid can be calculated as in (3.1).

$$\Delta V_i = \Delta V_{1i} + \Delta V_{2i} \tag{3.1}$$

where:

$$\begin{cases} \Delta V_{1i} = Z_{1(i)} * I_{1(i)} \\ \Delta V_{2i} = Z_{2(i)} * I_{2(i)} \end{cases} \tag{3.2}$$

Since the distribution grid normally has a radial configuration, the buses of each feeder are connected in a consecutive order, i.e. each bus is normally connected to its upper bus. However, having more than one bus connected to an upper bus is not unusual. Therefore, the voltage drop is divided into two equations, as shown in (3.2). Here, $Z_1(i)$ is a matrix which represents the impedance of the consecutive bus connections for feeder 'i', and matrix $I_1(i)$ represents the current in the same impedance, as presented in (3.3). For non-consecutive connections which are not covered by $Z_1(i)$ and $I_1(i)$, matrices $Z_2(i)$ and $I_2(i)$ are defined, as presented in (3.4).

$$\begin{cases} Z_{1(i)} = [Z_{T1(i)}, Z_{12(i)}, Z_{23(i)}, \ldots, Z_{(k-1)(k)(i)}] \\ I_{1(i)}{}^{T} = [I_{T1(i)}, I_{12(i)}, I_{23(i)}, \ldots, I_{(k-1)(k)(i)}] \end{cases} \tag{3.3}$$

$$\begin{cases} Z_{2(i)} = [Z_{13(i)}, \ldots, Z_{1k(i)}, Z_{24(i)}, \ldots, Z_{2k(i)} \ldots, Z_{(k-2)(k)(i)}] \\ I_{2(i)}{}^{T} = [I_{13(i)}, \ldots, I_{1k(i)}, I_{24(i)}, \ldots, I_{2k(i)} \ldots, I_{(k-2)(k)(i)}] \end{cases} \tag{3.4}$$

In these equations, the notion "T_1" represents the connection between the transformer and the first bus of the feeder. The impedance '*Z(k-1)(k)(i)*' represents the connection between bus '*k-1*' and bus '*k*', and '*I(k-1)(k)(i)*' is the current flowing between the two buses. As mentioned, for the aggregation purpose, all the loads of the feeder are moved and located at the very end of the feeder. The equivalent impedance of the feeder, Z_{eq}, can be calculated using impedance matrices, $Z_1(i)$ and $Z_2(i)$. For a feeder with consecutive bus connections, the equivalent impedance can be easily calculated by summing up all the impedances between the buses, as expressed in (3.26). However, for feeders with both consecutive and non-consecutive connections, calculating the equivalent impedance depends on the feeder configuration.

Applying such change to the feeders, the voltage drop among feeder '*i*' can be calculated, as expressed in (3.5):

$$\Delta V_i(agg) = Z_{eq\_i} * (I_1 + I_2 + ... + I_k) \qquad (3.5)$$

Comparing (3.1) and (3.5), it can be easily realized that putting all the loads at the end of the feeder will increase the voltage deviation, i.e. $\Delta V_i > \Delta V$. Therefore, aggregating all the loads at the end of the feeder is a conservative approach. By other words, such aggregation will easily catch all the potential voltage issues in the feeder. Therefore, the equivalent of each of the grid feeders can be obtained.

3.2.2. AGGREGATION OF ALL FEEDERS

Applying step1 to each of the grid feeders will provide the aggregated model on feeder level. Having such model, step2 will aggregate all the feeders into one feeder. The voltage across the aggregated load of different feeders depends on the voltage drop of each feeder. The voltage drop of each feeder is a function of the feeder current, and the impedance of the lines. However, based on voltage standards and measures, the voltage across different loads in the grid should not violate a certain value (5%) [92]. Therefore, the maximum difference between the voltage of a strong bus and the voltage of a weak bus of the grid is around 5%. On the other hand, by applying step1, all the loads are located at the weak bus of each feeder (end of each feeder). Therefore, the voltage difference between the loads of different feeders would be around 5%.

3.3. IMPEDANCE CALCULATION

In distribution networks, the R/X ratios of different feeders are almost similar. In such case, the following simplified method gives accurate calculation for parallel impedances. The mathematical proof of the proposed method is presented here.

3.3.1. SIMPLE CASE

3.3.1.1 Hypothesis

The hypothesis can be stated in two ways, as mentioned in the following statements.

Statement1: If a number of impedances are connected in parallel, and if the R/X ratio of all the impedances is similar, the resistance and reactance values can be decoupled and treated separately.

Statement2: If a certain number of impedances are connected in parallel, and the impedance angle is the same for all the impedances, the resistance and reactance values can be decoupled and treated separately.

3.3.1.2 Mathematical proof

Based on circuit basic laws, the equivalent impedance of circuit in Fig. 3.1 should be calculated as follows:

$$\frac{1}{Z_{eq}} = \frac{1}{Z_1} + \frac{1}{Z_2} \tag{3.6}$$

In which:

$$\begin{aligned} Z_1 &= R_1 + jX_1 \;\; ; \; \frac{R_1}{X_1} = n \\ Z_2 &= R_2 + jX_2 \;\; ; \; \frac{R_2}{X_2} = n \end{aligned} \tag{3.7}$$

To have a more general case, impedance number 2 is considered to be *k* times bigger than impedance number 1. Eq.(3.8) and (3.9) expresses the general case.

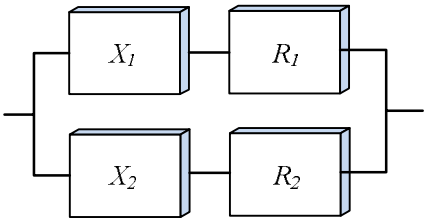

Fig. 3.1. A circuit with two parallel impedances.

$$Z_2 = k * Z_1 \Rightarrow \begin{cases} R_2 = k * R_1 \\ X_2 = k * X_1 \end{cases} \qquad (3.8)$$

$$for\ Z_1 \rightarrow \begin{cases} X_1 = \beta \\ R_1 = nX_1 = n\beta \end{cases} \qquad for\ Z_2 \rightarrow \begin{cases} X_2 = k * X_1 = k\beta \\ R_2 = k * R_1 = kn\beta \end{cases} \qquad (3.9)$$

To calculate the equivalent impedance, it's easier to solve the problem with the admittance values.

$$y_1 = \frac{1}{Z_1} = \frac{R_1}{(R_1^2 + X_1^2)} - j\frac{X_1}{(R_1^2 + X_1^2)} \Rightarrow y_1 = \frac{n}{(n^2+1)\beta} - j\frac{1}{(n^2+1)\beta}$$

$$y_2 = \frac{1}{Z_2} = \frac{R_2}{(R_2^2 + X_2^2)} - j\frac{X_2}{(R_2^2 + X_2^2)} \Rightarrow y_2 = \frac{n}{(n^2+1)k\beta} - j\frac{1}{(n^2+1)k\beta} \qquad (3.10)$$

Having these values, the admittance can be calculated.

$$y_{eq} = y_1 + y_2 = \frac{(k+1)n}{(n^2+1)k\beta} - j\frac{(k+1)}{(n^2+1)k\beta} \Rightarrow Z_{eq} = \frac{\frac{(k+1)n}{(n^2+1)k\beta} + j\frac{(k+1)}{(n^2+1)k\beta}}{\frac{(k+1)^2(n^2+1)}{(n^2+1)^2(k\beta)^2}} \Rightarrow \qquad (3.11)$$

$$Z_{eq} = (\frac{kn}{k+1} * \beta) + j(\frac{k}{k+1} * \beta) \Rightarrow \begin{cases} R_{eq} = \frac{kn}{k+1} * \beta \\ X_{eq} = \frac{k}{k+1} * \beta \end{cases} \qquad (3.12)$$

Considering the proposed change in Fig. 3.2, the equivalent resistance and reactance are calculated in Eq.(3.13).

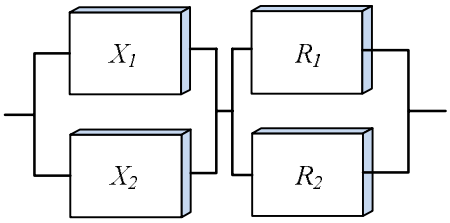

Fig. 3.2. The proposed replacement for circuit in Fig. 3.1.

$$\frac{1}{R_{eq}} = \frac{1}{R_1} + \frac{1}{R_2} = \frac{1}{n\beta} + \frac{1}{kn\beta} = \frac{k+1}{kn\beta} \Rightarrow R_{eq} = \frac{kn}{k+1}\beta$$

$$\frac{1}{X_{eq}} = \frac{1}{X_1} + \frac{1}{X_2} = \frac{1}{\beta} + \frac{1}{k\beta} = \frac{k+1}{k\beta} \Rightarrow X_{eq} = \frac{k}{k+1}\beta \quad (3.13)$$

As can be seen, the equivalent impedance values of the proposed configuration are equal to the equivalent impedance of the circuit, obtained in Eq.(3.12).

3.3.2. GENERAL CASE

3.3.2.1 Hypothesis

For a distribution system, the number of feeders connected to each transformer is limited. Normally, each distribution transformer feeds between 4 to 7 feeders. The following statement can be applied for parallel circuits with limited number of branches.

Statement: If a certain number of impedances with different R/X ratios are parallel with each other, with R bigger than X in all the impedances, then the circuit in Fig. 3.3 can be simplified to Fig. 3.4.

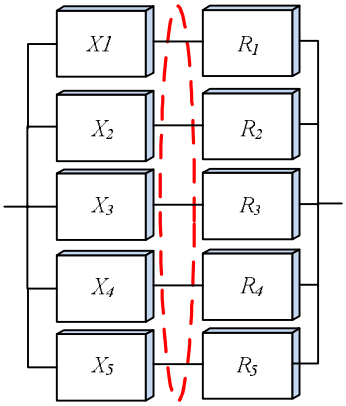

Fig. 3.3. Parallel connection of 5 impedances.

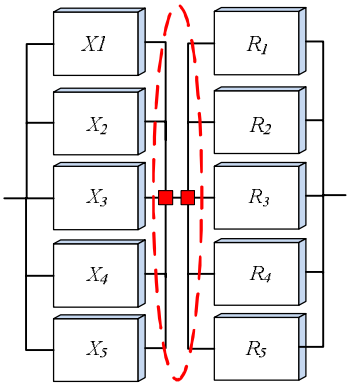

Fig. 3.4. The proposed replacement for Fig. 3.3.

3.3.2.2 Proof

Considering Fig. 3.3, the impedances of branches can be stated as follows:

$$for\ Z_1 \rightarrow \begin{cases} X_1 = \beta \\ R_1 = nX_1 = n\beta \end{cases} \qquad for\ Z_2 \rightarrow \begin{cases} X_2 = 2*X_1 = 2\beta \\ R_2 = 2*R_1 = 2n\beta \end{cases}$$

$$for\ Z_3 \rightarrow \begin{cases} X_3 = 3*X_1 = 3\beta \\ R_3 = 3*R_1 = 3n\beta \end{cases} \qquad for\ Z_4 \rightarrow \begin{cases} X_4 = 4*X_1 = 4\beta \\ R_4 = 4*R_1 = 4n\beta \end{cases}$$

$$for\ Z_5 \rightarrow \begin{cases} X_5 = 5*X_1 = 5\beta \\ R_5 = 5*R_1 = 5n\beta \end{cases}$$

(3.14)

The admittance of each of the branches is calculated in Eq.(3.15)–(3.19).

$$y_1 = \frac{1}{Z_1} = \frac{R_1}{(R_1^2 + X_1^2)} - j\frac{X_1}{(R_1^2 + X_1^2)}$$
$$y_1 = \frac{n\beta}{((n\beta)^2 + \beta^2)} - j\frac{\beta}{((n\beta)^2 + \beta^2)} \Rightarrow y_1 = \frac{n}{(n^2+1)\beta} - j\frac{1}{(n^2+1)\beta} \qquad (3.15)$$

$$y_2 = \frac{1}{Z_2} = \frac{R_2}{(R_2^2 + X_2^2)} - j\frac{X_2}{(R_2^2 + X_2^2)} \Rightarrow y_2 = \frac{n}{(n^2+1)*2\beta} - j\frac{1}{(n^2+1)*2\beta} \qquad (3.16)$$

$$y_3 = \frac{1}{Z_3} = \frac{R_3}{(R_3^2 + X_3^2)} - j\frac{X_3}{(R_3^2 + X_3^2)} \Rightarrow y_3 = \frac{n}{(n^2+1)*3\beta} - j\frac{1}{(n^2+1)*3\beta} \tag{3.17}$$

$$y_4 = \frac{1}{Z_4} = \frac{R_4}{(R_4^2 + X_4^2)} - j\frac{X_4}{(R_4^2 + X_4^2)} \Rightarrow y_4 = \frac{n}{(n^2+1)*4\beta} - j\frac{1}{(n^2+1)*4\beta} \tag{3.18}$$

$$y_5 = \frac{1}{Z_5} = \frac{R_5}{(R_5^2 + X_5^2)} - j\frac{X_5}{(R_5^2 + X_5^2)} \Rightarrow y_5 = \frac{n}{(n^2+1)*5\beta} - j\frac{1}{(n^2+1)*5\beta} \tag{3.19}$$

Therefore, we can calculate the equivalent admittance and the equivalent impedance.

$$y_{eq} = y_1 + y_2 + y_3 + y_4 + y_5 \Rightarrow y_{eq} = \frac{n(1+\frac{1}{2}+\frac{1}{3}+\frac{1}{4}+\frac{1}{5})}{(n^2+1)\beta} - j\frac{(1+\frac{1}{2}+\frac{1}{3}+\frac{1}{4}+\frac{1}{5})}{(n^2+1)\beta} \tag{3.20}$$

Considering that: $\left(1+\frac{1}{2}+\frac{1}{3}+\frac{1}{4}+\frac{1}{5}\right)=\frac{137}{60}$, we can write:

$$Z_{eq} = \frac{1}{y_{eq}} \Rightarrow Z_{eq} = (\frac{60}{137}*n\beta) + j(\frac{60}{137}*\beta) \Rightarrow \begin{cases} R_{eq} = \frac{60}{137}*n\beta \\ X_{eq} = \frac{60}{137}*\beta \end{cases} \tag{3.21}$$

By applying the proposed configuration, the circuit will look like Fig. 3.4. Considering this figure, the equivalent resistance and reactance can be calculated.

$$\frac{1}{R_{eq}} = \frac{1}{R_1} + \frac{1}{R_2} + ... + \frac{1}{R_5} \Rightarrow \frac{1}{R_{eq}} = \frac{1}{n\beta} + \frac{1}{2n\beta} + ... + \frac{1}{5n\beta} \Rightarrow R_{eq} = \frac{60}{137}n\beta \tag{3.22}$$

$$\frac{1}{X_{eq}} = \frac{1}{X_1} + \frac{1}{X_2} + ... + \frac{1}{X_5} \Rightarrow \frac{1}{X_{eq}} = \frac{1}{\beta} + \frac{1}{2\beta} + ... + \frac{1}{5\beta} \Rightarrow X_{eq} = \frac{60}{137}\beta \tag{3.23}$$

As can be seen, the proposed change provides the exact answer, while it is much simpler and its calculation time is much less.

3.3.3. CASE STUDY FOR IMPEDANCE CALCULATION

To prove the results, the equivalent impedance of the original circuit and the proposed simplified circuit are calculated and compared for a wide range of R/X ratios, and for different number of branches. For a certain number of branches, the R/X ratios of different branches are changed to realize the accuracy of the proposed simplified model. Considering the normal R/X ratio in distribution systems, it could be seen that this ratio is normally bigger than 2 (R/X>2). The calculations and comparisons are presented below, considering this ratio. Fig. 3.5 presents different R/X ratios for a 4-branch circuit. To keep the figure clear, only some of the R/X samples are presented in this figure. Each line in Fig. 3.5 presents the R/X values of different branches, comparing to other branches. Table 3–1 presents the percentage error of the proposed model. The same calculation is applied for circuits with 5 branch, 6 branch, 7 branch, 8 branch, 9 branch, and 10 branches. The results are presented in tables below. The error of the proposed method for different number of branches and with different R/X ratios for each circuit is presented in Fig. 3.8. As can be seen, the error is less than 0.3% in the worst case.

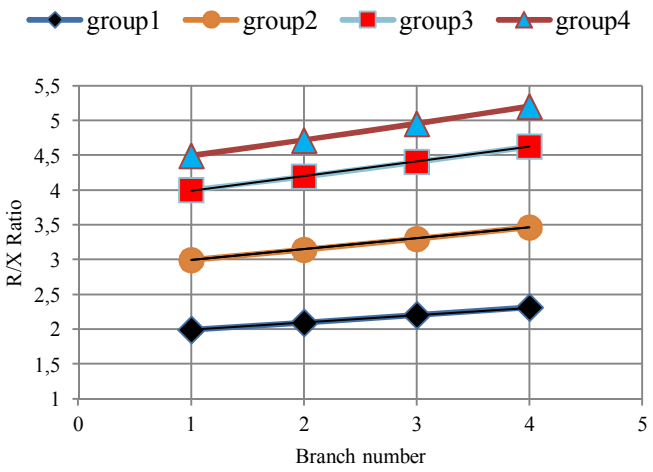

Fig. 3.5. R/X ratios for a 4-branch circuit

Table 3–1. Error of the proposed model in percentage for a 4-branch circuit

Group	R1/X1	R2/X2	R3/X3	R4/X4	% R_error	% X_error
1	2	2,1	2,205	2,31	0,05285	0,24376
2	2,1	2,205	2,315	2,431	0,04875	0,24785
3	2,2	2,31	2,425	2,5467	0,04508	0,25151
4	2,3	2,41	2,536	2,66	0,04179	0,25479
5	2,4	2,52	2,646	2,7783	0,03883	0,25774
6	2,5	2,62	2,756	2,89	0,036158	0,260401
7	2,6	2,73	2,866	3,0098	0,033742	0,262809
8	2,7	2,83	2,976	3,1256	0,031551	0,264992
9	2,8	2,94	3,087	3,2413	0,029559	0,266976
10	2,9	3,04	3,197	3,3571	0,027744	0,268785
11	3	3,15	3,3	3,47	0,026086	0,270436

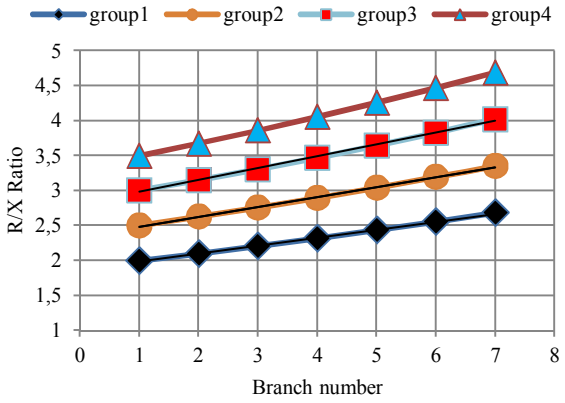

Fig. 3.6. R/X ratios for a 7-branch circuit

Table 3–2. Error of the proposed model in percentage for a 7-branch circuit

	R1/ X1	R2/ X2	R3/ X3	R4/ X4	R5/ X5	R6/ X6	R7/ X7	% R_error	% X_error
1	2	2,1	2,205	2,31	2,43	2,55	2,68	0,15	0,792
2	2,5	2,62	2,756	2,89	3,038	3,19	3,35	0,102	0,84
3	3	3,15	3,3	3,47	3,646	3,83	4,02	0,0733	0,868
4	3,5	3,67	3,86	4,05	4,25	4,467	4,69	0,055	0,887

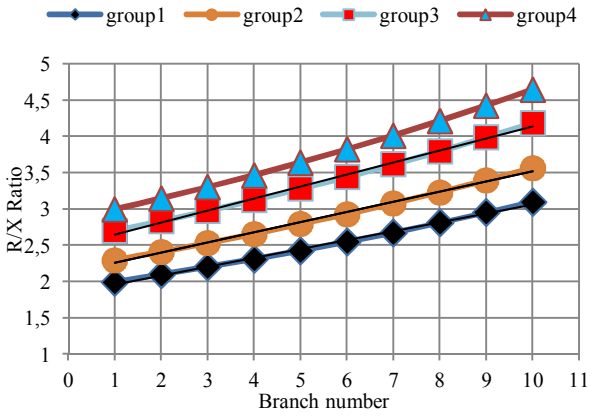

Fig. 3.7. R/X ratios for a 10-branch circuit

Table 3–3. Error of the proposed model in percentage for a 10-branch circuit

	1	2	3	4
R1/X1	2	2,3	2,7	3
R2/X2	2,1	2,41	2,83	3,15
R3/X3	2,205	2,536	2,976	3,3
R4/X4	2,31	2,66	3,1256	3,47
R5/X5	2,43	2,795	3,28	3,646
R6/X6	2,55	2,935	3,446	3,83
R7/X7	2,68	3,082	3,618	4,02
R8/X8	2,81	3,236	3,8	4,2
R9/X9	2,95	3,399	3,99	4,43
R10/X10	3,1	3,569	4,19	4,65
% R_error	0,27	0,215	0,161	0,133
% X_error	1,64	1,707	1,75	1,78

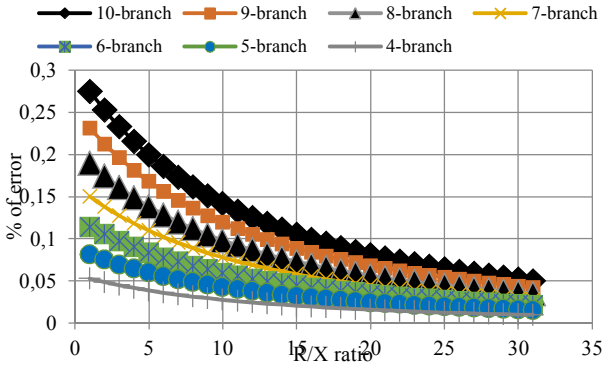

Fig. 3.8. Percentage of error for different circuits.

It can be seen from the results that the proposed model can be easily replaced with the main circuit. The error of such replacement, as presented in Table 3–1, Table 3–2, and Table 3–3, is ignorable.

Note 1: From the results in the tables, for a circuit with a certain number of branches, as the R/X ratios increase, the error of resistance decreases, while the error in reactance increases.

Note 2: The proposed method was applied to the circuits with different number of branches. As the number of parallel branches increases to 30, the error in resistance estimation is still below 1%. However, the error in reactance increases sharply. In fact, the error in estimating reactance increases to more than 10%, as the number of parallel branches increases to 30.

Note 3: It should be mentioned that all the results and discussions presented here are for the cases where (R/X >1). If (R/X <1), the same results can be inferred. The only difference is that the results explained for resistance would be true for reactance, and vice versa.

3.4. AGGREGATION TECHNIQUE: CASE STUDY

To evaluate the validity of the proposed method, the method is applied to a case study. PV panels and electric vehicles are also considered in this study to demonstrate the viability of the method in different circumstances. Also, EVs are considered as aactive player in the study, i.e. EVs are allowed ti participate in grid support applications. The grid support strategy, details of the grid, the aggregation procedure, and simulation results of the study are presented in this section.

It should be noted that modeling of EVs and PV panels is similar to modeling details of Chapter 2. Also, the driving patterns of EVs are similar to the patterns presented in Chapter 2.

3.4.1. PROPOSED GRID SUPPORT STRATEGY

To enable the grid support feature in the network, it is assumed that the grid operator can use the EV battery capacity for grid support; either for discharging (V2G(-) in Fig. 3.10), or for charging (V2G(+) in Fig. 3.10). The EV can be used for grid support only if it is idle and connected to the grid. Also, the battery limits of the EV should allow charging or discharging of the EV. The minimum and maximum charging limits of the battery should be between 20% and 90%, due to battery lifetime issues [20]. Besides, the driving requirements of customer should be considered for determining battery's minimum state of charge (SOC).

Fig. 3.9 presents the proposed algorithm for the grid support. The algorithm calculates the grid operating limits in presence of PV panels. These operating limits act as an input for the "EV Block". The "EV Block" determines the role of EVs for the grid support. Then, the output of the "EV block" will be used for the "Grid Operation" block to determine grid operating indices in presence of EVs. The "EV

Block" checks the status of each EV and separates idle EVs from moving EVs, using EVs' distance profile (DP). For grid support application, it is assumed that when EV is idle, it is connected to the grid and can be utilized for grid support. The moving EVs cannot be used for grid support. Therefore, the algorithm only calculates their SOC based on the distance that each EV will move for that time interval. For idle EVs, the algorithm identifies the EV location, including EV's bus and EV's feeder. Then, the maximum voltage along the EV's feeder (Vmax), as well as the minimum voltage along the feeder (Vmin), will be determined for the time interval. These parameters are obtained considering the voltage values of different buses of the feeder. The algorithm checks these values with its predefined criteria, V_{max}*(upper)* and V_{min}*(lower)* in Fig. 3.10, and decides whether to utilize the EVs for grid support or not. In case of overvoltage in the feeder (due to power production of PV panels), the EVs will be used for storing the extra energy. If the voltage drops below a certain limit, then the algorithm utilizes the stored energy in the EV storage for supporting the grid.

There might be special cases through which both upper and lower voltage limits are violated. Such cases occur mainly in long and weak feeders. In such cases, the algorithm checks the distance between EV's bus and the feeder's buses which cause such voltage issues. If the EV is closer to the bus with the overvoltage problem, the algorithm uses the EV storage for positive balance, i.e. it charges the EVs. However, if the EV is closer to the bus with the undervoltage problem, the algorithm discharges the EV to support the grid (negative balance).

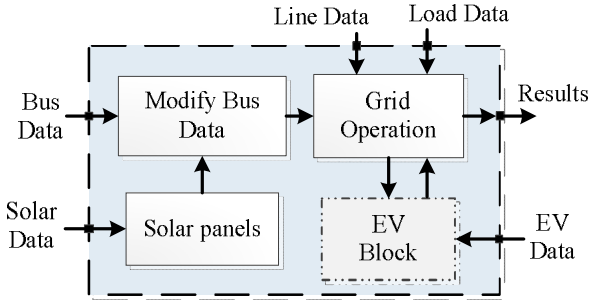

Fig. 3.9. Proposed algorithm for grid support applications

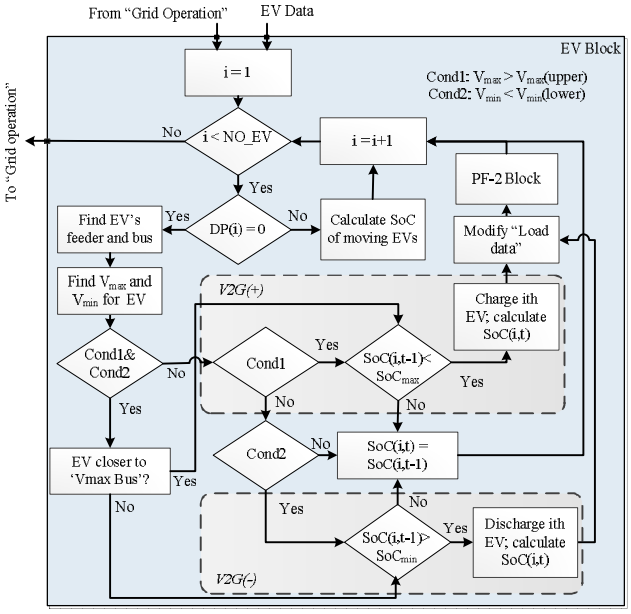

Fig. 3.10. Algorithm of the "EV Block" in Fig. 3.9.

3.4.2. CASE STUDY DETAILS

The system under discussion is a residential grid, which is fed by a 20kV/0.4kV, 630kVA transformer. The grid configuration is presented in Fig. 3.11. The number of households on each feeder is given in Table 3–4. The symbols of Fig. 3.11 are presented to depict the grid view, and do not define the number of households on each bus. The data of the cables are obtained using grid data presented in [16] 2 and Appendix A. Load profiles are obtained using "Velander method" [24]. The load power factor is assumed to be 0.95 [25]. The cable values presented in Table 3–4 are all in (p.u). The values of cables are transferred to (p.u.), with 0.4 kV as the base value of voltage, and 100 MVA as the base value of apparent power.

Table 3–4 Details of feeders, EVs, and grid cables.

Number of households on grid feeders						
Feeder	1	2	3	4	5	6
No. of household	20	33	27	28	17	42

Details of EVs					
	% of EVs	Battery (kWh)	Average consumption (Wh/km)	Charger power (kW)	Daily distance (km)
Commuter	80	30	150	7.2	40
Family car	20	30	150	7.2	25

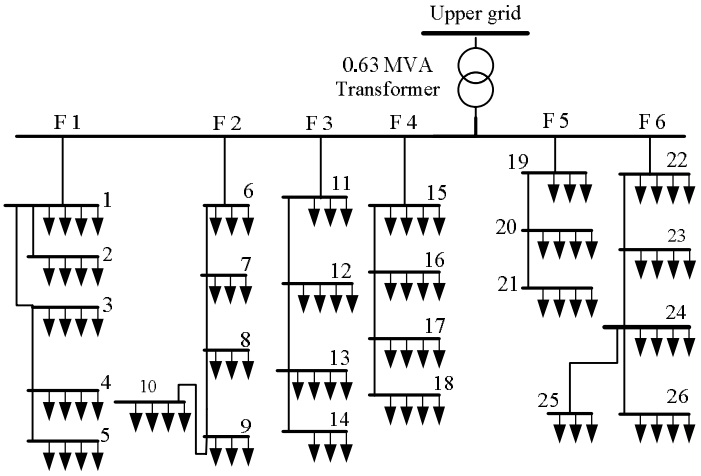

Fig. 3.11. Layout of Danish test system.

3.4.3. GRID AGGREGATED MODEL

The equivalent electric circuit for feeder1 of the original grid in Fig. 3.11 is presented in Fig. 3.12 (a). The equivalent circuit of the other feeders can be depicted similarly. From the DSO point of view, the grid customer is seen as a load with a certain demand in each time instant, i.e. DSO quantifies the loads based on their load profiles. Considering the fact that all the loads are connected in parallel in the distribution system, they would have similar voltage values at their point of connection (POC), with a small standard deviation [92]. Therefore, the difference between the power demands of different loads is reflected in the current. It should be noted that the distribution system is normally operated in a radial structure in Denmark. However, in some distribution grids, power switches are designed and implemented in the grid. The grid operators will use these switches under certain circumstances, which will change the grid configuration. In such cases, the aggregated model should be calculated for the new grid layout. Such case will not be challenging, considering the simplicity of the proposed method.

3.4.3.1 Step1: Aggregation of each feeder

To clarify the method, the details of applying the first step are presented for feeder1 of the grid in Fig. 3.11. Considering the electric circuit of feeder1 in Fig. 3.12 (a), the worst voltage drop along feeder1 can be obtained, using (3.24):

$$\begin{aligned}\Delta V_1 &= Z_{T1} * (I_1 + I_2 + I_3 + I_4 + I_5) \\ &+ Z_{13} * (I_3 + I_4 + I_5) + Z_{34} * (I_4 + I_5) + Z_{45} * I_5\end{aligned} \tag{3.24}$$

On the other hand, the voltage drop for the aggregated model of the feeder, presented in Fig. 3.12 (b), can be calculated using (3.25) and (3.26):

$$\Delta V_1(agg) = Z_{eq\_F1} * (I_1 + I_2 + ... + I_5) \qquad (3.25)$$

$$Z_{eq\_F1} = Z_{T1} + \left[Z_{12} \parallel \left(Z_{13} + Z_{34} + Z_{45} \right) \right] \qquad (3.26)$$

Considering Table 3–4, and based on the decomposition of resistance and reactance, the equivalent resistance of feeder1 is obtained in (3.27).

$$\left.\begin{aligned} R_{12} &= 24.96 \\ R_{bus1-5} &= R_{1-3} + R_{bus3-4} + R_{bus4-5} = 115.722 \\ R_{eq\_F1} &= (R_{12} \parallel R_{bus1-5}) + R_{T1} = 74.233 \ (p.u.) \end{aligned}\right\} \qquad (3.27)$$

By applying similar procedure, the equivalent reactance is obtained as X_{eq_F1} = 24.91 (p.u.).

By applying the same procedure for all the feeders, the equivalent parameters of all the feeders are obtained, as presented in Table 3–5.

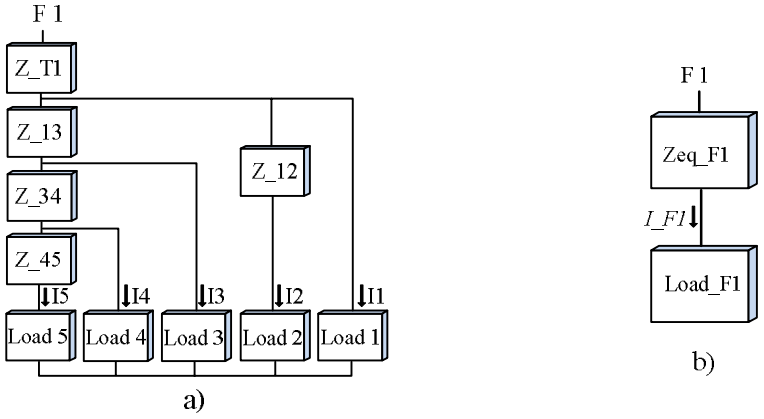

Fig. 3.12. Feeder1: a) electric equivalent circuit; b) aggregated model.

Table 3–5 Equivalent parameters of each feeder

	F1	**F2**	**F3**	**F4**	**F5**	**F6**
R_{eq}	74.233	92.43	86.67	77.223	116.73	61
X_{eq}	24.92	36.728	27.83	31.185	13.867	22.516

3.4.3.2 Step2: Aggregation of all Feeders

Having the aggregated model of each feeder, step2 will aggregate all the feeders into one feeder. By applying step2, Fig. 3.13 can be replaced by the circuit in Fig. 3.14. Considering Fig. 3.14, the impedances of the feeders are in parallel with each other. The proposed decomposition method in Section 3.3 is applied in this step as well. Therefore, the resistance and reactance terms of feeder impedance can be written, as expressed in (3.28) and (3.29), respectively.

$$\frac{1}{R_{eq}} = \frac{1}{R_{eq\_F1}} + \frac{1}{R_{eq\_F2}} + \frac{1}{R_{eq\_F3}} + ... + \frac{1}{R_{eq\_Fn}} \tag{3.28}$$

$$\frac{1}{X_{eq}} = \frac{1}{X_{eq\_F1}} + \frac{1}{X_{eq\_F2}} + \frac{1}{X_{eq\_F3}} + ... + \frac{1}{X_{eq\_Fn}} \tag{3.29}$$

By applying step2 to the case study in Fig. 3.11, the equivalent aggregated impedance of the grid is obtained, as in (3.30):

$$Z_{eq\_agg} = 14.7927 + j*4.055\,(p.u.) \tag{3.30}$$

In Fig. 3.14, the equivalent current, *I_eq*, can be obtained from (3.31):

$$I\_eq = I\_F1 + I\_F2 + I\_F3 + ... + I\_Fn \tag{3.31}$$

The calculation of resistance and reactance is based on the proposed decomposition. Fig. 3.15(a) presents the aggregated model for the grid in Fig. 3.11.

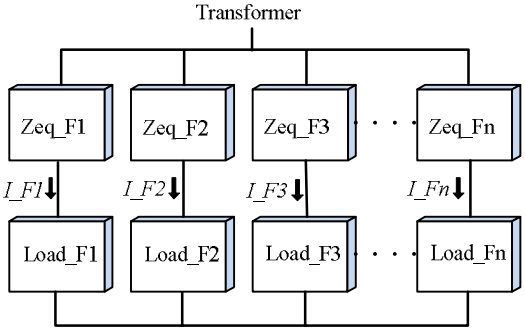

Fig. 3.13. Aggregated model of the grid on feeder level

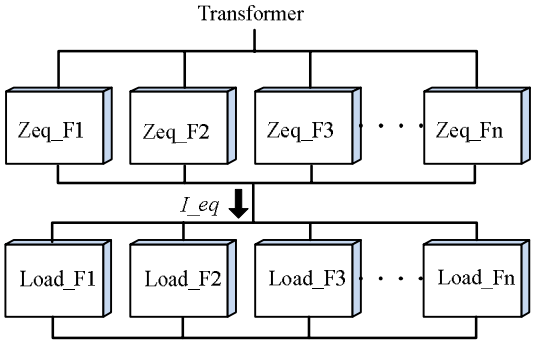

Fig. 3.14. Grid estimated model

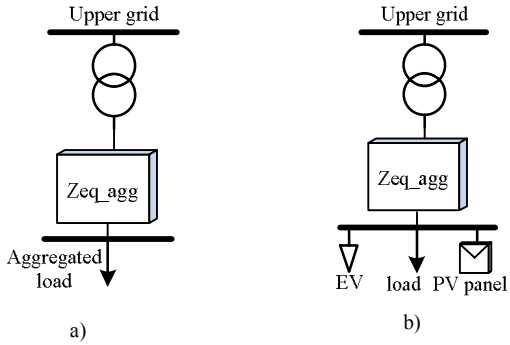

Fig. 3.15. Aggregated model of the grid: a) original grid; b) with PV and EV

3.4.3.3 The role of PV and EV

To evaluate the validity of the proposed method, the aggregated model was tested in presence of PV panels and EVs as well. For this purpose, an aggregated PV panel is added to the aggregated model. The overall model in this case is shown in Fig. 3.15 (b). The size of the PV panel is equal to the number of panels distributed among the original grid.

3.5. SIMULATION RESULTS

The validity of the proposed model is tested under different scenarios. The details of each scenario, as well as the simulation results, are presented in this section.

3.5.1. SCENARIO 1: BASE CASE

In this case, the grid existing condition is evaluated. Based on the number of households and the length of the lines, steady state analysis clarifies that bus10 is the worst grid bus, in terms of voltage profile. The voltage profile of bus10 is presented

in Fig. 3.16. The voltage profile of the aggregated model is also presented in this figure for comparison. The difference of the two voltage profiles of Fig. 3.16 is presented in Fig. 3.17 as the error of the aggregated model, compared to the original grid. It can be seen from Fig. 3.17 that the error of the aggregated model is always less than 0.009 (p.u.). Based on the error values in Fig. 3.17, the average error in voltage estimation is 0.0053 (p.u.) for a 24-hour period. Fig. 3.18 presents the transformer power profiles of the original and aggregated model. Considering Fig. 3.18, the average error of transformer power profile is 1.54% for a 24-hour period. It is important to point that the transformer profile of aggregated model in this point is overestimated comparing to the original grid. Such overestimation represents less available capacity of transformer compared to the results of the original grid, as the transformer loading in this case is higher than the real case. As a result, the proposed aggregation will not jeopardize the transformer operating limits. The average error of the transformer profile is less than 1.5%. Table 3–6 presents the difference between the results of the original grid and the results of the proposed aggregated model. In Table 3–6, "$V_{error}(max)$" represents the maximum difference between the voltage of the aggregated bus and the voltage of bus10 from the original grid. In other words, this value shows the error of the aggregated model in capturing the voltage drop on the grid critical bus. Also, "$V_{error}(avg)$", the average voltage error, is obtained by comparison of the two voltages for a 24-hour period.

3.5.2. SCENARIO 2: ADDING PV PANELS TO THE GRID

Adding PV panels would change grid characteristic, as these energy sources provide power to the grid and change the power profile of the grid. Different number of PV panels was added to the grid. The distribution of panels in the grid is proportional to the number of houses on each feeder. The 'penetration level' of PV panels in this work represents the number of customers which install a 3-kW PV panel, compared to the total number of customers in the grid. To have a more realistic evaluation of the effect of PV panels, the simulations are performed for a summer day with high solar irradiation. Considering Table 3–6, the error of the aggregated model in presence of PV panels is always below 0.009 (p.u.), for different penetration levels of PV panels. For 100% PV penetration, the average error in voltage estimation is 0.0037 (p.u.) for a 24-hour period. As mentioned in scenario 1, bus10 is the worst bus in the grid. Therefore, the error of the model is obtained by comparing the voltage profile of aggregated bus with the voltage profile of bus10 in Fig. 3.11. Simulation results in Table 3–6 demonstrate that the error of the aggregated model is trivial, which verifies the validity of the model in presence of PV panels.

3.5.3. SCENARIO 3: IMPACT OF EVS ON THE GRID

In this scenario, the effect of EVs on the grid was simulated. Different number of EVs was added to the grid and simulated. In all the simulations with different number of EVs, 80% of EVs are commuters, while the rest of EVs are family cars,

as mentioned in Table 3–4. The power factor of EVs is assumed to be 1. Different penetration levels of EVs are considered in this case. The EV characteristics and their DP are explained in Section II. The number of EVs in different grid buses depends on the number of customers on the bus. Simulations are performed for different EV penetration levels up to 50% penetration, i.e. the case where half the customers own an EV. The power rating of all EVs is similar to the data in Table 3–4. In this scenario, the EV charging is limited to the night time, i.e. EVs will be charged during the night, between 22:00 until 07:00.

10% EV penetration: In this case, 16 EVs are distributed in the grid. Comparing the voltage deviations, it can be observed that the error of the aggregated model is less than 1% for voltage, as mentioned in Table 3–6.

25% EV penetration: Here, 40 EVs are distributed in the grid. From Table 3–6, for this scenario, the maximum voltage error, $V_{error}(max)$, is less than 1%, and the average voltage error, $V_{error}(avg)$, is less than 0.5%.

50% EV penetration: In this case, 80 EVs are located in the grid. Table 3–6 demonstrates that the maximum error on the voltage, $V_{error}(max)$, is 1.25%.

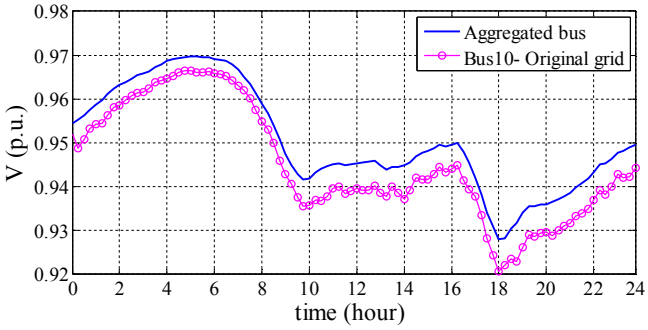

Fig. 3.16. Voltage profiles of the original and the aggregated model

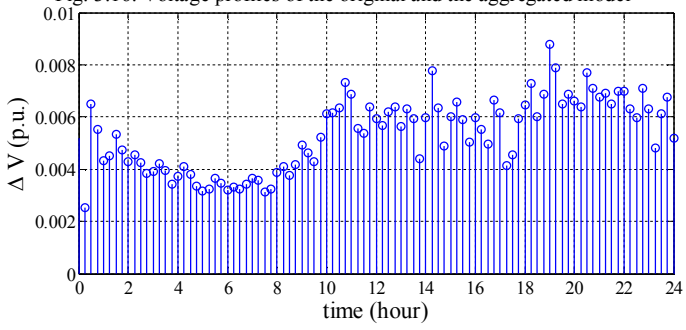

Fig. 3.17. Error of the voltage of the proposed model

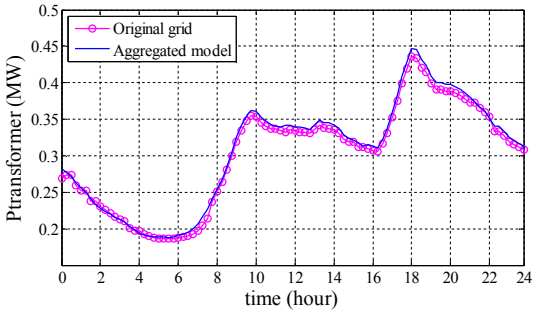

Fig. 3.18. Transformer power profile: original and the aggregated model

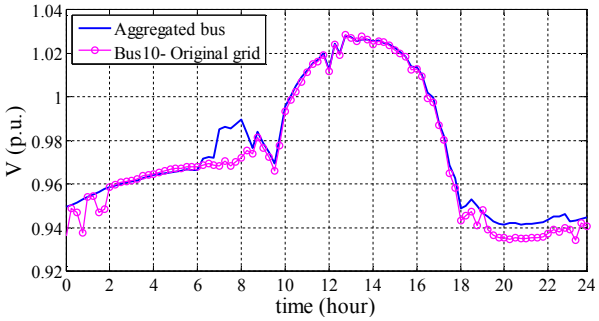

Fig. 3.19. Voltage of original grid and aggregated model (scenario 4)

Table 3–6 Simulation results of bus10 in different scenarios

Scenario	Case	Verror (max)	Verror (avg)
Base case		0.009	0.0053
PVs	10%	0.0082	0.0032
	20%	0.0071	0.00049
	50%	0.0072	0.0062
	100%	0.009	0.0037
EVs	10%	0.0097	0.0049
	25%	0.00978	0.0042
	50%	0.0125	0.0023
100% PV + EV (Grid support)	10% EV	0.0165	0.0038
	25% EV	0.026	0.0045

3.5.4. SCENARIO 4: GRID WITH PVS AND EVS

This scenario represents the proposed grid support algorithm which is presented in Section 3.4.1. In this study, it is assumed that all the grid customers own PV panels, and a certain number of customers own an EV. Strictly speaking, the PV penetration level is assumed to be 100%, and different EV penetration levels are investigated. From Table 3–6, it can be realized that the maximum voltage error, $V_{error}(max)$, is 1.65% for the scenario with (100% PV+10% EV) in the grid, and the average

voltage error, $V_{error(avg)}$, is less than 0.4%. For the scenario with (100% PV+25% EV), $V_{error(max)}$ is 2.6%, and $V_{error(avg)}$ is less than 0.5%.

To further verify the results, the voltage profile of the aggregated model, and the voltage profile of bus10 in Fig. 3.11 is presented in Fig. 3.19 for (100% PV+25% EV) in the grid. From Fig. 3.19, it can be realized that the aggregated model presents a reasonable track of bus10 of the original grid. To further evaluate the validity of the aggregation technique, maximum voltage deviation of each of the grid buses in different scenarios is presented for 'scenario 1' and 'scenario 2' in Table 3–7, and for 'scenario 3' and 'scenario 4' in Table 3–8. In these tables, maximum voltage deviation is the difference between the highest voltage of each bus during the 24-hour period and the minimum voltage of that bus during similar time period. It can be seen from Table 3–7 and Table 3–8 that, in different scenarios, the aggregated model presents good track of the behavior of the original grid. Comparing the voltage deviations of different grid buses with the aggregated model of the grid in different scenarios demonstrate the capability of the aggregated model in capturing the maximum voltage deviations of different grid buses. Also, it can be realized that in all the scenarios, maximum voltage deviation occurs for bus10 on feeder2. Therefore, comparing the results of the aggregated model with bus10 of feeder2 captures the potential violations of the grid in different scenarios.

Table 3–7 Maximum voltage deviation of buses: "base case" and "with PV panels in the grid"

Grid		Scenario1: Base Case		Scenario2: PV in the grid							
				10%		20%		50%		100%	
Feeder	Bus	Original	Agg.	Original	Agg.	Original	Agg.	Original	Agg.	Original	Agg.
1	1	,0187	,0422	,0179	,0418	,0181	,0419	,0245	,0419	,0443	,0774
	2	,0211		,0203		,0205		,0272		,0496	
	3	,0266		,0255		,0258		,0362		,0656	
	4	,0327		,0316		,0320		,0413		,0758	
	5	,0349		,0338		,0343		,0428		,0785	
2	6	,0198		,0191		,0193		,0212		,0356	
	7	,0258		,0248		,0251		,0273		,0460	
	8	,0373		,0359		,0363		,0383		,0645	
	9	,0432		,0425		,0430		,0460		,0800	
	10	,0457		,0440		,0444		,0491		,0864	
3	11	,0088		,0085		,0085		,0106		,0178	
	12	,0134		,0128		,0129		,0162		,0270	
	13	,0167		,0161		,0162		,0202		,0339	
	14	,0205		,0201		,0201		,0248		,0412	
4	15	,0149		,0141		,0142		,0178		,0299	
	16	,0189		,0179		,0181		,0228		,0385	
	17	,0214		,0203		,0205		,0261		,0449	
	18	,0218		,0207		,0209		,0268		,0464	
5	19	,0197		,0189		,0191		,0219		,0347	
	20	,0276		,0266		,0269		,0291		,0455	
	21	,0327		,0315		,0317		,0339		,0524	
6	22	,0275		,0264		,0266		,0258		,0410	
	23	,0333		,0320		,0323		,0310		,0489	
	24	,0388		,0373		,0376		,0356		,0557	
	25	,0416		,0399		,0402		,0381		,0599	
	26	,0429		,0411		,0415		,0388		,0601	

Table 3–8 Maximum voltage deviation of buses: "EVs in the grid" and "PV panels+ EVs" in the grid

Grid		Scenario3: EV in the grid				Scenario4: 100% PV+EV (grid support)			
Feeder	Bus	10%		50%		10% EV		25% EV	
		Original	Agg.	Original	Agg.	Original	Agg.	Original	Agg.
1	1	,0187	,0423	,0237	0,0485	,0389	0,0867	,0389	0,0955
	2	,0211		,0258		,0449		,0449	
	3	,0266		,0314		,0625		,0625	
	4	,0326		,0372		,0777		,0776	
	5	,0349		,0394		,0846		,0819	
2	6	,0198		,0248		,0322		,0462	
	7	,0258		,0302		,0450		,0627	
	8	,0373		,0410		,0684		,0825	
	9	,0442		,0473		,0874		,0926	
	10	,0457		,0490		,0924		,1045	
3	11	,0088		,0153		,0113		,0131	
	12	,0134		,0198		,0219		,0258	
	13	,0167		,0230		,0301		,0353	
	14	,0205		,0274		,0368		,0446	
4	15	,0149		,0232		,0242		,0272	
	16	,0189		,0284		,0340		,0380	
	17	,0213		,0322		,0411		,0469	
	18	,0218		,0331		,0428		,0491	
5	19	,0197		,0250		,0305		,0341	
	20	,0276		,0324		,0431		,0464	
	21	,0327		,0370		,0522		,0541	
6	22	,0274		,0318		,0396		,0486	
	23	,0332		,0372		,0493		,0593	
	24	,0387		,0422		,0574		,0695	
	25	,0415		,0449		,0613		,0769	
	26	,0427		,0457		,0633		,0757	

3.6. SUMMARY

A new aggregation technique is proposed in this paper which enables the grid operators to quickly assess the grid operating limits under different loading conditions. The method is tested on part of a Danish distribution grid under different scenarios. Grid existing condition, the effect of PV panels, and the effect of EVs were tested on the grid. To provide a comprehensive analysis, the aggregation method was also tested in a grid support scenario. A grid support strategy is proposed in this study for active distribution networks. The grid support algorithm utilizes the EV storage for supporting the grid, based on the grid operating parameters, and with respect to EVs' location in the grid.

Different scenarios have been tested and simulated to demonstrate the validity of the method. Simulation results demonstrate that in all the scenarios, the error of the aggregated model is less than 1%, compared to the original grid, considering the "average voltage error" index. For the "maximum voltage error" index, the error is below 2% in all scenarios, except for the grid support scenario, in which the maximum error reaches 2.6%.

.

CHAPTER 4. RES INTEGRATION IN MV GRID IN PRESENCE OF MICROGRIDS

This chapter investigates the impact of RESs and EVs in a medium voltage (MV) network. A steady state analysis of the MV network in presence of RESs, EVs, and DCHP units demonstrates the capability of the MV and LV networks for supporting upper network, i.e. high voltage (HV) transmission system. Modeling approach for PV panels and EVs are similar to the models which are presented in Chapter 2. Steady state modeling details of wind turbines and DCHP units will be presented in this chapter. Different placements of wind turbines have been studied and simulated to determine MV network bottlenecks. Dynamic modeling of wind turbines and DCHP units will be presented in Chapter 5.

4.1. INTRODUCTION

Despite huge challenges of integrating large-scale renewable energy resources (RESs) in power system due to their uncertainties and their variable inherent [93], [94], the interest towards RESs and their increasing penetration in today's power system cannot be ignored. Among different kinds of renewable energy, wind energy is considered as one of the most promising resources. Due to its zero fuel costs, and considering its environmentally-friendly inherent, wind is considered a one of the best replacements for conventional power plants. Due to these reasons, there is a major attempt to increase the use of RESs in the power system using the incentive policies such as Renewable Portfolio Standard (RPS) [95]. Renewable policies such as fixed tariff in countries such as Germany, Denmark and Spain have made rapid progress of this energy [95]. Table 4–1 presents the installed wind power capacity in different countries [93]. Denmark is a leading country in Europe in the integration of wind energy into the power system, with more than 24% of its electric consumption supplied by wind energy [96]. This value has increase to 39% in 2013 [97]. On the other hand, different policies and tariffs for supporting solar panels in the system have been defined in the last few years, which have sharply increased the penetration level of solar PV panels in the power system, especially in the residential areas [22]. However, as mentioned, high penetration of renewable energy in the system can be challenging, considering the

uncertainty of these resources. Such uncertainties might lead to issues for the grid operating conditions, such as bus voltages and line nominal currents [21].

Considering new developments in smart grid technologies, especially the increasing role of information and communication technology, customers' behavior is predicted to be affected, and they are expected to role as active participants in the power system and energy market [98]. In this regard, flexible demand can be seen as a major player in balancing the demand and supply, and maximizing the utilization of RESs in the system. One of the most promising players in this regard is electric vehicles, considering their promising technology. Despite the uncertain speed in the development of EVs, the number of EVs can grow fast and the impact of these flexible loads on the power system can be remarkable [98]. Fast evolution toward the smart grid in recent years has made it feasible to propose and apply different smart charging algorithms for electric vehicles. Such potential leads to new opportunities for different parties to use the capacity and flexibility of EVs for different purposes and different objectives [57], [99]. Some algorithms are proposed in order to minimize the charging costs of EVs based on the real-time price [57]. On the other hand, some methods utilize EVs for frequency regulation and/or real-time balancing of power [57]. Another interesting objective among smart charging algorithms is using EVs for reducing peak demand, because shifting the demand to off-peak hours increases the grid ability to transport the energy from the RESs to the upper grid, and hence avoiding/delaying reinforcing investment [96].

Table 4–1 Installed wind power generation [MW] [93].

Areas	2010	2020
Norway	545	6600
Sweden	1250	10000
Finland	350	3000
Denmark	3700	6000
Germany	24900	57300
Netherlands	1000	2950
Belgium	2800	10400

4.2. MODELING APPROACH

The study investigates the impact of different energy sources, as well as the impact of electric vehicles (EVs). The energy sources in this study include residential PV panels, MV wind turbines, and decentralized combined heat and power (DCHP) units. Modeling approach for EVs and PV panels is similar to the models presented in Chapter 2.

Two types of EVs are considered for MV grid analysis: commuters and family cars. The driving patterns of EVs are similar to driving patterns of commuters and family

card in Chapter 2. Also, regardless of the number of EVs in different buses, the ratio of "commuter/family car" is taken to be the same, and 80% of EVs would be commuters. Furthermore, EVs are located in residential buses in this study.

4.2.1. WIND TURBINE MODELING

Wind turbine modeling is done using the common models, as noted in (4.1) [100].

$$P_{WT} = \begin{cases} 0 & V < Vc\_in \\ P_r \times \left(A + B \times V + C \times V^2 \right) & Vc\_in \le V < V_r \\ P_r & V_r < V < V_{c\_out} \\ 0 & V > V_{c\_out} \end{cases} \quad (4.1)$$

Here, 'V_{c_in}' is the cut-in speed, 'V_r' is the rated speed of the turbine, and 'V_{c_out}' is the cut-out speed of the wind turbine. 'A', 'B', and 'C' are constants that are determined by the wind turbine characteristics [100]. Considering the available turbines in the market, a 2-MW wind turbine is considered in this study. The data of the turbine is presented in Table 4–2 [101]. The wind speed data in this study is obtained from the historic measurements [97]. However, since the wind measurement is done at a certain height where the measurement device is installed, the wind speed should be modified with respect to the height of the wind turbine hub. In this study, wind speed is modified using (4.2) [102].

$$Vs(h2) = Vs(h1) \frac{ln\left(\frac{h2}{Z_0}\right)}{ln\left(\frac{h1}{Z_0}\right)} \quad (4.2)$$

Here, $V_s(h1)$ is the measured wind speed at height h1, h2 is the hub height, and Z_0 is the roughness factor. Z_0 depends on the type of the environment where the turbine is installed [102]. Considering the focus of this work, which is MV grid in the cities and industrial areas, Z_0 is assumed to be 0.1. Applying the modified wind speed data to the model of the 2-MW unit, the output power of the unit is calculated. The calculation is done for 2012, 2013, and 2014. Based on the output power of the wind turbine for the whole year, the average power and energy production of the unit is calculated, as presented in Table 4–3. From Table 4–3, the average annual energy production of a 2-MW wind turbine is obtained in (4.3).

$$\begin{aligned} Eavg &= \left(E\_2012 + E\_2013 + E\_2014\right)/3 = 8917\ MWh \\ \%\ of\ annual\ consumption &= 8917/106385 = 8.38\% \end{aligned} \tag{4.3}$$

Comparing to (2), it can be seen that a 2-MW wind turbine can provide 8.38% of the annual energy demand of the grid.

4.2.2. DCHP MODELING

DCHP units are considered as PQ sources. Two DCHP units are placed in the network, with the maximum capacity of 3MW for each unit. The detailed model of the DCHP units, including the dynamics of governor and turbine of DCHP, will be explained in chapter 5. The placement of DCHP units in the network will be presented in Section 4.5.

4.3. CIGRE BENCHMARK NETWORK

The study is performed on a CIGRE benchmark grid. The grid layout is presented in Fig.4.1, and the load demand of different grid nodes is presented in Table 4–4 [103]. The load modeling approach is also presented in this section, although the main methodology is based on the "Velander method" which was presented in Chapter 2.

4.3.1. GRID LAYOUT

The grid layout is presented in Fig.4.1. The grid consists of two 25 MVA medium voltage transformers. By default, all the circuit breakers are open in the grid. The grid is combined of residential and industrial loads, with different power factors and different demands. Table 4–4 presents the demand of loads on different buses [103].

Table 4–2 Details of wind turbine [101].

Rated Power	2000 kW
Cut-in speed (Vc_in)	3 m/s
Rated speed (Vr)	11 m/s
Cut-out speed (Vc_out)	20 m/s
Hub height	125 m

Table 4–3 Average power and energy of a 2-MW wind turbine.

Year	**2012**	**2013**	**2014**
Eavg (MWh)	9268	8502.8	8980.2
Pavg (kW)	1055.2	970.63	1025.1

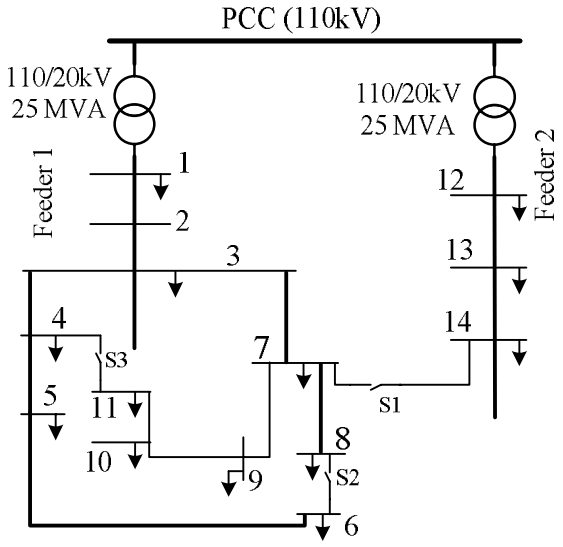

Fig.4.1. Grid layout [103].

Table 4–4 Demand on each grid bus [103].

Node	Apparent Power (kVA)		Power Factor	
	Residential	*Industrial*	*Residential*	*Industrial*
1	15300	5100	.98	.98
2	----	----	----	----
3	285	265	.97	.85
4	445	----	.97	----
5	750	----	.97	----
6	565	----	.97	----
7	----	90	----	.85
8	605	----	.97	----
9	----	675	----	.97
10	490	80	.97	.85
11	340	----	.97	----
12	15300	5280	.98	.95
13	----	40	----	.85
14	9215	390	.97	.85

4.3.2. GRID DEMAND AND LOAD MODELING

Modeling the load profiles of different industrial and residential loads are based on a measured Danish grid profile. To apply the study to the network in Fig.4.1, it is necessary to scale the bus demands in Table 4–4 with respect to Danish load profiles, which is available in (p.u.) scale. Load profiles are created in 2 steps.

In the first step, the demand profiles of each bus in Fig.4.1 were created by scaling up the demand profiles. The scaling factors are based on the demands of the buses in Table 4–4, as well as their power factor. It should be noted that the demand profiles of industrial and residential loads are with respect to typical demand profile in Denmark, as shown in Fig. 4.2. In the second step, the demand profiles of the buses were scaled with respect to the grid overall demand, as presented in Table 4–4.

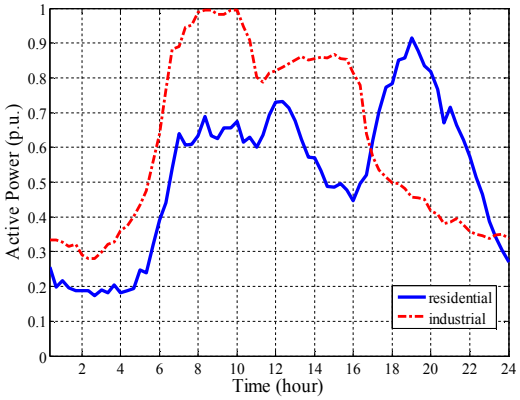

Fig. 4.2. Typical demand profile for residential and industrial load (p.u.).

4.3.3. ANNUAL ENERGY CONSUMPTION

As mentioned before, the demand profiles of different buses were created based on the annual profile, typical residential and industrial profiles, and demand of each bus in Table 4–4. Considering the main focus of this work, i.e. determining maximum penetration level of RESs in the grid without reinforcing the grid, it is necessary to know the annual energy consumption of the grid. However, there was no measured data available for this study. Therefore, the following procedure is used to give a rough estimation of grid annual energy demand. For such estimation, 3 different summer days and 3 different winter days were picked, and the calculation for the whole year was performed based on that, as presented in (4.4).

$$\begin{aligned} Summer: & \begin{cases} day\,1: & Et = 213.7\ MWh \\ day\,2: & Et = 220\ MWh \\ day3: & Et = 214\ MWh \end{cases} \\ Winter: & \begin{cases} day\,1: & Et = 360\ MWh \\ day\,2: & Et = 361\ MWh \\ day\,3: & Et = 363\ MWh \end{cases} \end{aligned} \tag{4.4}$$

Summer days are picked among different days of April until September. On the other hand, winter days are picked among days of October until March. With respect

to these values, the daily average energy demand of the grid, and the annual energy demand of the grid is obtained, presented in (4.5).

$$\begin{aligned} &Average\ \ day = 289\ kWh \\ &Annual\ \ Energy\ \ demand\ = 289 * 365\ = 105485\ kWh \end{aligned} \tag{4.5}$$

4.4. PROPOSED CONTROL ALGORITHM

The algorithm for managing high integration of RESs into MV grid is presented in this section for two states: without the EVs in the grid, and with EVs in the grid.

4.4.1. GENERAL ALGORITHM WITHOUT EVS IN THE GRID

The first algorithm, i.e. the grid without the presence of EVs is presented in Fig. 4.3. The 'PF-1 Unit' is the load flow calculation block. It takes the load data and the grid data as the input. Wind data, solar data, and CHP data act as inputs for 'wind units', 'PV panels, and 'CHP units', respectively. Then, it calculates the grid operating parameters, including voltages of different buses, power flow through transformers and lines, and power loss in the grid. it should be noted that the overall production of the RESs in the grid (i.e. wind and solar) also affect the power production of the CHP units in the system; i.e. if the power production from RESs in the grid is more than the grid consumption, then the CHP units do not produce power. Otherwise, they would produce power with respect to their nominal power and their operating point, as they also provide reactive power for the grid.

4.4.2. IMPACT OF EVS ON THE PROPOSED ALGORITHM

The details of EVs are explained in section II. As mentioned, the located EVs in each grid node are the aggregated model of the commuters and family cars for the node. Similar to solar panels, the penetration level of EVs for different nodes is with respect to the residential demand of the nodes. In this study, 20% EV penetration is considered. The proposed algorithm for grid analysis in presence of EVs can be seen in Fig. 4.4 and Fig. 4.5. The algorithm evaluates the grid without the effect of EVs, as shown in Fig. 4.4. Then, the results act as an input for 'EV Unit' block in this figure. The updated results with the effect of EVs are sent to "PF-3 Unit" for the grid analysis. Fig. 4.5 presents the "EV Unit" in details. As can be seen from Fig. 4.5, the algorithm takes the data from "PF-1 Unit", and checks the availability of all the EVs in different grid buses. If the EV is moving, it cannot be used for the grid support. Otherwise, the EVs will be sorted based on their state of charge (SoC). Then, the EV location (bus and feeder where the EV is connected) will be checked. Then, based on the maximum and minimum voltage of the feeder where the EV is connected ('Vmax' and 'Vmin' in Fig. 4.5), the algorithm decides how to use EV; either for positive balance (i.e. power from the grid to the EV), shown by V2G(+),

or for negative balance (i.e. power from EV to the grid), denoted by V2G(-). The decision is made based on the voltage conditions (voltage set points), mentioned by 'Cond1' and 'Cond2' in Fig. 4.5. In case where both conditions are satisfied (both 'Cond1' and 'Cond2'), the algorithm makes decision based on the distance between the EV bus and the buses which caused 'Vmax' and 'Vmin' in this interval. Based on the algorithm decision, the SOC of the EV and the "Load data" will be modified. Then, the "PF2" block analyses the grid to find the new status of the grid and to obtain the new values for 'Vmax' and 'Vmin'. When all the EVs in the grid are analyzed, the results will be sent to "PF-3 Unit" in Fig. 4.4 for grid analysis in presence of the EVs.

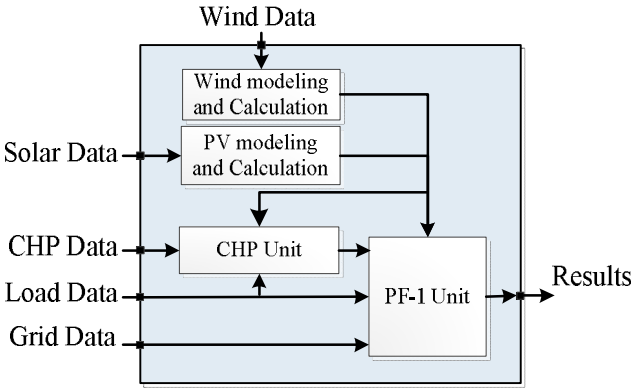

Fig. 4.3. Calculation process without EVs.

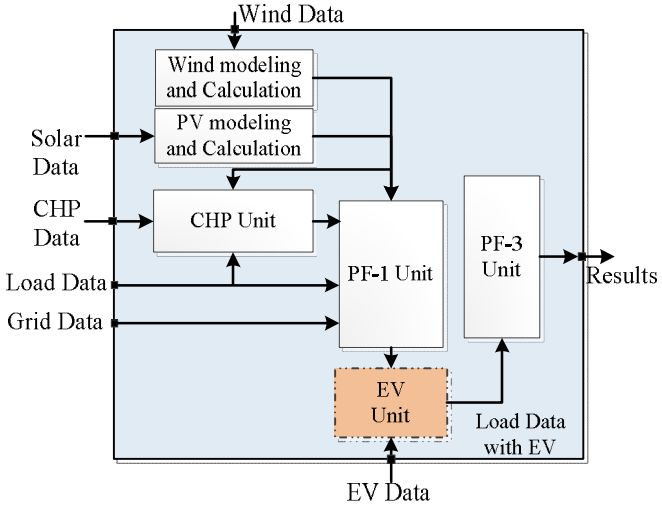

Fig. 4.4. Grid analysis in presence of EVs.

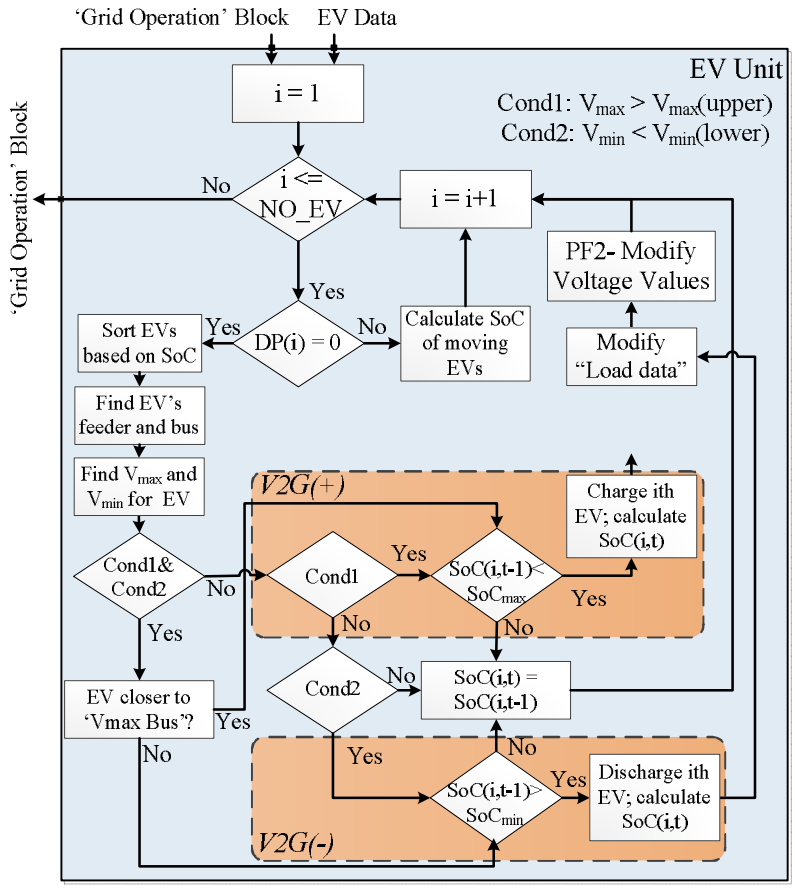

Fig. 4.5. The interaction between the grid and EVs.

4.5. SIMULATION RESULTS

Different scenarios have been simulated to demonstrate the viability of the algorithm. Besides, considering the siginificant difference between summer and winter load profiles, different summer and winter scenarios have been defined and investigated. Table 4–5 defines different winter and summer scenarios in this study. The load demand of the grid for each scenario is also presented in Fig. .4.6. As a comparison, Table 4–6 presents the output power of a 2-MW wind turbine for each of the scenarios of Table 4–5, in which 'Day 1' and 'Day 2' is based on the definition of Table 4–5. As presented in Table 4–6, the wind power production is much higher in a 'winter windy day', compared to other scenarios. Therefore, the grid is more prone to voltage and transformer issues in a 'winter windy' scenario than other scenarios. As mentioned in section III, the placement of PV panels in the grid is proportional to the residential demand of the grid buses, which is presented in

Table 4–4. Table 4–7 presents different placement of RESs in the grid in each case study. From Table 4–7, the cases can be divided into 2 categories: a) cases where the wind turbine placement is near the load center (case 1 and case 2); b) cases where the wind turbines are located far from the load centers (case 3 and case 4).

In general, the wind turbines are preferred to be located at the buses far from the load centers [95]. It should be mentioned that in scenarios where DCHP is also included, 2 DCHP units are located in the grid: a 3-MW unit in bus 1 on feeder 1, and a 3-MW unit on bus 12 on feeder 2. Also, for the cases with PV panels in the grid, it is assumed that the solar penetration is around 20% in the grid, with respect to the grid residential demand. This is due to the fact that the study is focused on the residential PV panels.

The simulation results for different cases are presented in the next section. As a major grid operating index, the voltage of different grid buses under different scenarios are presented and evaluated.

Table 4–5 Different winter and summer scenarios.

	Day 1	**Day 2**
Winter	Low wind	Windy
Summer	Low wind	Windy

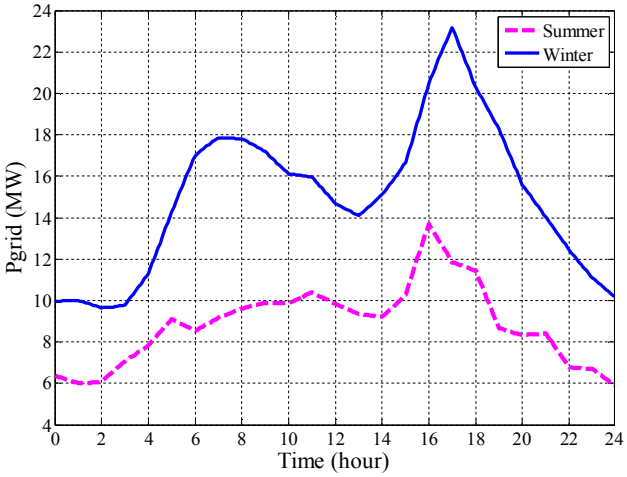

Fig. .4.6 Grid demand for summer and winter scenarios.

Table 4–6 Output of a 2-MW wind turbine in different scenarios.

		E_t (kWh)	**P_{avg} (kW)**	**% of turbine capacity**
Summer	***Day1***	937.65	39.06	1.9
	Day2	24705.5	1029.4	51.47
Winter	***Day1***	8776.2	365.67	18.3
	Day2	45811.2	1908.8	95.4

Table 4–7 Different RES placements in the grid.

	NO. Wind turbines				**NO. Wind turbines + NO. PV panels**			
Bus No.	***Case 1***	***Case 2***	***Case 3***	***Case 4***	***Case 1***	***Case 2***	***Case 3***	***Case 4***
1	2	4	0	0	2 + 1000	4 + 1000	0+ 1000	0 + 1000
2	0	0	0	0	0 + 0	0 + 0	0 + 0	0 + 0
3	0	0	0	0	0 + 0	0 + 0	0 + 0	0 + 0
4	1	1	0	0	1 + 0	1 + 0	0 + 0	0 + 0
5	0	0	1	0	0 + 50	0 + 50	1 + 50	0 + 50
6	0	0	0	0	0 + 0	0 + 0	0 + 0	0 + 0
7	0	0	1	0	0 + 0	0 + 0	1 + 0	0 + 0
8	1	1	1	0	1 + 50	1 + 50	1 + 50	0 + 50
9	0	0	0	0	0 + 0	0 + 0	0 + 0	0 + 0
10	0	0	0	1	0 + 50	0 + 50	0 + 50	1 + 50
11	0	0	0	1	0 + 0	0 + 0	0 + 0	1 + 0
12	2	4	1	1	2 + 500	4 + 500	1 + 500	1 + 500
13	1	1	4	5	1 + 0	1 + 0	4 + 0	5 + 0
14	1	2	1	2	1 + 500	2 + 500	1 + 500	2 + 500

Table 4–8 Maximum voltage deviation in the grid for different winter and summer scenarios.

		Winter		**Summer**	
Scenario		***Day 1: low wind***	***Day 2: windy day***	***Day 1: low wind***	***Day 2: windy day***
Base		.0259	.0258	.0129	.0124
Wind	***Case 1***	.0362	.0302	.0176	.0369
	Case 2	.0405	.0302	.0189	.0353
	Case 3	.046	.0367	.0223	.0556
	Case 4	.0402	.0332	.0196	.0448
PV		.0259	.0258	.0094	.0113
Wind + CHP	***Case 1***	.0356	.0296	.0174	.0368
	Case 2	.0394	.0292	.0186	.035
	Case 3	.0455	.0353	.0221	.055
	Case 4	.0384	.0317	.0193	.0446
Wind + PV	***Case 1***	.0362	.0302	.0143	.0382
	Case 2	.0405	.0302	.0147	.0359
	Case 3	.046	.0367	.019	.0567
	Case 4	.0402	.0332	.0163	.0462
Wind + PV + CHP	***Case 1***	.03562	.02965	.0141	.038
	Case 2	.0395	.02925	.0144	.0356
	Case 3	.0455	.0353	.0188	.0566
	Case 4	.0384	.0317	.0161	.046

4.5.1. GRID ANALYSIS WITHOUT EVS IN THE GRID

The impact of RESs without the impact of EVs is presented here. In the following, the impact of wind turbines, PV panels, and DCHP untis is discussed separately.

4.5.1.1 Wind Turbines

Table 4–8 presents the voltage deviation of different grid buses. In this table, different possible RES scenarios are compared with the grid base case, i.e. the case where no RES and no CHP is in the grid. To obtain the values of Table 4–8, the maximum and minimum voltage of each grid bus is calculated for each day. Then,

the voltage deviation of each grid bus is obtained. Comparing the voltage deviations of different grid buses, the worst voltage deviation of the grid under a certain scenario is obtained. Analyzing different cases and scenarios, it can be realized that when the wind turbines are located at the remote buses, i.e. buses with the distance from the main transformer, the voltage deviation of the buses increases significantly. Case 3 and case 4 in Table 4–7 represent such scenarios. Due to the structure of feeder 2, the high number of wind turbines doesn't cause serious voltage deviation, since the last bus on feeder 2 is also a big load center. However, feeder 1 has a different situation. Feeder 1 has many remote buses with low demand on the buses, such as bus 9, bus 10, and bus 11. Locating the wind turbines at these buses causes serious voltage deviations in the grid, as can be realized from case 3 and case 4 in Table 4–8. In case 4, two wind turbines are located in the far end buses of feeder 1. In this case, although RESs cause no issues for transformers and the lines have, the voltage deviations are quite significant. In case 3, although only 3 wind turbines are located in the middle of the feeder, the voltage deviation of the grid (especially bus 12 on feeder 1) exceeds 5%, which is a standard voltage deviation of the buses. Such case needs to be handled by changing the tap changers of the main transformers of the feeder.

4.5.1.2 PV panels

Considering the PV panels, Table 4–9 shows that a 3-kW panel provides around .001% of the grid annual demand. Considering 20% solar penetration in this study, which is 2150 3-kW panels in the grid, the panels provide around 2% of the grid annual demand in this study. However, it should be noted that most of the solar power production is during the summer time, where the solar irradiation is high. Therefore, separating the summer and winter times during the year, and considering the fact that the grid energy consumption in the summer time is almost half of the grid energy consumption in the winter time, it can be seen that the role of solar panels increases significantly for the summer scenarios. Separating the solar power production of the grid for summer and winter scenarios suggests that the solar panels produce more than 95% of their annual energy production during the summer time. Therefore, for the case study in this work, which is 20% residential panel penetration, the solar panels provide up to 6% of the grid summer demand, while their participation in providing the grid winter demand is ignorable. Analyzing the effect of panels on the grid voltage deviation would be interesting. As expected, the panels hardly have any effect on the grid in the winter scenario. Considering the 'solar' scenario in Table 4–8, in the summer scenarios where the solar production is significant, the solar panels lead to less voltage deviation on the MV grid. On the other hand, in cases where 'wind+ solar' exist in the grid, the solar panels have no significant effect on the voltages, as expected. On the other hand, in summer scenarios with 'low wind' ('Day 1' of the summer scenario), solar panels helped improve the voltage profile of the grid and reduce the voltage deviation. However, in 'windy day' of 'summer scenario', the solar panels have negative effect on

voltage deviations and increase the voltage deviations, compared to the cases where only 'wind' is in the grid.

Table 4–9 Average power and energy of a 3-kW PV panel.

Year	2012	2013	2014
Eavg (kWh)	1011	1022	1050
Pavg (kW)	117	116.5	121

4.5.1.3 DCHPs

Considering the scenarios where DCHPs are also added to the grid, it can be realized that in all the cases the DCHPs have had positive effect and reduced the voltage deviations. However, the significance of DCHPs is different for different cases. To have a better view, the scenarios should be divided. Comparing the 'winter' cases with similar 'summer' cases, it can be realized that the positive effect of DCHPs is more significant in the winter scenarios. The reason is the output power production of DCHP units in winter scenarios. Due to the need of the customers in winter scenarios, the set points of DCHPs are much higher in winter time, compared to the summer time. The other point to consider in evaluating the role of DCHPs is the location of RESs in the grid. Going through the results, in cases where the wind turbines are located near load centers (case 1 and case 2 in Table 4–8), the DCHPs have a much more significant effect on reducing the voltage deviation. However, in case 3 and case 4 where the wind turbines of feeder 1 are located on remote buses, the effect of DCHPs on reducing voltage deviations would be less.

4.5.2. IMPACT OF EVS ON THE PROPOSED ALGORITHM

To realize the effect of EVs on the grid, the voltage deviation of different scenarios in presence of EVs is presented in Table 4–10. Comparing to the values for "wind+ solar" scenario in Table 4–8, two points can be addressed. In the scenarios of "low wind" days, both in winter and in summer scenarios, the presence of EVs has helped reducing the voltage deviation in the grid. As the load demand increases during the evening time, the EVs strat supporting the grid by injecting power into the grid (negative balance, V2G(-)). As a result, they help reducing voltage deviations in the grid. However, in the "windy" scenarios, the EVs hardly have a positive effect. The reason is that in these days, the power production of the wind turbines is very high, and it increases voltage of the grid buses. However, the EVs capacity for storing the extra energy is limited. Therefore, they have a very small effect on reducing the voltage deviations in these scenarios. It should be noted that the EV penetration is 20% in this study, as mentioned in section IV.B. To find out the EV interaction with the grid, the state of charge (SOC) of some of the grid EVs under some scenarios are presented below. Fig. 4.7 presents the SOC of grid EVs for 'winter' scenario, in 'case 4' with wind turbines and solar PV panels in the grid. As presented in Fig. 4.7, in 'low wind' case, as the grid buses demand more energy and the wind power

production is low, the EV role in supporting the grid is considerable (EV discharging for grid support). Especially, in the evening time, as the load demand increases, the role of EVs becomes more significant. On the other hand, in 'windy day' case, due to high wind power production, the EVs are used by the grid to store energy, but their capacity is limited.

An interesting fact about the presence of EVs in the grid is their role in increasing the penetration of wind turbines. From Table 4–10, the voltage deviations on 'low wind' scenarios are higher than 'windy' scenarios. The presence of EVs reduces the maximum voltage deviation in 'low wind' scenarios, as mentioned above, and enables increasing wind penetration in the grid. For case 4 for 'winter' scenario with "wind+ solar", the use of EVs allows installing at least 1 more 2-MW turbine at bus 9, without causing more than 5% voltage deviation.

4.5.3. RES PENETRATION

Considering the case scenarios in Table 4–8 and Table 4–10, it can be seen that for cases where the wind turbines are installed near the load centers, the overall RES penetration can increase significantly. As explained in section III, a 2-MW wind turbine can produce around 8.38% of the grid annual energy demand. Therefore, in cases where the wind turbines are installed near the load centers, such as case 1 and case 2, the wind penetration can be increased to more than the grid annual energy demand (case 2 in this study). However, if the wind turbines are installed far from the load centers, the wind penetration level will be limited by voltage deviation. For grid in Fig.4.1, case 3 and case 4 represent the cases where the wind turbines are installed far from the load centers on feeder 1. Although the overall wind penetration is still high in these cases (up to 85% of the grid annual energy demand in case 4), feeder 1 has serious limits in these scenarios. Due to high voltage deviations, the maximum wind penetration for this feeder is around 17% of its annual energy demand. However, as mentioned above, the use EVs enables installing at least 1 more 2-MW wind turbine, which leads to 8.35% higher wind penetration. Therefore, the overall wind penetration on feeder 1 can increase from 17% to 25%. On the other hand, considering the positive effect of CHPs on reducing voltage deviations, the voltage deviations in the winter time are well limited by the help of CHPs in the winter scenarios. This would offer a potential on increasing the wind penetration. However, checking the summer scenarios reveals that the CHPs didn't have much effect on reducing voltage deviations for summer scenarios. Therefore, installing more wind turbines in the grid might lead to voltage deviations above 5%.

Table 4–10 Maximum voltage deviation in the grid for different winter and summer scenarios.

Scenario		Winter		Summer	
		Day 1: low wind	***Day 2: windy day***	***Day 1: low wind***	***Day 2: windy day***
Wind + PV + CHP + EV	***Case 1***	.0338	.0289	.0126	.038
	Case 2	.0327	.0287	.0129	.0358
	Case 3	.0437	.0351	.0173	.0566
	Case 4	.0367	.0317	.0146	.046

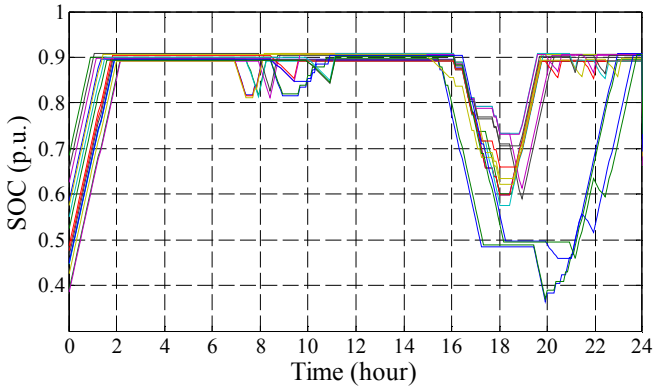

a)

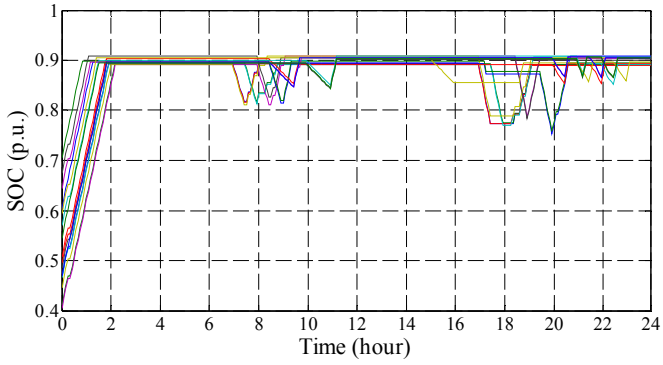

b)

Fig. 4.7. SOC of EVs in case 4 (winter day):a) low wind; b) windy.

4.5.4. POWER TRANSFER AT THE PCC

To find out the power exchange of the grid with the upper network, the power flow of the grid at the point of common coupling (PCC in Fig.4.1) is presented below for case 4 of Table 4–8 and Table 4–10 in winter scenarios. All the scenarios are compared with the 'winter base case', i.e. the case where only the grid base demand

exists, and no wind, solar, CHP, or EV is added to the grid. Therefore, in the base case, all the grid demand is provided by the upper hand network.

Solar production is very low in winter scenarios and almost has no effect on the overall power exchange at the PCC. Therefore, the cases with the "solar panels" are not presented in these figures to avoid confusion. The plots present the power flow from the upper network to the MV grid at the PCC. Therefore, a positive value in the figure represents the power flowing from the upper network to the MV grid, while the negative values of the figure reveal the reverse power flow (from the MV grid to the upper network).

4.5.4.1 No EV in the grid

Fig. 4.8 and Fig. 4.9 present the power exchange at the PCC, ignoring the effect of EVs. Fig. 4.8 presents the power exchange for a 'low wind' scenario. Compared to the base case, it can be realized that the wind power provides part of the grid demand, and therefore, the grid imports less power from the upper network. On the other hand, when considering DCHP units in the grid, the role of DCHPs in providing a significant part of the grid demand is easy to recognize. During the peak hour, i.e. between 16:00 to 18:00, comparing the plots reveal that the DCHP units are producing power at their maximum capacity, as both DCHP units in the grid are 3 MVA units.

On the other hand, considering the 'windy' scenario in Fig. 4.9, the wind power production in the grid is very high. Therefore, the wind power provides the whole demand in the grid, and it also sends the extra power to the upper network. Therefore, the power exchange at the PCC is negative for most of the day, indicating the reverse power flow from the MV grid to the upper network. However, due to low wind power production between 15:30 to 18:00, the upper network has to provide part of the grid demand.

Considering the case where the DCHP units are also in the grid in Fig. 4.9, it can be realized that the output power of the DCHP units is almost zero for many hours. However, considering the low wind period in the evening, i.e. between 15:30 to 18:00, it can be realized that the DCHPs are providing power at this period and supply part of the grid demand, compensating the shortage of power due to the low wind power production.

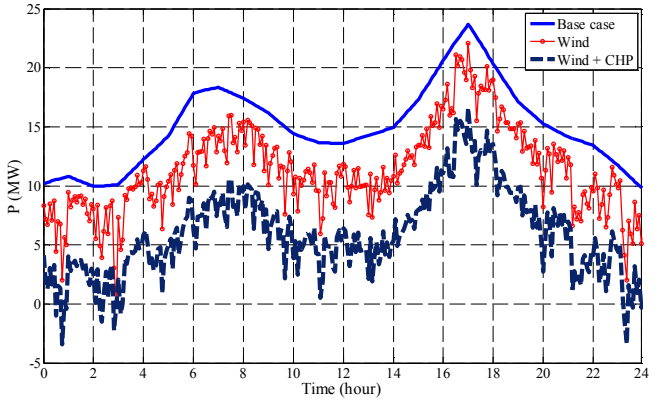

Fig. 4.8. Power exchange at the PCC for winter 'low wind': case 4.

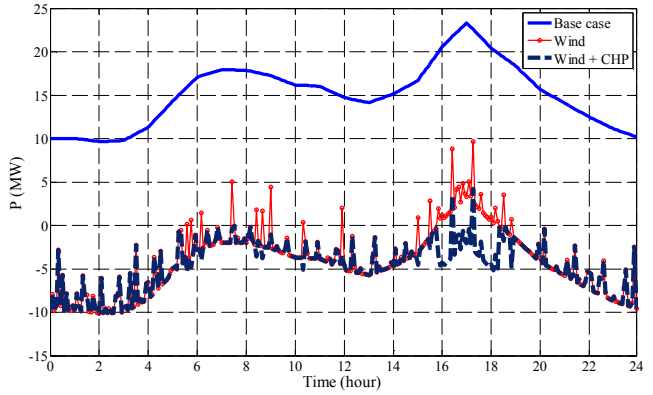

Fig. 4.9. Power exchange at the PCC for winter 'windy': case 4.

4.5.4.2 The effect of EVs in the grid

To figure out the role of EVs on the grid overall behavior, the power exchange of the grid at the PCC is presented in Fig. 4.10 and Fig. 4.11 for similar scenarios as above: 'low wind' winter day, and 'windy' winter day. As before, the results are for case 4 in Table 4–10.

Considering a 'low wind' day, as presented in Fig. 4.10, it can be realized that during the night time, i.e. between 00:00 to 2:00, adding the EVs to the grid has led to increase in power flow from the upper network to the grid. The extra power requirement is due to the charging requirements of the EVs. However, an interesting fact in Fig. 4.10 is the effect of EVs on shifting high demand of the grid. In the evening time, i.e. between 16:00 to 18:00, the EVs start discharging and supporting the grid (V2G(-) in the proposed algorithm in Fig. 4.5). This way, the power flow from the upper network to the grid decreases. This is a great advantage for the upper network, as the overall demand is very high during the evening time, and reducing

and shifting the peak demand of the grid removes part of the high demand from the upper network.

On the other hand, in the 'windy' scenario, plotted in Fig. 4.11, it can be seen that the EVs hardly affect the power exchange at the PCC. Their main effect is during the midnight time, i.e. between 00:00 to 2:00, where the EVs are getting charged. However, during the day time, the EVs cannot have much role in supporting the grid (V2G(+) in Fig. 4.5). The reason is that the available storage of the EVs is limited, as it mainly depends on the driving requirements and the distance profiles (DP) of EVs, as explained in section II. Therefore, EVs can only absorb a fraction of the extra power in the grid. While analyzing the voltage deviations in Table 4–10, it could be realized that the EVs have a very small effect on reducing the maximum voltage deviation in 'windy day' scenarios.

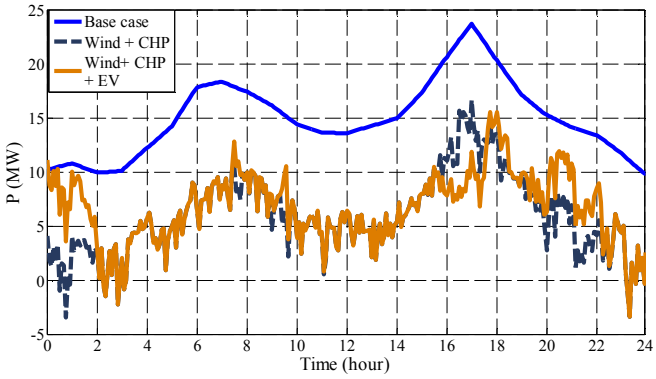

Fig. 4.10. Power exchange at the PCC: winter 'low wind' day: case 4.

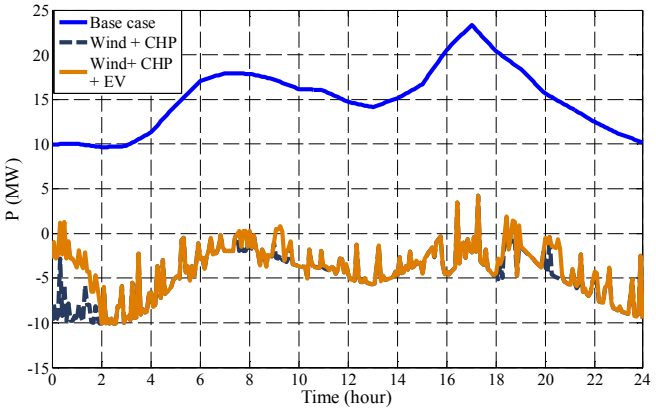

Fig. 4.11. Power exchange at the PCC: winter 'windy' day: case 4.

4.6. SUMMARY

A steady state analysis is performed in this chapter to demonstrate the impact of high RES penetration in MV grid, and the interaction between the MV grid and the upper network (HV network). Results show that, for the winter loading in the grid, the main players are the wind turbines, as the PV power production is very low in the winter time. Among all the cases which were investigated in this study, 'case 3' of the 'windy summer day' with both wind turbines and solar panels in the grid shows maximum voltage deviation. Two parameters cause such deviation. The first parameter is the location of the wind turbines in the grid, which are located in the remote buses. The second reason is the impact of significant PV production in the summer scenario.

EVs, as one of the grid flexible loads, are used in this study for grid support applications. Considering the number of EVs in this scenario, and due to the fact that the EV battery capacity is considered to be 30 kWh, EVs have a high potential of participating in the upper network regulation, although all this capacity cannot be used by the grid and the driving requirements of the EV owners should be considered. EVs can participate in the grid support (up-regulation), in case the grid requires power, such as a 'low wind' scenario.

CHAPTER 5. DCHP-BASED MODIFIED LOAD FREQUENCY CONTROL

Different placement of RESs in MV grid has been investigated in Chapter 4. In this chapter, a modified secondary control is proposed based on the capacity of DCHP units in the MV grid. The main objective is to improve the frequency response of the power system by incorporating DCHP units in traditional "Load Frequency Control" (LFC). Details of the modified LFC, modeling approach for DCHP untis, and the effectiveness of the proposed modification are demonstrated in this chapter.

5.1. INTRODUCTION

Renewable policies such as fixed tariff in countries such as Germany, Denmark and Spain have made rapid progress of renewable energy penetration [95]. Denmark is a leading country in Europe in the integration of wind energy into the power system, with more than 39% of its electric consumption supplied by wind energy in 2013 [96], [97]. On the other hand, different policies and tariffs for supporting solar panels in the system have been defined in the last few years, which have sharply increased the penetration level of PV panels in the power system, especially in the residential areas. However, as mentioned, high penetration of renewable energy in the system can be challenging, considering the uncertainty of these resources. Such uncertainties might lead to issues for grid operating conditions, such as bus voltages and line currents [21]. Considering new developments in smart grid technologies, and regarding the increasing interest in electric vehicles (EVs), EVs are considered as active players, both for energy management and for frequency control purposes [98], [99]. Some algorithms are proposed in order to minimize the charging costs of EVs based on the real-time price [9]. On the other hand, some methods utilize EVs for frequency regulation and/or real-time balancing of power [57]. An important parameter in such applications is to consider EV owner's requirements, as well as EV availability. An optimization method is proposed in [104] to optimally involve EVs in load frequency control (LFC). However, EVs are treated as an aggregated device in this work, which might not be accurate, especially for an MV microgrid with limited number of EVs. On the other hand, the possibility of utilizing the MV microgrid units and flexible loads in the LFC are quantified in [23], [105], [106]. In [105], the potential of refrigeration systems for frequency

response is quantified. In this work, assuming the significant number of such systems in power system, a simplified aggregated model of refrigeration systems are considered, which might not be accurate for a small-scale MV microgrid. In [106], a hierarchical control structure is proposed for microgrids, which requires communication infrastructure for accurate implementation of the method. Including wind turbines and PV panels in the LFC is proposed in [107] and [108]. However, most grid codes in Europe do not allow participation of small-scale MV wind turbines and small PV panels in LFC [97].

Decentralized combined heat and power plants (DCHPs) play an important role in energy systems in many European countries. Most cities in Denmark are equipped with DCHP units which are responsible for provide heat consumption. As a co-product, these units produce electricity [109]. Considering the fast response of DCHP units, adding these units in frequency control strategies could provide new potentials in the power system [104]. A general rule regarding traditional LFC is that, the system operating conditions, i.e. voltages in the grid and currents of the lines, are not considered in the load frequency control concepts [108]. However, in order to have a right evaluation of the MV microgrid participation in the LFC, it is necessary to verify the potential of the MV microgrid for locating RESs and EVs in the grid.

5.2. PROPOSED CONTROL LAYOUT

The proposed algorithm consists of two control modules: the ‘Steady State’ (SS) module, and the ‘LFC module’. Fig.5.1 presents the general layout of the proposed algorithm. The ‘SS’ control module runs in 5-minute intervals. The output vector of this module includes the power production of wind turbines and PV panels, the available storage of EVs, the primary power production of DCHPs, and the load demand. The output vector of ‘SS’ module acts as an initial input for MV microgrid for responding to signals from LFC. On the other hand, the “Frequency Block” obtains the system frequency, using the data of the system.

5.2.1. STEADY STATE CONTROL

The overall structure of the proposed ‘SS’ control module for the MV microgrid control is presented in Fig. 5.2(a). The ‘Grid Operation’ block evaluates the steady state operating conditions of the MV microgrid. It takes the load data and the microgrid data as inputs. Also, the power production of the RESs in the grid, as well as the power production of the DCHP units acts as input for the ‘Grid Operation’ block. The ‘Grid Operation’ block calculates the grid operating parameters, including voltages of different buses and power flow through transformers and lines.

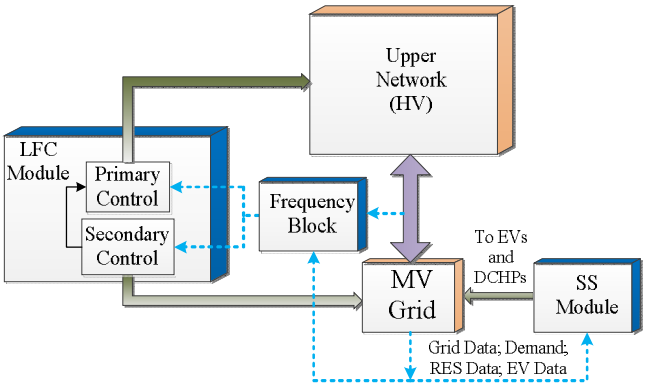

Fig.5.1. Proposed control algorithm: an overview.

Wind data, solar data, and 'total load data' in Fig. 5.2(a) act as inputs for 'wind units', 'PV panels', and 'DCHP units', respectively. It should be noted that the overall production of the RESs in the grid (i.e. wind and solar) also affect the power production of the DCHP units in the system; i.e. if the power production from RESs in the grid is more than the grid consumption, then the DCHP units do not produce power. Otherwise, they would produce power with respect to their nominal power and their operating points. From Fig. 5.2(a), the "EV Unit" is responsible for evaluating the availability of EVs for grid support. Fig. 5.2(b) presents the details of the EV unit. The output of 'Grid Operation' block in Fig. 5.2(a) acts as an input for 'EV Unit' block. The output of the 'EV Unit' acts as feedback for the 'Grid Operation' block in Fig. 5.2(b). Considering Fig. 5.2(b), the algorithm takes the data from 'Grid Operation' block in Fig. 5.2(a), and checks the availability of all the EVs in different buses. If the EV is moving, it cannot be used for grid support. Otherwise, the EVs will be sorted based on their state of charge (SoC). Then, the EV location (EV's bus and the feeder where the EV is connected) will be checked. Based on the maximum and minimum voltage of the feeder where the EV is connected ('V_{max}' and 'V_{min}' in Fig. 5.2(b)), the algorithm decides how to use EV. The decision is made based on voltage set points, mentioned by 'Cond1' and 'Cond2' in Fig. 5.2(b). Based on the decision, the EV will be used:

- For positive balance (charging the EV), shown by V2G(+);
- Or for negative balance (discharging the EV), denoted by V2G(-) [43];
- In case where both conditions are satisfied (both 'Cond1' and 'Cond2'), the algorithm makes decision based on the distance between the EV bus and the buses which caused 'V_{max}' and 'V_{min}' in this interval.

Based on the algorithm decision, the SoC of the EV and the "Load data" will be modified. Then, the "PF2" block analyses the grid to find the new status of the grid and to obtain the new values for 'V_{max}' and 'V_{min}'.

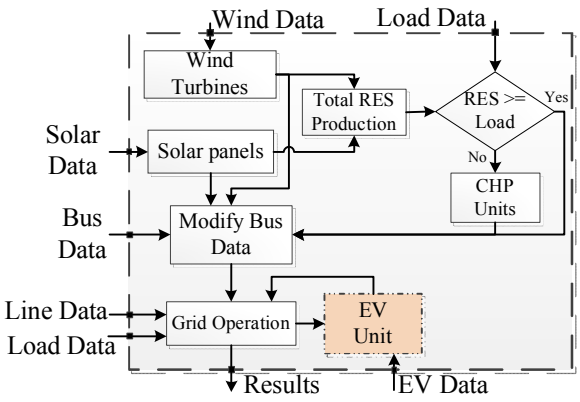

a)

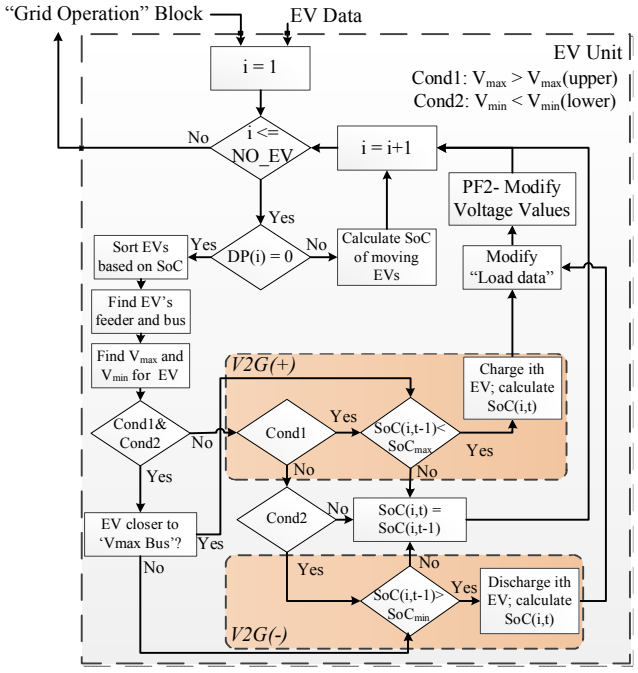

b)

Fig. 5.2. a) Proposed 'SS' module; b) Details of 'EV Unit' in 'SS' module.

5.2.2. LFC CONTROL: MODIFIED SECONDARY CONTROL

The general concept of the 'DCHP-based modified LFC model' is presented in Fig. 5.3. From Fig. 5.3, the MV microgrid is added in the secondary control loop and responds to the frequency deviations with respect to its available capacity. The frequency feedback of the network acts as an input for the proportional integral (PI)

controller. The output of the PI controller acts as an input for the "MV microgrid" and the "Upper Network", and each block responds to the signal with respect to their participation factor, denoted by 'α_{MV}' and '$\alpha_{network}$' in Fig. 5.3. The relation between 'α_{MV}' and '$\alpha_{network}$' is presented in (5.1):

$$\alpha_{MV} + \alpha_{network} = 1 \Rightarrow \alpha_{network} = 1 - \alpha_{MV} \qquad (5.1)$$

Fig. 5.4 presents the calculation procedure for participation factors. The algorithm checks the availability of DCHP units based on frequency error. For $\Delta f<0$, if DCHP units can produce more power, then the algorithm would use DCHP units. Otherwise, the 'Upper Network' will compensate frequency deviation. For $\Delta f>0$, the system needs to reduce its production. In such case, DCHP units will participate in the secondary control if they're able to reduce their output power. Otherwise, their participation factor will be zero.

The details of the "Upper Network" block in Fig. 5.3 are presented in the following, and the "MV microgrid" details are presented in Chapter 4. A major difference between the typical LFC models and the model which is used in this work should be mentioned here. In traditional LFC models, the output power of the "Upper Network", i.e. the output of the equivalent generator cannot be negative [108]. However, this value is allowed to become negative in this work. The reason is that this work is focused on the high penetration of RESs in the MV microgrid and their capability to provide ancillary service. Therefore, such change enables the MV microgrid to provide ancillary service for the upper network.

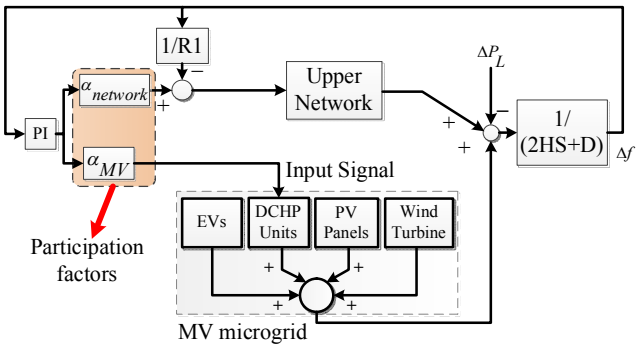

Fig. 5.3. Modified LFC with DCHP participation.

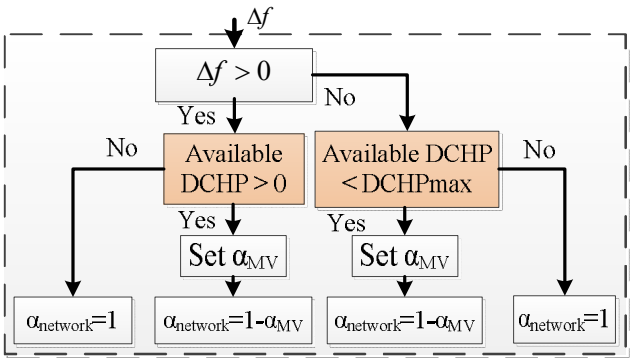

Fig. 5.4. Decision procedure for participation factors

5.2.2.1 Upper-network role in the LFC

In this study, the upper network is modelled as a generator with a turbine and a governor with a droop control [104]. Such aggregation is demonstrated to be valid for power systems with stiff transmission lines, both mathematically and practically [105]. Generally, the governors are designed to have a 4% droop characteristic, i.e. a 4% drop in frequency leads to 100% increase in the generator output [105]. Also, the generator's spinning output power alters with the "set point frequency", i.e. the frequency that the generator output spinning reserve is zero. The generator responds to the changes in the grid frequency by changing its output power, using (5.2):

$$P_{TG} = \left(\frac{f_s - f_m}{R_{droop} * f_n} \right) * P_{SR} \qquad (5.2)$$

where P_{TG} is the target power which generator should produce to get the frequency back to its nominal value (50Hz). P_{SR} is the spinning reserve capacity, fs is the set point frequency of the generator, f_m is the grid measured frequency, f_n is the grid nominal frequency (50Hz), and R_{droop} is the droop characteristic of the governor, which is considered to be 4% [105].

Considering (5.2), the output power of generator can be calculated in order to reduce the difference between the output power of generator, P_G, and the target power for the generator, P_{TG}, as explained in (5.3):

$$P_G(t+dt) = P_G(t) + \left(P_{TG} - P_G(t) \right).G_g \,.dt \qquad (5.3)$$

where Gg is the gain of governor, and P_G is the output power of generator. Gg is assumed to be 0.3 [105].

5.2.2.2 Released demand and grid inertial storage

A significant part of the loads in the grid are "rotating-machine" type loads. These loads are frequency-dependent loads, i.e. as the frequency drops, these loads slow down and consume less power [105]. Empirical results demonstrate that a 1% frequency drop leads to 1%-2% drop in the power demand of these loads [23]. This demand drop depends on the load-damping constant, represented by "*D*" in Fig. [23]. This effect, known as "released demand", is modelled using (5.4). *D* is considered to be 1.2 in this study [105].

$$P_R = -D.\,P_L.\left(\frac{f_m - f_n}{f_n}\right) \qquad (5.4)$$

On the other hand, considering the number of generators and spinning loads in the system, the effect of the stored inertial energy in these machines should be considered. The inertial capacity of a power system is defined by "inertial constant", represented by *H* in Fig.. As a typical case, this parameter changes between 2s to 8s [23]. In general, changing this parameter between 2 and 8 does not have a significant effect on the dynamic response of the system [104]. Modeling all the inertia in the system with a flywheel with the momentum of "*I"* which rotates with the grid frequency, f_m, the stored energy of the system can be obtained using (5.5) and (5.6) [104]:

$$E_S = \frac{1}{2}.\,I.(2\pi f_m)^2 \qquad (5.5)$$

$$I = \frac{2.\,P_{GM}.\,H}{\left(2\pi f_n\right)^2} \qquad (5.6)$$

where 'P_{GM}' is the total generation capacity.

5.2.3. GRID FREQUENCY CALCULATION

Considering the parameters mentioned above, the system new frequency for each time step is obtained using (5.7):

$$\omega\left(t+dt\right) = \sqrt{\omega^2(t) + \frac{2.\,P_T.\,dt}{I}} \qquad (5.7)$$

where P_T is obtained using (5.8):

$$P_T(t) = P_G(t) + P_{wind}(t) + P_{PV}(t) + P_{DCHP}(t) - P_{EV}(t) - P_L(t) \quad (5.8)$$

In (5.8), Pwind is the total wind production in the MV microgrid, P_{PV} is the total PV power production, P_{DCHP} is the power production of DCHP units, P_L is the total load demand in the microgrid, and P_{EV} is the total power of the EVs.

5.3. MODELING DETAILS OF DCHP, WIND TURBINES, AND PV PANELS

Modeling details of EVs and PV panels are presented in Chapter 2. Wind turbines are also modelled in Chapter 4. MV grid in this study is the CIGRE benchmark network which was presented in Chapter 4. The layout of the network is presented in Fig.5.5.

In this section, modeling details of DCHP units for LFC are presented. Besides, the dynamic modeling of wind turbines and PV panels for LFC control are presented in this section.

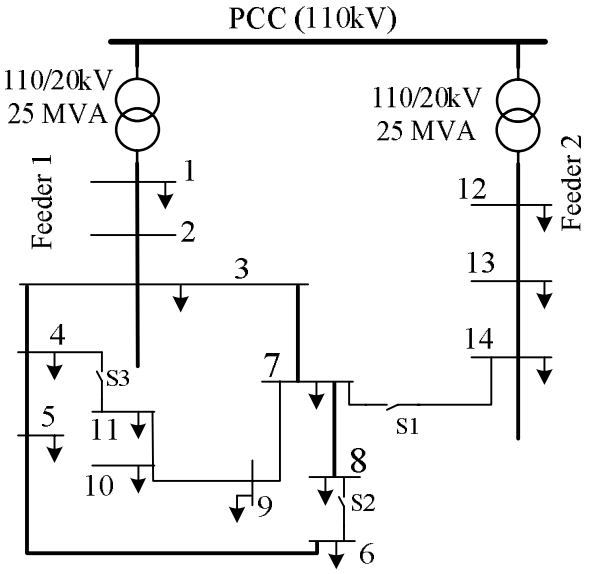

Fig.5.5. CIGRE benchmark network [103].

5.3.1. DCHP UNITS

An important fact about Danish network is the role of DCHP units in power production. In Danish scenario, it is highly likely that an MV microgrid has at least one DCHP unit, which is responsible for producing power and heat for a load center

(such as a city). In this study, 2 3-MW DCHP units are located in bus 1 and bus 12. Fig. 5.6 presents the details of DCHP modeling [109]. In this figure, "governor dead zone" defines the minimum frequency deviation for which the DCHP responds to the frequency error signal. The "DCHP power limits" determines the maximum and minimum output power of the DCHP, with "0" as its lower value and "DCHP nominal power" as its upper value.

5.3.2. WIND TURBINE

The output power of wind turbine is calculated based on the models of Chapter 4. The main equations are presented below as well.

The output power of wind turbine is calculated using (5.9), which is a common modeling approach [100]. The wind speed data in this study is obtained from the historic measurements [97]. However, since the wind measurement is done at a certain height where the measurement device is installed, the wind speed should be modified with respect to the height of the wind turbine hub. In this study, wind speed is modified using (5.10) [102].

$$P_{WT}=\begin{cases}0 & V<V_{c\_in}\\ P & V_{c\_in}\le V<V_r\\ P_r & V_r<V<V_{c\_out}\\ 0 & V>V_{c\_out}\end{cases} \tag{5.9}$$

$$Vs(h2)=Vs(h1)\left[ln\left(\frac{h2}{Z_0}\right)/ln\left(\frac{h1}{Z_0}\right)\right] \tag{5.10}$$

In this equation, "*Vc_in*" is the cut-in speed of the wind turbine, "*Vr*" is the rated speed of the turbine, "*Vc_out*" is the cut-out speed of the turbine, and "*Pr*" is the rated power of the wind turbine. Also, "*P*" is the wind turbine output power in different wind speeds which is obtained from the wind turbine power curve [110]. The details of wind turbine modeling are presented in Fig. 5.7. In this figure, "speed modification" block represents the modification of wind speed using (5.10). The "Turbine power calculation" block in Fig. 5.7 represents turbine power, which is presented in (5.9). The turbine transfer function is modelled with a first-order function [108].

5.3.3. PV PANELS

The nominal output power of the PV panels is calculated using the PV panel models in Chapter 2. As the main focus is on residential solar panels, only the grid buses with residential demand are considered for placement of PV panels. In all the studies, the penetration level of solar panels on different grid buses is similar, i.e. the number of panels on different buses is determined with respect to the residential demand of the bus. Fig. 5.8 presents the details of solar panel modeling, in which the "solar model" block is the representative of the PV output power, as presented in Chapter 2. The first-order block in Fig. 5.8 represents the inverter which connects PV panels to the grid.

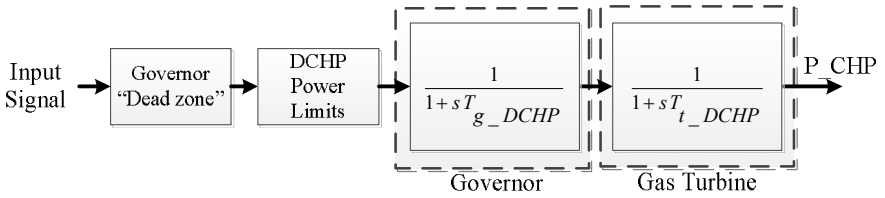

Fig. 5.6. modeling details of DCHP.

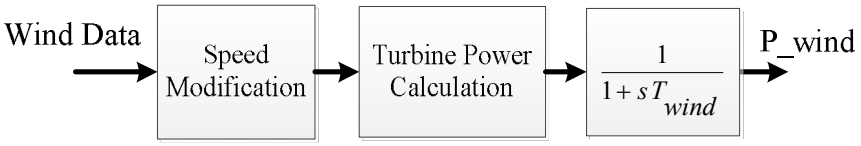

Fig. 5.7. modeling details of wind turbine.

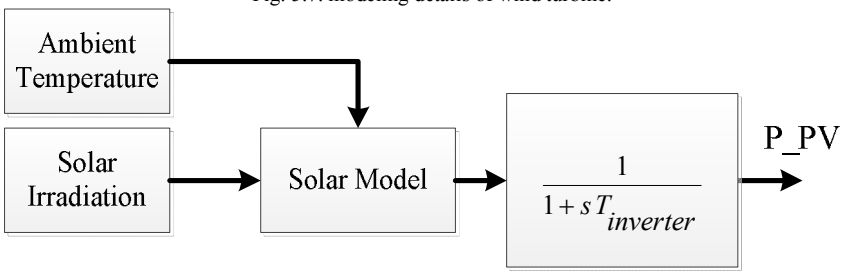

Fig. 5.8. Modeling details of PV panels.

5.4. CASE STUDIES

Different scenarios have been simulated to demonstrate the viability of the modified LFC in improving system frequency response. The simulation results are divided into two parts: the steady state results, which are related to "SS Control" block, and the frequency response results, which are related to "LFC Block".

In all the scenarios, the PV penetration is assumed to be 20% in certain grid buses, as the focus is on residential PV panels [110]. Also, the EV penetration is assumed to be 20% for certain grid buses with residential demand [110]. The simulation is done for 1000 EVs in the grid. Table 5–1 presents the number and location of different RESs, EVs, and DCHP units in the grid. 2 DCHP units with 3-MW capacity are located in the MV microgrid, on bus 1 of feeder 1 and on bus 12 of feeder 2 in Fig.5.5.

Table 5–1 Number and placement of RESs, DCHPs, and EVs in microgrid

Bus No.	No. Wind Turbines	No. PV Panels	No. EVs	No. DCHP
1	0	1000	400	1
2	0	0	0	0
3	0	0	0	0
4	0	0	3	0
5	0	50	6	0
6	0	0	3	0
7	0	0	0	0
8	0	50	3	0
9	0	0	0	0
10	1	50	3	0
11	1	0	2	0
12	1	500	400	1
13	4	0	0	0
14	1	500	180	0

5.4.1. SIMULATION RESULTS FOR ‘SS MODULE’

5.4.1.1 Winter ‘low wind’ scenario

Considering the low level of power production from RESs in this scenario, the grid voltages tend to drop during high demand period. In such case, the algorithm utilizes EVs storage to support the grid and provide part of the grid demand. It can be seen from Fig. 5.9 that the available EVs, i.e. EVs which are idle and have certain level of charge, start discharging between 16:00 to 18:00, and help improve the grid voltages. The total power exchange between the EVs (1000 EVs) and the grid is also plotted in Fig. 5.10, which clarifies the overall behavior of EVs in the “low wind” scenario. It can be realized that the EVs have a significant effect on the grid demand requirements.

5.4.1.2 Winter 'windy' scenario

In this case, the wind power production is very high, and the wind turbines are providing maximum power (16 MW) for most of the day. Therefore, the power production from RESs easily covers the grid demand for most of the day. There would also be extra power during some hours which the system should consume. In such case, the controller utilizes the storage of EVs for storing the extra power production by the RESs. However, due to the low available EV storage for such case, the extra power would be sent to the upper network. The SoC of EVs in such scenario is presented in Fig. 5.11. It can be seen from the figure that the EVs cannot provide a considerable support to the grid. The total power exchange between the EVs and the grid, which is presented in Fig. 5.12, also clarifies the role of EVs in windy scenario.

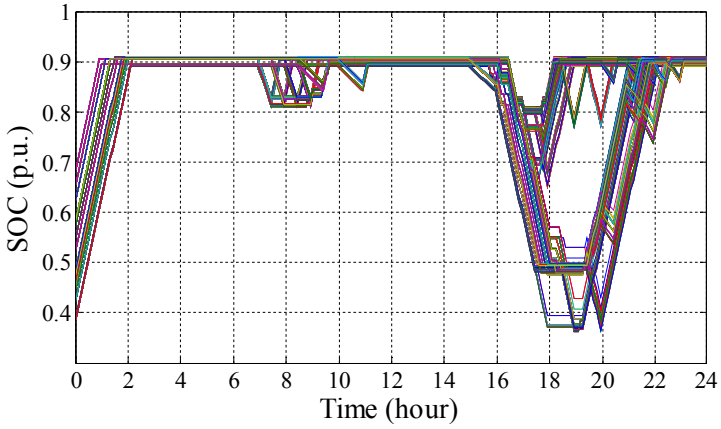

Fig. 5.9. SoC of EVs in the grid: low wind scenario.

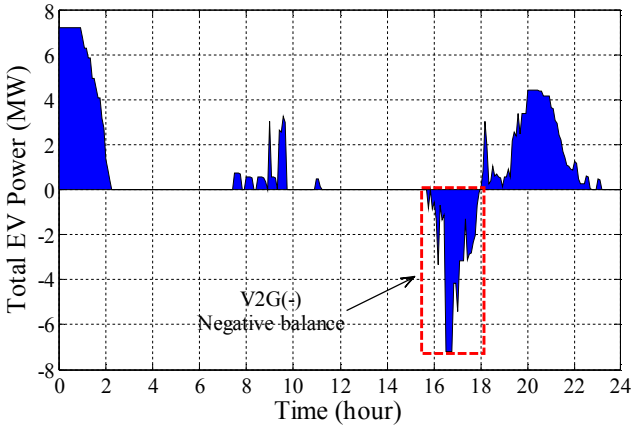

Fig. 5.10. Power exchange between EVs and grid: low wind scenario.

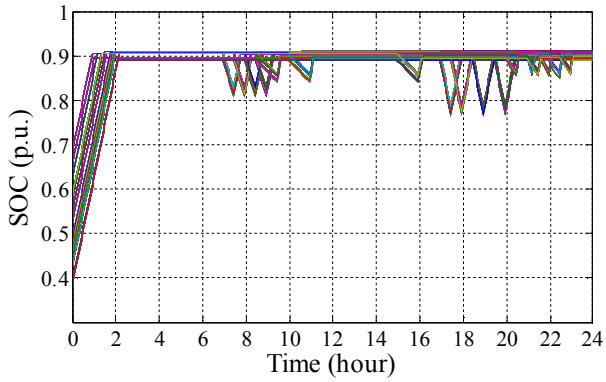

Fig. 5.11. SoC of EVs in the grid: windy scenario.

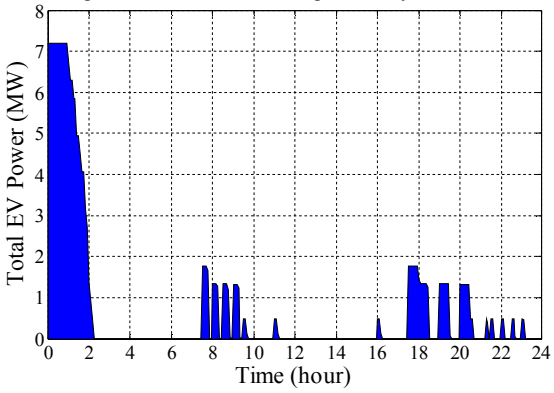

Fig. 5.12. Power exchange between EVs and grid: windy scenario.

5.4.2. SYSTEM FREQUENCY RESPONSE: LFC MODULE

The participation of DCHP units in the secondary control loop of the LFC is determined by the 'participation factor', as mentioned in (5.1) and in Fig. 5.3. Increasing the participation factor of MV microgrid units, i.e. DCHP units in this study, will increase the role of these units in system frequency response, which in turn leads to less participation of the upper network in the frequency response. Different cases are simulated below to evaluate the impact of DCHP participation in the LFC.

5.4.2.1 Case 1: under-frequency scenario

If the power production of the RESs in the grid is less than the total grid consumption, the frequency tends to drop. In such case, the LFC system responds to the frequency changes to bring the frequency back to its nominal value. Adding DCHP units to the LFC will generally improve system frequency response, as these units have faster response compared to the upper network. This can be realized in

Fig. 5.13, by comparing the system original frequency response with the frequency response in presence of DCHP units. Different participation factors are simulated to clarify the effectiveness the LFC control. From Fig. 5.13, increasing the participation of DCHP units in the frequency control improves the frequency response. The output power of DCHP units is presented in Fig. 5.14.

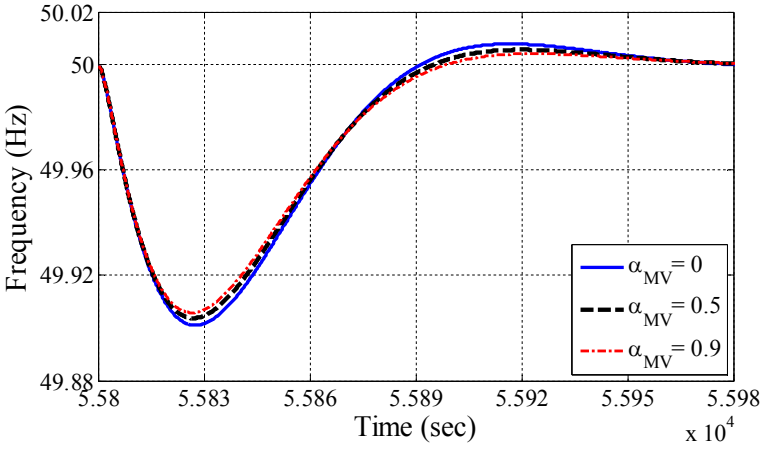

Fig. 5.13. System frequency response: Case 1.

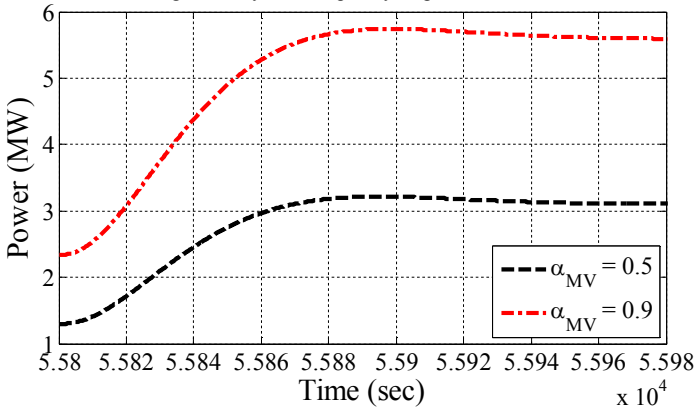

Fig. 5.14. DCHP participation in frequency control: Case 1.

5.4.2.2 Case 2: DCHP limits for under-frequency scenario

In some cases, the power production of the RESs in the grid is very low, and the difference between the "total grid consumption" and the "total RES production" is greater than the capacity of the DCHP units. In such cases, the impact of DCHP units on the frequency response is determined by two parameters: 1) the amount of total grid consumption which should be compensated by DCHP units (due to low power production of RESs); and 2) the 'participation factor'. As can be seen in

Fig. 5.15, high load demand in the grid causes the system frequency to drop. In the original LFC, shown by the blue line in Fig. 5.15, the upper network is responsible for supporting the frequency. By including DCHP units in the frequency response, the system response tends to improve. However, when the 'participation factor' of DCHP units increases more than a certain value, the DCHPs make the frequency response worse. Considering the green line in Fig. 5.15, in which α_{MV}=0.75, DCHPs have a totally negative impact on the frequency. To clarify the reason, the output power of DCHPs is presented in Fig. 5.16. As can be seen, due to high demand in the grid, high participation of DCHP units in the LFC leads to early saturation of these units, i.e. the units produce power at their maximum capacity from an early stage. Therefore, they cannot further support the frequency, as they cannot provide power for grid demand. Regarding Fig. 5.3, the PI controller divides the error signal between the upper network and the DCHPs based on their 'participation factor'. Higher 'participation factor' requires DCHPs to produce power at a higher rate. As a result, when DCHPs reach their maximum capacity, they cannot respond to the error signal anymore. Consequently, the LFC cannot completely compensate the frequency error. Therefore, allocating a proper 'participation factor' to DCHPs is an important parameter in improving frequency response.

5.4.2.3 Case 3: Over-frequency scenario

There are cases where the power production of RESs in the grid exceeds the total grid consumption. In such case, the frequency tends to increase. In the traditional LFC, i.e. without participation of MV grid units (α_{MV}=0), the upper network deals with frequency and brings frequency back to its nominal value. This can be seen by the blue solid line in Fig. 5.17. By adding DCHP units in the LFC, the PI controller divides the error signal between the upper network and the DCHP units. As the system faces over-frequency, the DCHP units should reduce their power production to help bringing frequency to its nominal value. However, if the output power of DCHP units is already zero, they cannot reduce their output power any further. On the other hand, they cannot consume power. Therefore, they cannot respond to the frequency error signal. In such case, only the upper network is responding to the error signal of PI controller. As a result, part of the error signal remains in the system for a longer time, compared to the traditional LFC (i.e. blue line in Fig. 5.17). In such cases, the participation factor of MV grid becomes zero (α_{MV}=0), and the upper network deals with over-frequency.

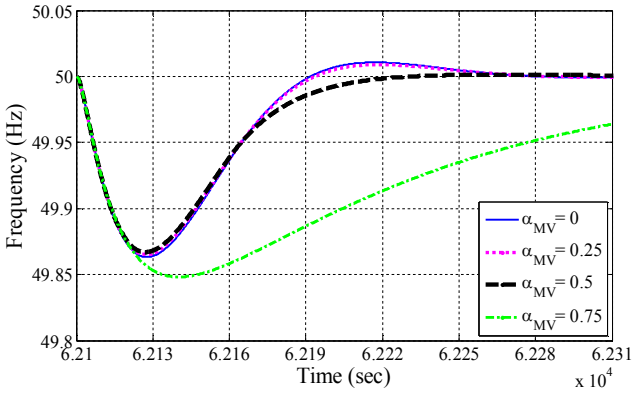

Fig. 5.15. System frequency response: Case 2.

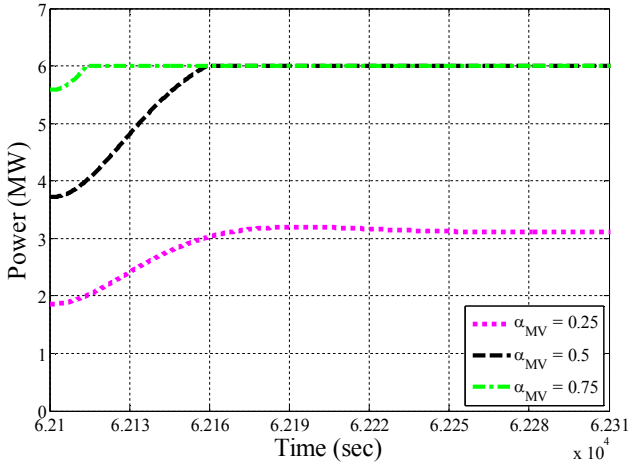

Fig. 5.16. DCHP participation in frequency control: Case 2.

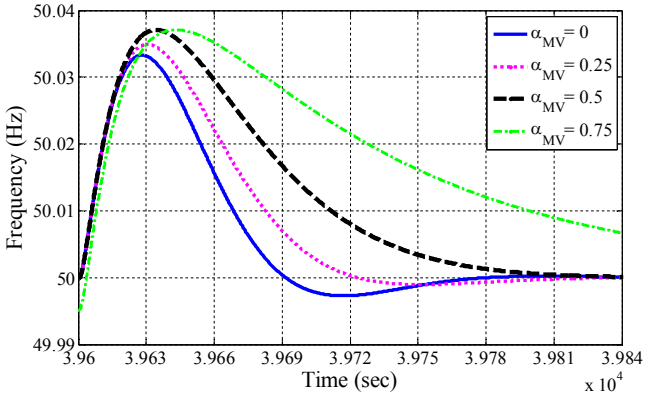

Fig. 5.17. System frequency response: Case 3.

5.5. SUMMARY

A combined control layout for the medium voltage (MV) microgrid is proposed and discussed in this chapter. The control structure consists of a steady state control module, and a frequency control module. The proposed steady state control strategy manages the grid operating limits under high penetration of RESs by intelligent management of the EV storages in the grid. The proposed algorithm in this regard considers the customer's quality of service (QoS) as a requirement for utilizing the EVs' storage in the grid. The second part of the control layout, i.e. the frequency control, implements a modified load frequency control (LFC) to utilize the DCHP units of the MV microgrid in the frequency response of the system. Despite the usual LFC models, the proposed modified LFC model enables the MV microgrid to involve in system frequency response. Simulation results reveal the effectiveness of the proposed algorithm in utilizing the EVs for grid support purposes, without endangering customers' QoS. On the other hand, the results from the frequency response of the system clarify that adding DCHPs in the LFC can improve system frequency response, if the 'participation factor' of these units are defined correctly under different operating conditions.

.

CHAPTER 6. CONCLUSIONS AND FUTURE WORKS

This chapter summarizes the results and the work which have been done in this project. It also outlines the main contributions of the project, including smart management of high RES penetration, aggregation method for distribution networks, energy interaction between MV/LV networks and the HV transmission network, and modified load frequency control (LFC). Some interesting perspectives are proposed at the end for further investigations on the topic.

6.1. SUMMARY

In this project, the main objectives include:

a) Evaluating and quantifying the impact of PV panels and electric vehicles (EVs) on low voltage (LV) distribution networks;

b) Evaluating the impact of wind turbines and decentralized combined heat and power (DCHP) units on medium voltage (MV) networks and their interactions with the high voltage (HV) transmission network;

Chapter 2 and Chapter 3 address the first objective of the project, while the second objective is covered in Chapter 4 and Chapter 5,

Chapter 2 evaluates the impact of residential PV panels on distribution networks. It also quantifies the impact of PV panels on distribution networks, and the effect of PV panels on reverse power flow. The impact of EVs on distribution network is also addressed in this chapter. Different charging strategies have been proposed for EVs to avoid potential issues which are caused by EVs. Furthermore, a smart energy management strategy has been developed in Chapter 2 to enable the potential of EVs for grid support purposes. The developed algorithm manages the interaction of PV panels and EVs with the electric network to avoid potential issues in the network, while supporting the network via PV panels and EVs. Modeling details of PV panels and EVs are discussed in Chapter 2, and these models have been used in the rest of the project as well.

Chapter 3 proposes an aggregation method for distribution networks, considering PV panels and EVs. The number of distribution transformers which are connected to an MV transformer is generally significant. Considering the significant number of customers under each distribution transformer, each distribution system operator (DSO) deals with a huge number of customers, and adding new players such as EVs and PV panels makes the circumstance more complex. Therefore, a good aggregated model of distirubion networks alleviates the calculation complexity for determining available flexibility of distribution networks. Details of the proposed method are explained in Chapter 3. Different scenarios have been defined and simulated to demonstrate the validity of the method. The method is also tested in presence of PV panels and EVs.

Chapter 4 presents a steady state analysis of medium voltage (MV) network in presence of wind turbines and decentralized combined heat and power (DCHP) units. The role of distribution networks, as discussed in Chapter 2 and Chapter 3, is also included in the MV network. Bu other words, the impact of PV panels and EVs are also considered in the MV network studies. The interaction between MV network and high voltage (HV) transmission system is discussed and demonstrated in Chapter 4, by quantifying the power and energy exchange between the MV network and the HV transmission network.

In Chapter 5, active participation of MV networks in system frequency response has been investigated. A modified secondary control is proposed in this chapter to incorporate MV network units in traditional load frequency control (LFC). A modified procedure has been proposed for determining "Particpation factor" of different units in the LFC. Different scenarios have been simulated to demonstrate the positive impact of MV network on the system frequency response, as well as quantifying potential limitations of MV network units for participating in frequency response.

6.2. CONTRIBUTIONS FROM THE AUTHORS POINT OF VIEW

The main contributions of this project from the author's point of view are summarized as follows:

1) Developing a smart energy management strategy:

A smart energy management algorithm is proposed in this work to utilize the potential of PV panels and EVs for grid support requirements. To keep the algorithm as viable solution, the algorithm is mainly based on voltage measurements of grid buses. Based on the status of the grid buses, the first objective of EVs is to support their local area, i.e. EVs are utilized to support their direct connection bus and their feeder in the first place.

2) Proposing an aggregation technique for distribution networks:

A new aggregation procedure is proposed in this work for distribution networks. The main concept of the method is based on the concepts of electric circuits, as well as the operating requiremnts of distribution networks. The operating conditions of distribution networks validate the application of the proposed method for aggregation purposes. Furthermore, a simplified method is proposed for calculation of the grid impedances.

3) Proposing a modified secondary control:

A 2-level control strategy has been proposed for incorporating MV network in the HV control strategies. The strategy includes a steady state control layout, and a frequency control layout. The steayd state control layout manages the high penetration of wind turbines, PV panels, and EVs in the MV and LV networks, and utilizes the capability of these players for supporting HV transmission network. On the other hand, for the frequency control layout, a modified load frequency control (LFC) has been developed which incorporates small DCHP units of MV network in the LFC. The developed 2-level strategy has been tested to demonstrate its capability for responding to the potential requirements from HV network.

6.3. FUTURE WORKS

Some of the interesting issues which can be considered for further studies are listed below:

1) The impact of PV panels and EVs has been investigated in this study. However, the reverse power flow which is caused by PV and EV causes certain issues for protection devices in the network. The design and implementation of protection devices has always been based on the unidirectional power flow, from the HV network to the LV network and customers. These methods and calculations need to be modified for active distribution networks, where the power and energy can flow in both directions.

2) Regarding PV panels, this work was focused on small residential PV panels. Therefore, the potential control of PV converters, i.e. converters which connect the PV panels to the network, was not considerd in this study. However, considering the new concepts and roles which might appear in the future power systems, such as the role of Aggregator, there could be economic incentives for actively managing and controlling customers of the network. In such case, and under high penetration of PV panels in residential areas, it would be more logical to have control over small PV panels.

3) The proposed modified secondary control considered DCHP units of MV network for improving system frequency response. For this purpose, it was assumed that the LFC is able to utilize the whole capacity of DCHP units for frequency response purposes. However, due to main role of DCHPs in the system, i.e. providing heat for customers, the heat requirements of customers should be considered in the modeling of DCHP units in order to further improve the accuracy of the results. It should be noted that such requirements does not necessarily limit the capability of DCHP units for frequency response. For most of DCHP units, a heat storage system is incorporated in the units which stores the extra heat provided by the units for later consumptions.

4) Although the potential of EVs have been utilized for grid support, they have not been considered for frequency response. However, under potentially high penetration of EVs in the future power network, these vehicles can also be involved in the LFC to further improve the system frequency response. The main obstacles to address for such applications are the driving requirements of the EV owners and the availability of EVs for frequency applications, as well as the battery lifetime issues of EVs.

5) In current grid codes, small wind turbines cannot participate in frequency response. However, considering Danish milestones which encourage high penetration of small wind turbines, the number of these turbines will increase significantly in the near future. In such scenario, incorporating small wind turbines in the frequency response can be legitimate. Considering the potential participation of Danish power network in the European requlation market, such scenario brings a high incentive for investors to further invest on these untis. It should be noted that in such scenario, the interconnections between Danish network and other neighboring networks, such as Germany, Sweden, and Norway, should also be taken into consideration.

BIBLIOGRAPHY

[1] European Commission, "2030 framework for climate and energy policies," [Online]. Available: http://ec.europa.eu/clima/policies/2030/index_en.htm, 2014.

[2] European Commission, "European 20-20-20 targets," [Online]. Available: http://ec.europa.eu/clima/policies/package/index_en.htm, 2013.

[3] [Online]. Available: www.ens.dk.

[4] The Danish government, "Our future energy," Technical Report, Nov. 2011.

[5] P. Sorknæs, H. Mæng, T. Weiss, and A. N. Andersen, "Overview of the danish power system and res integration," Technical report, Jul. 2013.

[6] Energinet.dk, "Wind turbines reached record level in 2014," [Online]. Available: http://www.energinet.dk/EN/El/Nyheder/Sider/Vindmoeller-slog-rekord-i-2014.aspx , Jan. 2015.

[7] The Danish Ministry of Climate, Energy, and Building, "Smart grid strategy: The intelligent energy system of the future," Technical report, May 2013.

[8] Global wind energy council, "Global wind statistics 2014," Technical report, Feb. 2015.

[9] Energinet.dk, "Energinet.dk's analysis assumptions 2013-2035," Technical report, Apr. 2013.

[10] Energinet.dk, "Natural gas transmission and distribution system," [Online] Available: http://www.energinet.dk/EN/GAS/, 2014.

[11] Danish Energy Agency and Danish Board of District Heating, "district heating - danish and chinese experience," Technical Report, 2012.

[12] "Denmark in figures 2015," [Online]: Available: http://www.dst.dk/Site/Dst/Udgivelser/GetPubFile.aspx?id=19006&sid=denmark2015.

[13] Ministry of Transport and Statistics Denmark, "Key figures for transport 2011," Statistical Survey, Jun. 2012.

[14] Henrik Lund, "Wide perspective of smart grid," Course presentation.

[15] Energinet.dk, "Smart grid in denmark 2.0," Technical report, [Online]. Available:http://energinet.dk/SiteCollectionDocuments/Engelske%20dokumenter/Forskning/Smart%20Grid%20in%20Denmark%202.0.pdf.

[16] Technical regulation 3.2.1 for electricity generation facilities with a rated current of 16 A per phase or lower.

[17] CENELEC-ETSI, "CEN-CENELEC-ETSI smart grid coordination group-sustainable processes," Nov. 2012.

[18] Energinet.dk, "Strategy plan 2010," Technical report, 2010.

[19] V. Alimisis, and N.D. Hatziargyriou, "Evaluation of a hybrid power plant comprising used EV-batteries to complement wind power," *IEEE Trans. Sustain. Energy*, vol. 4, no. 2, pp. 286- 293, Apr. 2013.

[20] J.R. Pillai, and B. Bak-Jensen, "Integration of vehicle-to-grid in the western danish power system," *IEEE Trans. Sustain. Energy*, vol.2, no.1, pp. 12-19, Jan. 2011.

[21] R. Ahmadi Kordkheili, B. Bak-Jensen , J.R. Pillai, and Pukar Mahat, "Determining maximum photovoltaic penetration in a distribution grid considering grid operation limits," *in proc. IEEE PES general meeting*, July 2014, pp. 1-5.

[22] M. Thompson, and D. G. Infield, "Impact of widespread photovoltaics generation on distribution systems," *IET Renew. Power Gener.*, vol. 1, no. 1, pp. 33-40, March 2007.

[23] P. Kundur, *Power System Stability and Control*, New York: McGrawHill, 1993, pp. 581–592.

[24] V. Neimane, "On development planning of electricity distribution networks," doctoral dissertation, 2012, http://www.diva-portal.org/smash/get/diva2:9035/FULLTEXT01.pdf.

[25] J.R.Pillai, P. Thogersen, J. Moller, and B. Bak-Jensen, "Integration of electric vehicles in low voltage danish distribution grids," in *Proc. IEEE PES General Meeting*, July 2012, pp. 1-8.

[26] G. Carpinelli, P. Caramia, F. Mottola, and D. Proto, "Exponential weighted method and a compromise programming method for multi-objective operation of plug-in vehicle aggregators in microgrids," J. electrica power and energy syst., vol. 56, pp. 374-384, March 2014.

[27] R. T. Marler, and J. S. Arora, "Survey of multi-objective optimization methods for engineering," *Struct. Multidisc Optim*, vol. 26, pp. 369-395, March 2004.

[28] M. Mitchell, *An introduction to genetic algorithms*, MIT press, 1999.

[29] Hany M. Hasanien, and S. M. Muyeen, "Design optimization of controller parameters used in variable speed wind energy conversion system by genetic algorithms", *IEEE Trans. Sustain. Energy*, vol. 3, no. 2, pp. 200-208, April 2012.

[30] Hany M. Hasanien, "Design optimization of pid controller in automatic Voltage regulator system using taguchi combined genetic algorithm method", *IEEE Systems Journal*, vol. 7, no. 4, pp. 825-831, December 2013.

[31] Renewable development initiative, European bank for reconstruction and development (EBRD). [Online]. Available: http://www.ebrdrenewables.com/sites/renew/default.aspx.

[32] IEEE P2030, "Guide for smart grid interoperability of energy technology operation with electric power system (EPS), and end-use applications and loads," *IEEE Standards Association*, Sep. 2011.

[33] Farmer, Chris; Hines, Paul; Dowds, Jonathan; Blumsack, Seth; "Modeling the impact of increasing phev loads on the distribution infrastructure" Proceedings of the Annual Hawaii International Conference on System Sciences, 2010.

[34] W. H. Kersting, *Distribution System Modeling and Analysis*. Boca Raton, FL: CRC Press, 2007.

[35] L. P. Fernan´dez;, T. Román, R. Cossent, C. M. Domingo, and P. Frías, "Assessment of the impact of plug-in electric vehicles on distribution networks," *IEEE Trans. Power Syst.*, vol. 26, no. 1, pp. 206–213, Feb. 2011.

[36] C. Wen, J. Chen, J. Teng, and P. Ting, "Decentralized Plug-in Electric Vehicle Charging Selection Algorithm in Power Systems," IEEE Trans.Smart Grid, vol. 3, no. 4, pp. 1779–1789, Dec. 2012.

[37] C. Jin, J. Tang, and P. Ghosh, "Optimizing Electric Vehicle Charging: A Customer's Perspective," IEEE Trans. Vehicular Technology, vol. 62, no. 7, pp. 2919–2927, Sep. 2013.

[38] P. Richardson, D. Flynn, and A. Keane, "Local Versus Centralized Charging Strategies for Electric Vehicles in Low Voltage Distribution Systems," IEEE Trans. Smart Grid, vol. 3, no. 2, pp. 1020– 1028, 2012.

[39] I. Buchmann, *Batteries in a portable world: a handbook on rechargeable batteries for non-engineers*, Cadex Electronics, Inc; 2nd Edition, May 2001.

[40] M. A. Roscher, J. Assfalg, and O. S. Bohlen, "Detection of utilizable capacity deterioration in battery systems," IEEE Trans. Veh. Technol., vol. 60, no. 1, pp. 98–103, Jan. 2011.

[41] O. Sundstrom, and C. Binding, "Flexible charging optimization for electric vehicles considering distribution grid constraints," *IEEE Trans. Smart Grid*, vol. 3, no. 1, pp. 26-37, March 2012.

[42] Mohamed M. Aly, E. Abdelkarim, and M. Abdel-Akher, "Mitigation of photovoltaic power generation fluctuations using plug-in hybrid electric vehicles storage batteries," *International Trans. Electrical Energy Systems*, Early access.

[43] W. Kempton, and J. Tomic, "Vehicle-to-grid power implementation: from stabilizing the grid to supporting large-scale renewable energy," *J. Power Sources 144*, pp. 280–294, 2005.

[44] F. Katiraei and J. R. Agüero, "Solar pv integration challenges," IEEE P&E Mag., vol. 9, no. 3, pp. 62–71, May-Jun. 2011.

[45] S. Morozumi, S. Kikuchi, Y. Chiba, J. Kishida, S. Uesaka, and Y. Arashiro, "Distribution technology development and demonstration projects in Japan," in Proc. 2008 IEEE Power and Energy Society General Meeting, Jul. 20–24, 2008, pp. 1–7.

[46] P. M. S. Carvalho, P. F. Corriea, and L. A. F. Ferriera, "Distributed reactive power generation control for voltage rise mitigation in distribution networks," IEEE Trans. Power Syst., vol. 23, no. 2, pp. 766772, May 2008.

[47] G.M. Shafiullah, A. M. T. Oo, D. Jarvis, A. B. M. S Ali, and P. Wolfs, "Potential challenges: integrating renewable energy with the smart grid," *in Proc. 20th AUPEC*, 2010, pp 1-6.

[48] W.A. Omran, M. Kazerani, and M.M.A Salama, "Investigation of methods for reduction of power fluctuations generated from large grid-connected photovoltaic systems," *IEEE Trans. Energy Conversion*, vol. 26, no. 1, pp. 318-327, March 2011.

[49] Y. Ueda, K. Kurokawa, T. Tanabe, K. Kitamura, and H. Sugihara, "Analysis results of output power loss due to the grid voltage rise in grid-connected photovoltaic power generation systems," *IEEE Trans. Ind. Electron.*, vol. 55, no. 7, pp. 2744–2751, Jul. 2008.

[50] R. Tonkoski, D. Turcotte, and T. H. M. EL-Fouly, "Impact of high pv penetration on voltage profiles in residential neighborhoods," *IEEE Trans. Sustain. Energy*, vol. 3, no. 3, pp. 518–527, Jul. 2012.

[51] D.Q. Hung, and N. Mithulananthan, "Multiple distributed generator placement in primary distribution networks for loss reduction," *IEEE Trans. Ind. Electron.*, vol. 60, no. 4, pp. 1700-1708, April 2013.

[52] A. Al-Sabounchi, J. Gow, and M. Al-Akaidi, "Simple procedure for optimal sizing and location of a single photovoltaic generator on radial distribution feeder," *IET Renew. Power Gen*., vol. 8, no. 2, pp. 160-170, March 2014.

[53] C.H. Lin, W.L. Hsieh, C.S. Chen, C.T. Hsu, and T.T. Ku, "Optimization of photovoltaic penetration in distribution systems considering annual duration curve of solar irradiation," *IEEE Trans. Power Syst.*, vol. 27, no. 2, pp. 1090-1097, May 2012.

[54] M.F. Shaaban, Y.M. Atwa, and E.F. El-Saadany, "DG allocation for benefit maximization in distribution networks," *IEEE Trans. Power Syst.*, vol.28, no. 2, pp. 639-649, May 2013.

[55] F. Alsokhiry, and K.L. Lo, "Distributed generation based on renewable energy ancillary services," *in Proc. IEEE POWERENG*, May 2013, pp. 1200-1205.

[56] Jasna Tomic, and Willett Kempton, "Using fleets of electric-drive vehicles for grid support," *Elsevier J. Power Sources*, vol. 168, no. 2, pp. 459-468, June 2007.

[57] E. Sortomme, M.A. El-Sharkawi, "Optimal charging strategies for unidirectional vehicle-to-grid," *IEEE Trans. Smart Grid*, vol. 2, no. 1, pp. 131-138, March 2011.

[58] V. V. Viswanathan, and M. kintner-Meyer, "Second use of transportation batteries: maximizing the value of batteries for transportation and grid services," *IEEE Trans. Vehic. Tech.*, vol. 60, no. 7, pp. 2963-2970, Sep. 2011.

[59] S. Gao, K. T. Chau, C. Liu, D. Wu, and C. C. Chan, "Integrated energy management of plug-in electric vehicles in power grid with renewables," *IEEE Trans. Vehic. Tech.*, vol. 63, no. 7, pp. 3019-3027, Sept. 2014.

[60] J. J. Escudero-Garzas, A. Garcia-Armada, and G. Seco-Granados, "Fair design of plug-in electric vehicles aggregator for V2G regulation," *IEEE Trans. Vehic. Tech.*, vol. 61, no. 8, pp. 3406-3419, Oct. 2012.

[61] F. Guo, E. Inoa, W. Choi, and J. Wang, "Study on global optimization and control strategy development for a PHEV charging facility," *IEEE Trans. Vehic. Tech.*, vol. 61, no. 6, pp. 2431-2441, July 2012.

[62] N. L. Diaz, T. Dragicevic, J. C. Vasquez, and J. M. Guerrero, "Intelligent distributed generation and storage units for dc microgrids-a new concept on cooperative control without communications beyond droop control," *IEEE Trans. Smart Grid*, vol. 5, no. 5, pp. 2476-2485, Sep. 2014.

[63] Dan Wu, Fen Tang, T. Dragicevic, J. C. Vasquez, and J. M. Guerrero, "A control architecture to coordinate renewable energy sources and energy storage systems in islanded microgrids," *IEEE Trans. Smart Grid*, vol. 6, no. 3, pp. 1156-1166, May 2015.

[64] R. Ahmadi Kordkheili, S.A. Pourmousavi, J.R. Pillai, H.M. Hasanien, B. Bak-Jensen, and M.H. Nehrir, "Optimal sizing and allocation of residential photovoltaic panels in a distribution network for ancillary services application," *in Proc. IEEE OPTIM*, May 2014, pp. 681-687.

[65] H. Saadat, *Power System Analysis*, 2nd Ed. New York, NY, USA:Mc- Graw Hill, 2002.

[66] J.R.Pillai, S.Huang, B.Bak-Jensen, P.Mahat, P.Thogersen, and J.Moller, "Integration of solar photovoltaics and electric vehicles in residential grids," *in Proc. IEEE PES general meeting*, 2013, pp.1-5.

[67] A.Affanni, A.Bellini, G.Franceschini, P.Guglielmi, and C.Tassoni, "Battery choice and management for new-generation electric vehicles," *IEEE Trans. Ind. Electron.*, vol. 52, no. 5, pp.1343-1349, Oct. 2005.

[68] L. Bird, and D. Lew, "Integrating wind and solar Energy in the U.S. bulk power system: lessons from regional integration studies," NREL, Sep. 2012.

[69] R. J. Bessa, and M. A. Matos, "Economic and technical management of an aggregation agent for electric vehicles: a literature survey," *European Trans. Electrical Power*, vol. 22, no. 3, pp. 334-350, Apr. 2012.

[70] C. Battistelli, L. Baringo, and A. J. Conejo, "Optimal energy management of small electric energy systems including v2g facilities and renewable energy sources," *J. Electric Power Systems Research*, vol. 92, pp. 50-59, Nov. 2012.

[71] Divya K. C, J. Østergaard, E. Larsen, C. Kern, T. Wittmann, and M. Weinhold, "Integration of electric drive vehicles in the danish electricity network with high wind power penetration," *European Trans. Electrical Power*, vol. 20, no. 7, pp. 872-883, Oct. 2010.

[72] B. Cosic, G. Krajacic, and N. Duic, "A 100% renewable energy system in the year 2050: the case of macedonia," *J. Energy*, vol. 48. no. 1, pp. 80-87, Dec. 2012.

[73] T. Krause, and G. Andersson, "The role of electric vehicles in smart grids," *Wiley Interdis. Reviews, Energy and Environment*, vol. 2, no. 4, pp. 384-400, Aug. 2013.

[74] K. Clement-Nyns, E. Haesen, and J. Driesen, "The impact of vehicle-to-grid on the distribution grid," *J. Electric Power Systems Research*, vol. 81, no. 1, pp. 185-192, Jan. 2011.

[75] H. Lund, and B. V. Mathiesen, "Energy system analysis of 100% renewable energy system-the case study of denmark in years 2030 and 2050," *J. Energy*, vol. 34. no. 5, pp. 524-231, May 2009.

[76] R. D'hulst, F. D. Ridder, B. Claessens, L. Knapen, and D. Janssens, "Decentralized coordinated charging of electric vehicles considering locational and temporal flexibility," *International Trans. Electrical Energy Systems*, Early access.

[77] G. Krajacic, N. Duic, Z. Zamijarevic, B. V. Mathiesen, A. A. Vucinic, and M. D. G. Carvalho, "Planning for a 100% independent energy system based on smart energy storage for integration of renewables and co2 emissions reduction," *J. Applied Thermal Engineering*, vol. 31, no. 13, pp. 2073-2083, Sep. 2011.

[78] F. D. Ridder, M. Hommelberg, and E. Peeters, "Demand side integration: four potential business cases and an analysis of the 2020 situation," *European Trans. Electrical Power*, vol. 21, no. 6, pp. 1902-1913, Sep. 2011.

[79] R. A. Jabr, "Minimum loss operation of distribution networks with photovoltaic generation," *IET Renew. Power Gener.,* vol. 8, no. 1, pp. 33-44, Jan. 2014.

[80] J. B. Ward, "Equivalent circuits for power flow studies," *AIEE Trans. Power Appl. Syst.*, vol. 68, pp. 373–382, 1949.

[81] H. Duran and N. Arvanitidis, "Simplification for area security analysis: a new look at equivalencing," *IEEE Trans. Power App. Syst.*, vol. PAS-91, no. 2, pp. 670–679, Mar. 1972.

[82] G. Irisarri, A.M. Sasson, and J. F. Dopazo, “Real-time external system equivalent for on-line contingency analysis,” *IEEE Trans. Power App. Syst.*, vol. PAS-98, no. 6, pp. 2153–2171, Nov. 1979.

[83] D. Shi, D. L. Shawhan, N. Li, and D. J. Tylavsky, “Optimal generation investment planning: Pt. 1: network equivalents,” in *Proc. 44th North Amer. Power Symp.*, Champaign, IL, USA, Sep. 2012, pp. 1–6.

[84] D. Shi, and D.J. Tylavsky, “A novel bus-aggregation-based structure-preserving power system equivalent”, *IEEE Trans. Power Syst.*, 2014.

[85] X. Cheng and T. J. Overbye, “PTDF-based power system equivalents,” *IEEE Trans. Power Syst.*, vol. 20, no. 4, pp. 1868–1876, Nov. 2005.

[86] H. Oh, “A new network reduction methodology for power system planning studies,” *IEEE Trans. Power Syst.*, vol. 25, no. 2, pp. 677–684, May 2010.

[87] G. Y. Yang, M. Mattesen, S. B. Kjær, R. D. Lazar, A. Constantin, J. Østergaard, and C. Stephansen, ”Analysis of thevenin equivalent network of a distribution system for solar integration studies”, IEEE ISGT Europe, pp. 1-5, 2013.

[88] A. Kechroud, J. M. A. Myrzik. and W. L. Kling, "A power system equivalent impedance based voltage control," in Power Energy Society General Meeting, 2009. PES '09. IEEE, July 2009, pp. 1-5.

[89] A.Z.M. Shahriar, G. Taylor, and M. Bradley, “Novel approach to updating network equivalents for different cardinal points,” in *Proc. IEEE UPEC*, Sep. 2014, pp. 1-6.

[90] S. Deckmann, A. Pizzolante, A. Monticelli, B. Stott, and O. Alsac, “Studies on power system load flow equivalencing,” *IEEE Trans. Power App. Syst.*, vol. PAS-99, no. 6, pp. 2301-2310, Nov. 1980.

[91] R. Ahmadi Kordkheili, B. Bak-Jensen, J. R-Pillai, and B. P. Bhattarai, “A fast approach for calculating the available flexibility of a residential distribution grid,” in Proc. IEEE PowerEng, May 2015, pp. 1-6.

[92] Standard EN 50160 ed. 3, "Voltage characteristics of electricity supplied by public distribution networks," 2011.

[93] T. Aigner, S. Jaehnert, G. L. Doorman, and T. Gjengedal, “The effect of large-scale wind power on system balancing in northern europe,” *IEEE Trans. Sustain. Energy*, vol. 3, no. 4, pp. 751–759, Oct. 2012.

[94] S. Vachirasricirikul and I. Ngamroo, “Robust lfc in a smart grid with wind power penetration by coordinated v2g control and frequency controller,”, IEEE Trans. Smart Grid, vol. 5, no. 1, pp. 371– 380, 2014.

[95] M. Moeini-Aghtaie, A. Abbaspour, and M. Fotuhi-Firuzabad, “Incorporating large-scale distant wind farms in probabilistic transmission expansion planning—Part I: Theory and algorithm,” *IEEE Trans. Power Syst.*, vol. 27, no. 3, pp. 1585–1593, Aug. 2012.

[96] N. Maisonneuve and G. Gross, “A production simulation tool for systems with integrated wind energy resources,” *IEEE Trans. Power Syst.*, vol. 26, no. 4, pp. 2285–2292, Nov. 2011.

[97] [Online]. Available: www.energinet.dk.

[98] E. Veldman, and R. A. Verzijlbergh, “Distribution grid impacts of smart electric vehicle charging from different perspectives,” IEEE Trans. Smart Grid, vol. 6, no.1, pp. 333-342, 2015.

[99] T. Kristoffersen, K. Capion, and P. Meibom, “Optimal charging of electric drive vehicles in a market environment,” Appl. Energy, vol. 88, no. 5, pp. 1940–1948, 2011.

[100] P. Siano and G. Mokryani, “Probabilistic assessment of the impact of wind energy integration into distribution networks,” *IEEE Trans. Power Syst.*, vol. PP, no. 99, pp. 1–8, 2013.

[101] [Online]. Available: www.vestas.dk.

[102] N. B. Negra, "Offshore wind power: grid connection and reliability," Doctoral Dissertation, Dept. Energy Technology, Aalborg University, Denmark, 2008.

[103] K. Rudion, A. Orths, Z. Styczynski and K. Strunz, "Design of benchmark of medium voltage distribution network for investigation of DG integration," in Proc. IEEE PES General Meeting, 2006.

[104] M. D. Galus, S. Koch, and G. Andersson, "Provision of load frequency control by PHEVs, controllable loads, and a cogeneration unit," *IEEE Trans. Ind. Electron.*, vol. 58, no. 10, pp. 4568-4582, Oct. 2011.

[105] J. A. Short, D. G. Infield, and L. L. Freris, "Stabilization of grid frequency through dynamic demand control," *IEEE Trans. Power Syst.*, vol. 22, no. 3, pp. 1284–1293, 2007.

[106] J. M. Guerrero, J. C. Vasquez, J. Matas, and L. G. de Vicuna, "Hierarchical control of droop-controlled ac and dc microgrids-a general approach toward standardization," *IEEE Trans. Ind. Elec.*, vol. 58, no. 1, pp. 158-172, Aug. 2010.

[107] H. Bevrani, F. Habibi, P. Babahajyani, M. Watanabe, and Y. Mitani, "Intelligent frequency control in an ac microgrid: on-line pso-based fuzzy tuning approach," *IEEE Trans. Smart Grid*, vol. 3, no. 4, pp. 1935–1944, Dec. 2012.

[108] H. Bevrani, *Robust Power System Frequency Control*, 1st ed., New York, NY, U.S.A.: Springer, 2009.

[109] A. Suwannarat, "Integration and control of wind farms in the danish electricity system," Doctoral Dissertation, Dept. Energy Technology, Aalborg University, Denmark, 2007.

[110] [Online]. Available: www.ens.dk.

.

APPENDICES

Appendix A. Data of Danish distribution network

Table 1. Data of grid cables in different feeders

Bus number	R (Ω/km)	X (Ω/km)	R	X	R(p.u.)	X(p.u.)
Trafo→1 (Feeder1)	0,2080	0,086	0,0859	0,0355	53,703	22,204
1 to 2	0,6420	0,0870	0,0399	0,0054	24,958	3,382
1 to 3	0,6420	0,0870	0,0658	0,0089	41,128	5,573
3 to 4	0,6420	0,0870	0,0642	0,0087	40,125	5,438
4 to 5	0,3210	0,0860	0,0551	0,0148	34,467	9,234
Trafo→6 (Feeder2)	0,2080	0,0840	0,0539	0,0217	33,657	13,592
6 to 7	0,2080	0,0840	0,0186	0,0075	11,609	4,688
7 to 8	0,2080	0,0840	0,0448	0,0181	28,028	11,319
8 to 9	0,3210	0,0840	0,0544	0,0142	34,006	8,899
9 to 10	0,3210	0,0840	0,0258	0,0068	16,130	4,221
Trafo→11 (Feeder3)	0,2080	0,0840	0,0347	0,0140	21,671	8,752
11 to 12	0,2080	0,0840	0,0233	0,0094	14,560	5,880
12 to 13	0,3210	0,0840	0,0261	0,0068	16,331	4,274
13 to 14	0,3210	0,0840	0,0546	0,0143	34,106	8,925
Trafo→15 (Feeder4)	0,2080	0,0840	0,0613	0,0247	38,285	15,461
15 to 16	0,2080	0,0840	0,0223	0,0090	13,949	5,633
16 to 17	0,2080	0,0840	0,0267	0,0108	16,718	6,752
17 to 18	0,2080	0,0840	0,0132	0,0053	8,268	3,339
Trafo→19 (Feeder5)	0,2080	0,0860	0,0908	0,0376	56,771	23,473
19 to 20	0,3210	0,0840	0,0414	0,0108	25,901	6,778
20 to 21	0,6420	0,0870	0,0545	0,0074	34,066	4,616
Trafo→22 (Feeder6)	0,2080	0,0840	0,0590	0,0238	36,855	14,884
22 to 23	0,2080	0,0840	0,0146	0,0059	9,100	3,675
23 to 24	0,3890	0,0830	0,0204	0,0044	12,764	2,723
24 to 25	0,3890	0,0830	0,0311	0,0066	19,450	4,150
24 to 26	0,5260	0,0830	0,0395	0,0062	24,656	3,891